REPORT DOCUMENTATION PAGE

AFRL-SR-AR-TR-02-

O259

1. AGENCY USE ONLY (Leave blank)	2. REPORT DATE	3. REPORT
	19 JUL 2002	FINAL (01-N0V-98 TO 30-APR-02)

4. TITLE AND SUBTITLE
SPARTICLE SIMULATON OF PULSED PLASMA THRUSTER PLUMES

5. FUNDING NUMBERS
F49620-99-1-0040

6. AUTHOR(S)
IAIN D. BOYD

7. PERFORMING ORGANIZATION NAME(S) AND ADDRESS(ES)
CORNELL UNIVERSITY
246 UPSON HALL
ITHACA, NY 14853

8. PERFORMING ORGANIZATION REPORT NUMBER

9. SPONSORING/MONITORING AGENCY NAME(S) AND ADDRESS(ES)
AIR FORCE OFFICE OF SCIENTIFIC RESEARCH
801 N. RANDOLPH STRET
ARLINGTON, VA 22203

10. SPONSORING/MONITORING AGENCY REPORT NUMBER

11. SUPPLEMENTARY NOTES

12a. DISTRIBUTION AVAILABILITY STATEMENT

Approved for public release;
distribution unlimited.

12b. DISTRIBUTION CODE

13. ABSTRACT (Maximum 200 words)
This final report summarizes the research carried out on the development of numerical approaches for simulating the plumes of pulsed plasma thrusters. A significant amount of progress has bee made in the three years of this grant and this summarized in the 9 journals and conference papers that are included as appendices to this report. Our modeling had made progress in al aspects of simulating these complex devices including Teflon ablation, plasma formation, electro-magnetic acceleration, plume expansion, and particulate transport. Several different pulsed plasma thruster devices were modeled including an electro-thermal device (the PPT-4 developed at the University of Illinois by Dr. Rod Burton), and various micro-PPT's (developed at the Air Force Research Laboratory by Dr. Greg Spanjers and colleagues).

20020903 040

14. SUBJECT TERMS			15. NUMBER OF PAGES
			99
			16. PRICE CODE

17. SECURITY CLASSIFICATION OF REPORT	18. SECURITY CLASSIFICATION OF THIS PAGE	19. SECURITY CLASSIFICATION OF ABSTRACT	20. LIMITATION OF ABSTRACT
UNCLASSIFIED	UNCLASSIFIED	UNCLASSIFIED	

FINAL TECHNICAL REPORT

PARTICLE SIMULATION
OF PULSED PLASMA THRUSTER PLUMES

prepared by

Iain D. Boyd [1]

School of Mechanical and Aerospace Engineering
Cornell University,
246 Upson Hall
Ithaca, NY 14853.

June 2002

[1] Principal Investigator

1

32814 (handwritten)

Table of Contents

Summary

This final report summarizes the research carried out on the development of numerical approaches for simulating the plumes of pulsed plasma thrusters. A significant amount of progress has been made in the three years of this grant and this is summarized in the 9 journal and conference papers that are included as appendices to this report. Our modeling has made progress in all aspects of simulating these complex devices including Teflon ablation, plasma formation, electro-magnetic acceleration, plume expansion, and particulate transport. Several different pulsed plasma thruster devices were modeled including an electro-thermal device (the PPT-4 developed at the University of Illinois by Dr. Rod Burton), a Z-pinch device (the AZ-PPT developed at Princeton University by Dr. Eddie Choueiri), and various micro-PPT's (developed at the Air Force Research Laboratory by Dr. Greg Spanjers and colleagues).

Electrical Discharge in the Teflon Cavity of a Coaxial Pulsed Plasma Thruster

Michael Keidar, *Member, IEEE*, Iain D. Boyd, and Isak I. Beilis, *Member, IEEE*

Abstract—In this work, we analyze the physical processes of a pulsed discharge in a dielectric (Teflon) cavity. This type of discharge is generated in a coaxial pulsed plasma thruster (PPT) having a central Teflon cavity to produce a high-pressure cloud of ablation products during the discharge pulse. The primary intended role of this model is to provide upstream boundary conditions for particle simulation codes used to study the exhaust plume. The main features of the electrical discharge in the dielectric cavity include Joule heating of the plasma, heat transfer to the dielectric, decomposition of the dielectric followed by partial ionization, and acceleration of the plasma up to the sound speed at the cavity exit. We consider a diffuse type of discharge assuming that all plasma parameters are uniform in the cavity. The system of equations is based on the plasma energy balance, thermal conductivity, dielectric ablation, and mass balance. It is found that most of the energy of the plasma column is carried off by particle convection to the dielectric and by radiation. It is found that during the pulse, the electron density peaks at about 10^{24} m^{-3} and decreases to 10^{21} m^{-3} toward the end of the pulse, whereas the electron temperature peaks at about 2.2 eV and decays to 1.5 eV. Teflon surface temperature peaks at about 650 K. Predicted plasma temperature and ablated mass are found to be in agreement with available experimental data.

Index Terms—Ablation controlled discharge, near-wall sheath, pulsed plasma thruster (PPT).

I. INTRODUCTION

PULSED plasma thrusters (PPT's) have been investigated since the early 1960's and were among the earliest electric propulsion systems to be flown by the United States. First, plasma thruster designs were based on the plasma accelerators that were developed for high-energy plasma injection into thermonuclear reactors. Different configurations of plasma accelerators were proposed with electromagnetic [1], [2] and electrothermal [3] dominant acceleration mechanisms. The ratio between electromagnetic and electrothermal mechanisms of acceleration depends on thruster geometry and electrical discharge parameters. Both parallel rail electrode and coaxial concepts were developed [4]–[6] to produce the thrust. The principal advantage of the PPT is the simple propellant system design, which provides high reliability. However, the PPT has

poor performance characteristics. For instance, a flight-qualified PPT design had an efficiency of about 8% [7]. Several directions for improvement of PPT performance are under consideration [8].

A great interest in the development of small satellites occurs, which causes the PPT to be reconsidered as an attractive propulsion option [9], [10]. PPT's are expected to provide exact impulse bits to be used for accurate attitude control. PPT's can provide high specific impulse of 1000 s, impulse bit of about 30 μN-s per Joule, and can operate with arbitrary low power.

In order to assure successful operation of a PPT on the spacecraft, a complete assessment of the spacecraft integration effects is needed. The solid-fed PPT plume contains various ion and neutral species because of propellant decomposition and possible electrode erosion. The main integration issue is the deposition of highly condensible PPT plumes on spacecraft surfaces. Some attempts at PPT plume simulation using hybrid direct simulation Monte-Carlo particle-in-cell (DSMC-PIC) simulations were performed recently [11], [12]. In [11], however, some artificial starting conditions were employed. Accurate plume modeling requires the formulation of boundary and initial conditions, which depend on the specific PPT design and pulse parameters. Thus, it is necessary to analyze the physical processes involved in plasma generation and acceleration.

In this investigation, we will concentrate on a specific type of PPT, recently developed at the University of Illinois, so-called PPT-4 [9], [10]. This PPT has a coaxial configuration in which Teflon is ablated from a cylindrical cavity sitting in front of the central electrode. The device has a pulse length of about 10 μs, and the overall specific impulse was measured to be 830 s. The main physical processes in this type of PPT occur in the Teflon cavity. Rapid heating of a thin dielectric surface layer leads to decomposition of the material of the wall. As a result of heating, decomposition and partial ionization of the decomposition products, the total number of particles increases in the cavity. The PPT-4 also has a ceramic nozzle in which the plasma is presumed to be accelerated by both electrothermal and electromagnetic effects [9]. In principal, the ratio between electromagnetic and electrothermal acceleration mechanisms can be changed by using different operational parameters, such as cavity length, pulse form, and duration.

In the present work, a model of the physical process of plasma generation in the dielectric cavity will be developed. The present model allows calculation of the electron temperature, electron and neutral densities, dielectric surface temperature, and the sheath potential drops near the anode and dielectric. The present model helps us to understand plasma generation and energy balance in electrothermal PPT's. These calculation results will be
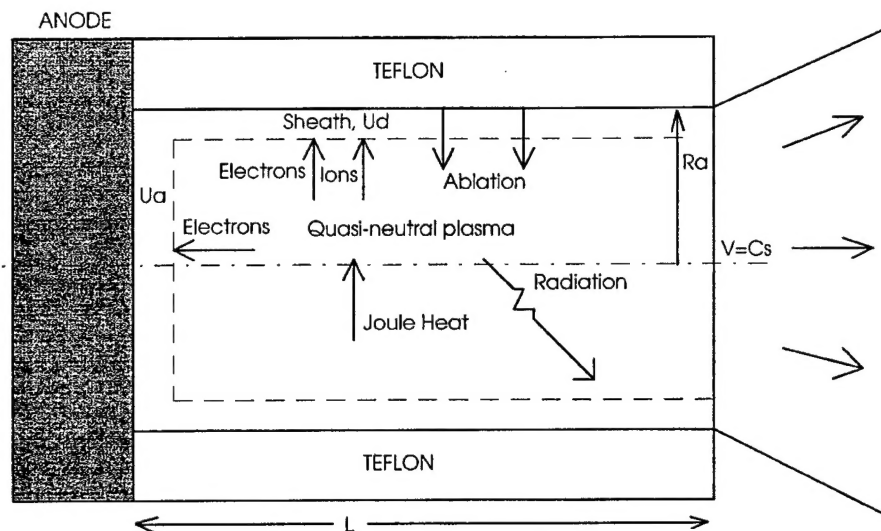
ANODE

Fig. 1.   Schematic of the problem geometry and energy balance.

used in other plasma plume model as time-dependent boundary conditions.

II. THE MODEL

The model presented here describes the physical processes of pulsed electrical discharge in a Teflon cavity sitting in front of the central electrode–anode, as shown in Fig. 1. The main features of electrical discharge in the dielectric cavity include heating of the plasma, heat transfer to the dielectric, decomposition of the dielectric followed by partial ionization, and electrothermal acceleration of the plasma up to the sound speed at the cavity exit. As a result of Teflon decomposition, the plasma density increases. Thus, the stored energy is expended in plasma generation, plasma, electrodes, and insulator heating, and acceleration. In the PPT-4, the two electrodes are connected with a 30° half angle nozzle, as shown in Fig. 1 (the annular electrode–cathode is not shown). Because of the specific geometry of this thruster, the current flow is mostly parallel to the plasma flow. In the initial stage of the discharge, the interelectrode gap is filled with a certain amount of plasma by a spark plug. The voltage- and surface-induced variations in the igniter plasma may lead to shot-to-shot variation of PPT thrust. However, usually the energy and mass of the first ignition plasma constitutes no more than a few percent of the total mass and energy involved in the discharge. Therefore, one may expect that the exact conditions of the igniter plasma will not substantially affect the performance of the PPT [9]. Because no experimental data for the initial plasma density exist, in the present model, the initial plasma density will be used as a free parameter of the problem (see Section III).

The main features of the discharge in the PPT Teflon cavity are analogous to the capillary discharge [13] and ablation controlled arcs [14]–[16]. During the discharge pulse, the plasma is heated by Joule heat and is cooled by radiation, energy losses from particle convection to the anode and dielectric, and ionization. Mechanisms of energy transfer from the plasma column to the wall of the Teflon cavity are also possible: heat transfer by particle fluxes and radiation heat transfer. As a result of this interaction of the plasma column with the walls of the cavity, the walls are heated rapidly. The temperature of the surface layer increases and reaches the critical temperature of phase transition. Further analyzes should include treatment of the kinetics of chemical reaction of material decomposition [17], [18]. The principal mechanism of thermal degradation of the dielectric is breaking the bonds in the backbone of the chain [17], which consumes the main portion of energy transferred.

During the discharge pulse, the nonuniformity in the discharge distribution across the Teflon surface may cause overheating followed by phase change of the propellant, which causes high pressure. High plasma pressure in the PPT channel may lead to Teflon macroparticle generation. However, the mechanism of such macroparticle generation from the propellant is not understood sufficiently for modeling. Another possible source of macroparticles is the spot attachment at the electrodes. Spot attachment at electrodes is a typical phenomenon in the early stages of discharge [9], [19]. The macroparticle generation phenomenon is beyond the scope of the present study.

During the discharge pulse, parameters change rapidly, so an important problem concerns the possibility of establishing local thermodynamic equilibrium (LTE). The typical PPT-4 pulse discharge duration is about 10 μs. In a homogeneous transient plasma [20], complete LTE may be obtained in 0.3 μs for a helium plasma with electron density of 10^{24} m^{-3}. An estimation of the characteristic times for ionization and recombination has shown that the ionization and recombination time scales for ground states of C and F are less than the typical time for discharge parameter changes (few microseconds) [21]. Therefore, LTE establishing may be considered during the discharge pulse. The calculation of relaxation time for higher excited levels shows, however, that the quasisteady state is not achieved for the second stage of ionization [20]. An estimate of the relaxation time for elastic collisions has shown that

in a plasma with density of 10^{22}–10^{24} m^{-3} and an electron temperature of 1–3 eV, equilibrium of electrons, ions, and neutrals is established on a time scale of microsecond [3]. Thus, the present model considers temperature equilibrium $T_e = T_i = T$, where T is the plasma temperature.

In the present model, we will assume that a diffuse discharge covers the entire surface of the anode. The anode current is carried by electrons and controlled by the potential drop in the anode sheath. The potential drop in the sheath depends on the plasma and current density and may have spatial variation. Generally, the sheath is slightly negative, to repel the excess of the thermal electron current, so that the electron current to the anode is equal to the circuit current

$$U_a = -T \ln(I_{th}/I) \tag{1}$$

where T is the plasma temperature in [eV], I_{th} is the random electron current, and I is the circuit current. The random electron current may be calculated as

$$I_{th} = \tfrac{1}{4} e n_e (8eT/\pi m_e)^{1/2} \pi R_a^2 \tag{2}$$

where

n_e is the electron density at the anode sheath–plasma interface;

m_e is the electron mass;

e is the electron charge;

R_a is the anode radius.

The electrostatic sheath also appears near the dielectric surface where quasineutrality condition breaks down. The transient sheath formation near the dielectric surface is determined by the dielectric permittivity. In the considered range of electron density (10^{21}–10^{24} m^{-3}), the characteristic charging time [22] is less than 10^{-10} s, which is much smaller than the characteristic time of the discharge parameter changes. Therefore, we will use a quasisteady-state sheath model. Furthermore, we will assume that the plasma density is so high that the sheath thickness ($\sim$Debye length) is much smaller than the electron Larmor radius (in the self magnetic field). This assumption will be justified later. As in the case of the anode sheath, the sheath voltage drop U_d should be negative to repel the excess of the thermal electron current, so that the electron current is equal to the ion current

$$U_d = -T \ln(I_{th}/I_i) \tag{3}$$

where I_i is the ion current given by the expression

$$I_i = 0.25 e Z_i n_e (8eT/\pi m_i)^{1/2} 2\pi R_a L. \tag{4}$$

Here, Z_i is the charge number, m_i is the ion mass, and L is the cavity length (see Fig. 1).

Starting from the above considerations, a simplified model of the pulsed discharge in the dielectric cavity is proposed using the following basic assumptions (some of these assumptions will be discussed in Section IV).

1) We have considered a diffuse type of discharge assuming that all plasma parameters are uniform within the plasma column.

2) The plasma is quasi-neutral.

3) The plasma column is in local thermodynamic equilibrium (LTE).

As a result of the foregoing assumptions, the following governing equation can be formulated to describe the time-dependent behavior of different plasma parameters and the relationship between them.

The electron energy balance in the quasineutral plasma column reads

$$\frac{3}{2} n_e \frac{dT}{dt} = \frac{j^2}{\sigma} - A Z_i^2 n_e n_i T^{1/2}(1 + \chi_g)$$
$$- \frac{j}{L}(2T + U_a) - \frac{2j_d}{R_a}(2T + U_d + T) \tag{5}$$

where the first term on the right-hand side represents the Joule heating of the plasma column, j is the current density $j = (I/\pi R_a^2)$, σ is the plasma conductivity, and j_d is the ion current density in the sheath near the dielectric $j_d = I_i/(2\pi R_a L)$. The second term describes the radiative emission energy losses [23], [24], A is the constant ($1.6 \cdot 10^{38}$ in SI units), n_i is the ion density, and $\chi_g = E_g/T_e$ is the E_g is the energy of the low excited state. The third term represents the energy losses caused by electron convection to the anode. The last term represents energy losses caused by convection of electrons and ions to the dielectric.

In general, the thermal regime of the Teflon will be considered to consist of two stages: the first stage involves initial heating, i.e., the Teflon surface heating up to the onset of phase transition, and the second stage of Teflon decomposition. A third stage also exists called late ablation [25], i.e., Teflon decomposition after the pulse, which is also under consideration.

The temperature can be calculated from the heat transfer equation

$$\partial T/\partial t = a \partial^2 T/\partial x^2 \tag{6}$$

where a is the thermal diffusivity, $a = \lambda/C_p\rho$, where λ is the thermal conductivity, C_p is the specific heat capacity, and ρ is the specific weight. Equation (6) is subject to the following boundary conditions [18]

$$-\lambda \partial T/\partial x (x = 0) = q(t) - \Delta H \cdot \Gamma - C_p(T_s - T_o)\Gamma$$
$$\lambda \partial T/\partial x (x = \infty) = 0$$
$$T(t = 0) = T_o \tag{7}$$

where

$x = 0$ corresponds to the inner dielectric surface;

ΔH is the ablation heat;

Γ is the ablated flux;

T_o is the initial room temperature;

$q(t)$ is the density of the heat flux;

consisting of the radiative and particle convection fluxes, determined according to (5), and T_s is the Teflon surface temperature.

In the first stage, which according to calculation is about 1.5 μs, the energy losses connected with decomposition are small and, thus, may be neglected in the energy balance. We will use an approximate solution for temperature within the Teflon [17], [18], which at the Teflon surface reads [21]

$$T_s(t) = T_o + \frac{q(t)}{3\lambda} \cdot \left[\frac{12\lambda}{q(t)C_p\rho} \int_0^t q(t)\, dt \right]^{0.5}. \tag{8}$$

After the surface reaches some critical temperature, material decomposition begins and ablation heat becomes significant in the energy balance. The principal mechanism of thermal degradation of the Teflon is the breaking the bonds in the backbone of the chain [17]. Heat transfer analysis shows that the temperature profile for the ablated Teflon is exponential [17]

$$T(x) = T_s \exp(-x\Gamma C_p/\lambda). \qquad (9)$$

We will use this approximate solution to estimate the temperature gradient at the Teflon surface. It should be noted, however, that the calculation shows little influence of the temperature gradient on the Teflon surface temperature.

Using (9) with boundary conditions (7), it is possible to calculate the temperature of the Teflon surface for known ablated flux Γ, which in turn depends on the equilibrium pressure. For known surface temperature, one can calculate the equilibrium pressure using the Teflon formula [9]

$$P = P_c \exp(-T_c/T_s) \qquad (10)$$

where P is the equilibrium pressure and P_c and T_c are the characteristic pressure and temperature, respectively. In the quasisteady state, the equilibrium pressure should be equal to the total pressure in the discharge column

$$P = P_n + P_i + \rho_{pl} V^2 \qquad (11)$$

where

P_n and P_i are the partial pressures of neutrals and ions, respectively, in the discharge column;
ρ_{pl} is the mass plasma density;
V is the plasma velocity.

In the cavity, the plasma velocity changes from zero near the anode up to a value equal to the local velocity of sound at the cavity outlet section. The considered plasma flow problem inside the cavity in principle is two-dimensional; however, in the main part of the plasma bulk this axial velocity is small [26]. In our pressure balance, we will use the plasma velocity as a parameter. Possible implications of this assumption will be discussed later. For known equilibrium pressure, one can calculate the ablation flux using the Langmuir law [27]

$$\Gamma = P\sqrt{\frac{m_i}{2\pi k T_g}} \qquad (12)$$

where T_g is the gas temperature. Our estimation shows that under considered conditions in the plasma, the bulk gas is in thermodynamic equilibrium with the ions and electrons and thus $T_g = T$, whereas near the surface the gas has a temperature equal to the Teflon surface temperature. Thus, for calculation of the ablation rate, we will use $T_g = T_s$. Generally, in the boundary layer near the Teflon surface, the temperature sharply changes from the plasma bulk temperature to the surface temperature. The temperature profile in this boundary layer is approximately linear [21]. The characteristic thickness of this temperature layer is about an electron–ion collision mean free path, which is about 10^{-4} m in the considered range of parameters and much smaller than the cavity radius.

The total mass of the dielectric material ablated during the entire discharge pulse may be calculated by integration of the net flux of ablation and deposition caused by back flux from the plasma. In equilibrium, the net ablated mass may be determined as follows:

$$M_a = 2\pi R_a L \int_o^{t_p} \Gamma(T)\, dt \qquad (13)$$

where t_p is the pulse duration.

For known equilibrium pressure and electron temperature, one can calculate the chemical plasma composition using models developed previously [28], [29]. In the considered range of electron temperature (1–2 eV) and plasma density (10^{21}–10^{24} m^{-3}), we will assume that polyatomic molecules C_2F_4 fully dissociate [29] and we will start our consideration from the point when we have gas containing C and F. The conservation of nuclei for the case of Teflon reads

$$2(n_C + n_C^+) = n_F + n_F^+ \qquad (14)$$

where n_C and n_F are the density of neutrals and n_C^+ and n_F^+ are the densities of ions, respectively. In LTE, the density of electrons n_e, ions n^+ and neutrals n_n depend on the plasma temperature according to the Saha equation [23]

$$\frac{n_e n_C^+}{n_n} = B\left(\frac{g_i}{g_n}\right)_C T^{3/2} \exp(-I_C/T) = A_C \qquad (15a)$$

$$\frac{n_e n_F^+}{n_n} = B\left(\frac{g_i}{g_n}\right)_F T^{3/2} \exp(-I_F/T) = A_F \qquad (15b)$$

where

B is a constant;
g_i and g_a are statistical weights of ion and electrons;
I_C, I_F are the ionization potentials of C and F, respectively.

In our case, the plasma consists of the electrons, neutrals C and F and ions C^+ and F^+. Thus, we have five unknown partial pressures. Therefore, an equilibrium composition can be calculated by solving (11), (14), and (15) supplemented with the quasineutrality condition

$$n_e = n_C^+ + n_F^+. \qquad (16)$$

From the system of equations (13)–(15) it is straightforward to find an equation for the electron density in an explicit form

$$2n_e^2(n_e + A_F) + n_e^2(n_e + A_C) - (n_h - 2n_e) \times \{2A_F(n_e + A_C) + A_C(n_e + A_F)\} = 0 \qquad (17)$$

where n_h is the total heavy particle density.

The heat deposited during the discharge pulse accumulates in the skin-layer $\delta = (\lambda t_p/\rho C_p)^{0.5}$ and propagates within the Teflon after the end of the discharge pulse ($t_p \sim 10 \cdot \mu$s in PPT-4, [31]). During the after-pulse cooling, the Teflon surface temperature can be estimated as follows [8], [30]:

$$T_s = T_o + (t_p/t)^{0.5}(T_{sp} - T_o) \qquad (18)$$

where T_{sp} is the Teflon surface temperature at the end of the discharge pulse.

III. RESULTS

In this section, we will present results of calculation of the plasma parameters during the discharge pulse in the PPT-4
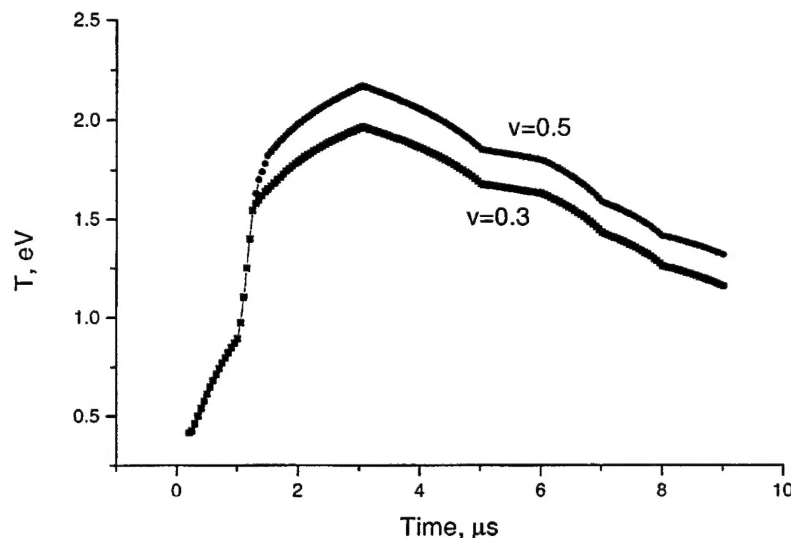
Fig. 2. Plasma temperature time distribution with plasma velocity as a parameter.

developed recently at the University of Illinois Urbana-Champaign [9], [31]. The set of the equation consists of nonlinear algebraic equations and a differential equation describing the energy balance. Equations (1)–(17) form a set of eight equations with the following unknowns: $T, T_s, U_a, U_d, n_C, n_F, n_C^+, n_F^+$. The differential equation was integrated numerically using the Runge–Kutta algorithm. Linearization of the experimental current waveform causes some kinks in the graphics presented below. In order to simulate the energy input during the pulse, the experimental current waveform has been used [9], [31]. The results presented in this section correspond to the following PPT-4 design and discharge parameters: $R_a = 3.15$ mm, $L = 8.3$ mm, current peak of about 8 kA, pulse duration is about 10 μs. The plasma velocity v is used as a parameter of the problem and is normalized by the sound speed $C_s = (2T/m_i)^{0.5}$. The initial plasma density is used as a parameter before Teflon heating. This density lies in the range of 10^{21}–10^{23} m^{-3} and weakly affects the results as shown below.

The time evolution of the plasma temperature is shown in Fig. 2. Initially, the plasma temperature sharply increases and peaks at about 2–2.3 eV, dependent on the velocity v. Toward the pulse end, the plasma temperature decreases to 1–1.5 eV. In the experiment [31] it was measured that the peak electron temperature lies in the range of 2–2.5 eV, decreases to about 1 eV, and varies slightly with axial distance from the thruster exit plane (not shown). The model predictions and experimental data have similar trend, which indicates that the model prediction reasonably agrees with experimental data. It should be noted, however, that the data were taken in the plasma plume at different axial distances from the thruster exit plane (up to 0.2 cm). Thus, the experimental and calculation time scales are different with a shift approximately equal to the plasma flight time from the cavity to the plane where data were taken.

The electron density distribution during the pulse is plotted in Fig. 3. It can be seen that the plasma density has a maximum of about 10^{24} m^{-3} and then decreases toward the discharge end.

The plasma density peaks at about 3 μs, which corresponds to the peak in the current pulse. One can also see that the high plasma density corresponds to the smaller velocity, which is a result of mass conservation.

The temperature of the Teflon surface is shown in Fig. 4. The temperature sharply increases during the first 2 μs of the discharge pulse and peaks at about 650 K, which is above the temperature of Teflon decomposition ($\sim$600 K, [8]). It should be noted that the Teflon surface temperature only slightly depends on plasma velocity v.

The anode sheath potential drop is displayed in Fig. 5 with initial potential drop U_{ao} as a parameter. The initial value of U_{ao} is a result of introducing the initial plasma density as a parameter. It can be seen that U_a is negative and has a maximum value of about $-6T$, regardless of the initial value of U_a. Toward the pulse end, the absolute value of the anode sheath potential drop decreases significantly.

The chemical composition of the plasma is shown in Fig. 6(a) for the case $v = 0.3$ and Fig. 6(b) for the case $v = 0.5$. One can see that all densities peak at about 3 μs. The fluorine (F) neutral density is larger than the carbon (C) neutral density, because originally Teflon has composition C_2F_4. However, the difference between fluorine ion density and carbon ion density is much smaller because carbon has a smaller ionization energy [ionization energy of carbon is 11.3 eV (at the first level), whereas fluorine has a corresponding ionization energy of 17.4 eV]. It can be seen that the ionization degree is higher in the case of larger velocity.

The distribution of the input energy density (by the Joule heat) and output (radiation, electron flux to the anode, and electron and ion convection to the Teflon) are shown in Fig. 7. It can be seen that the Joule heat density peaks at about 10^{13} W/m^3 and is mainly carried off by particle convection and radiation. The energy input is larger than output initially, for the time <3 μs (plasma heating), whereas for the time >3 μs, the energy input is slightly smaller than the output (plasma cooling). This corresponds to the plasma temperature behavior, as shown in Fig. 2.
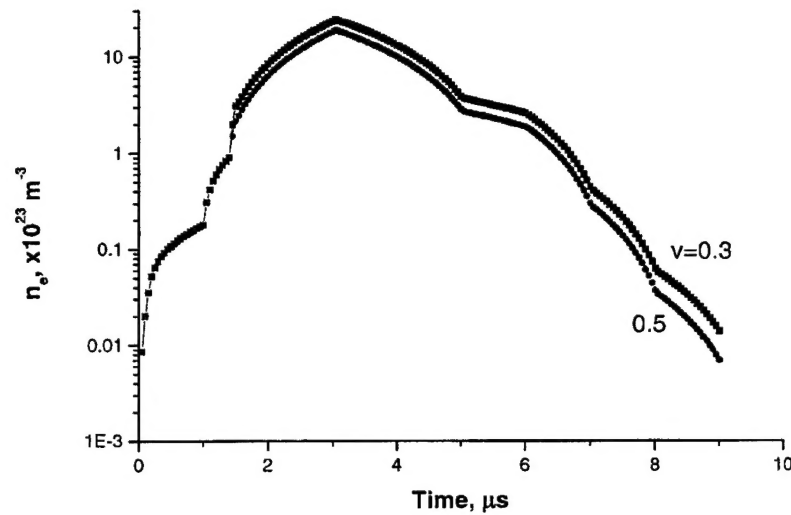
Fig. 3. Electron density distribution during the discharge pulse with plasma velocity as a parameter.
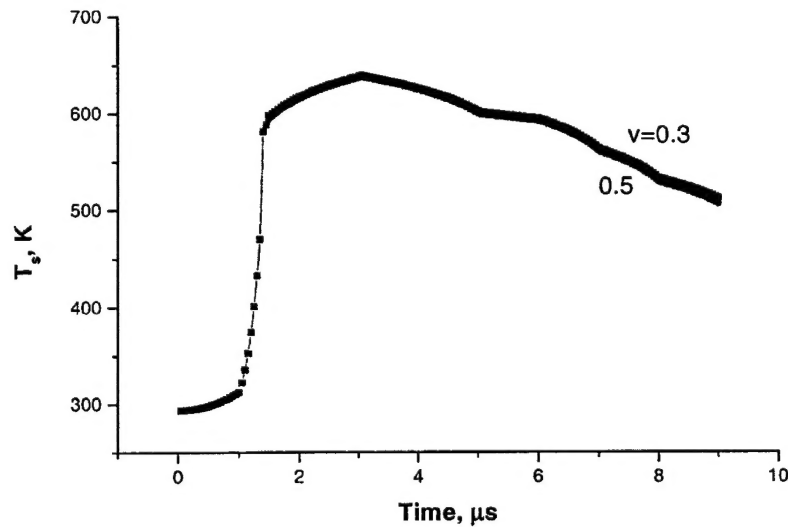

Fig. 4. Teflon surface temperature with plasma velocity as a parameter.

The ablated mass approximately increases linearly with cavity length, as shown in Fig. 8, where velocity is used as a parameter. It can be seen that in the case of smaller velocity, ablated mass is higher. For comparison, some experimental data [31] are also shown. One can see that generally good agreement between predicted and measured ablated mass is found.

It should be noted that ablation mass was measured over 1000 shots with a pulse rate of about 1.1 Hz [31]. Thus, it is possible that the Teflon surface temperature during the time between pulses may be higher than room temperature, which may increase the total mass ablation. However, calculation of the late time ablation shows that it consumes no more that 1 μg per pulse.

IV. DISCUSSION

In this section, we will discuss the implications of several of the assumptions used in the model described above.

The basic and strongest assumption is considering the plasma to be uniform in the cavity, which means that the plasma properties are described by average plasma parameters. In general, however, the problem is 2-D with plasma velocity and density variation in the radial and axial directions. Plasma velocity varies from zero near the anode up to the sound speed at the cavity exit plane, and thus, the plasma density should decrease toward the cavity exit plane. However, if ablation is approximately uniform along the cavity, the plasma velocity increases substantially only near the exit ($\sim$0.8 L, as shown in [13], [26]). In the plasma bulk, the velocity is about $(0.3–0.5)C_s$, as was used in the model. It was also found that the plasma velocity does not significantly affect the plasma density and temperature distributions during the discharge pulse. In spite of its simplicity, our approach is able to predict reasonable behavior of the plasma temperature and ablated mass, which are in reasonable agreement with an experiment.
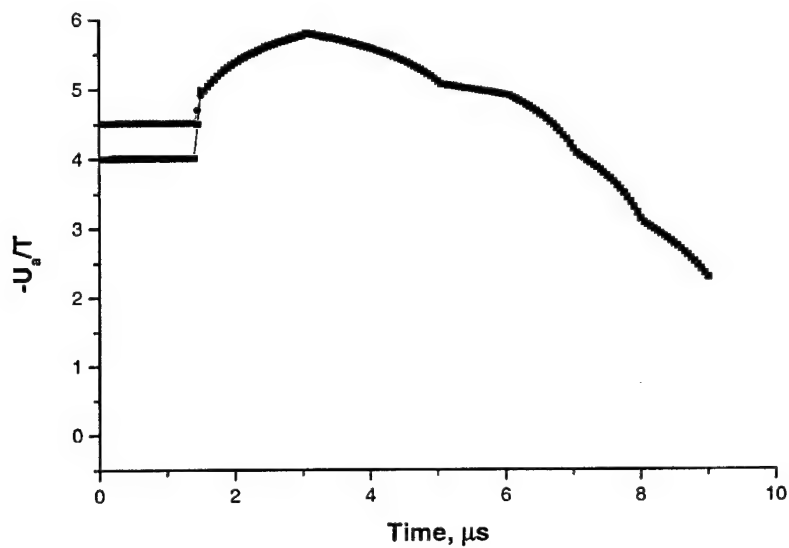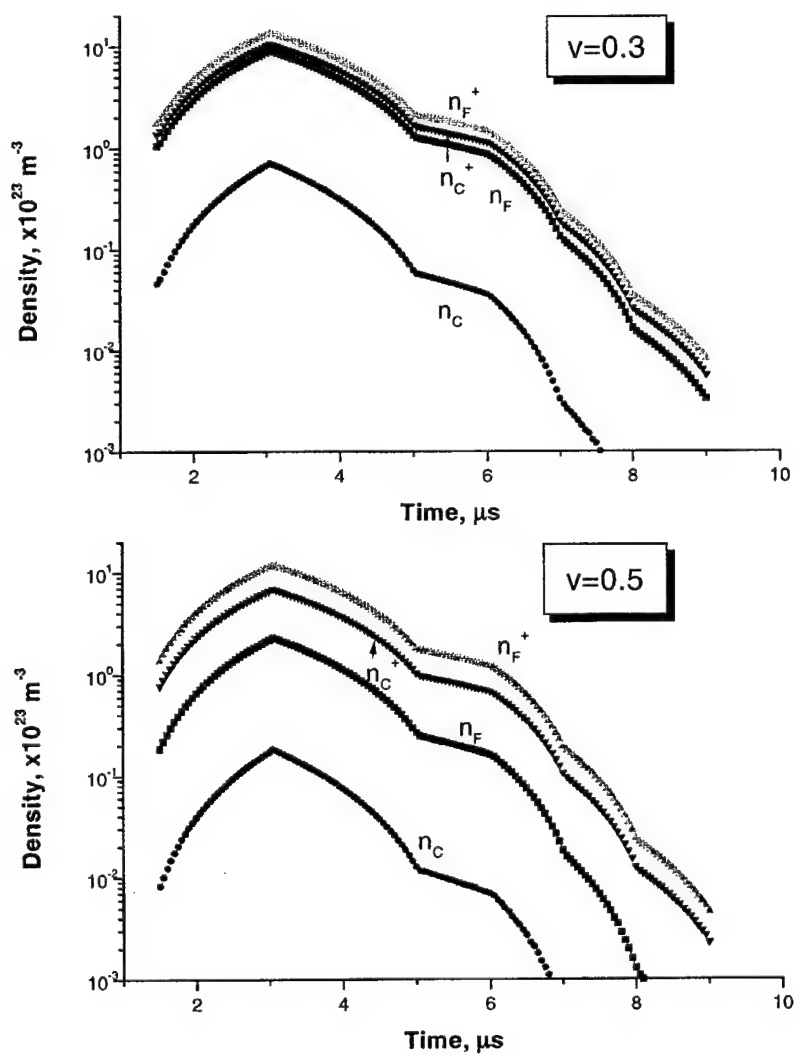
Fig. 5. Anode sheath potential drop time dependence.

Fig. 6. Chemical composition of the plasma during discharge pulse: (a) $v = 0.3$ and (b) $v = 0.5$.
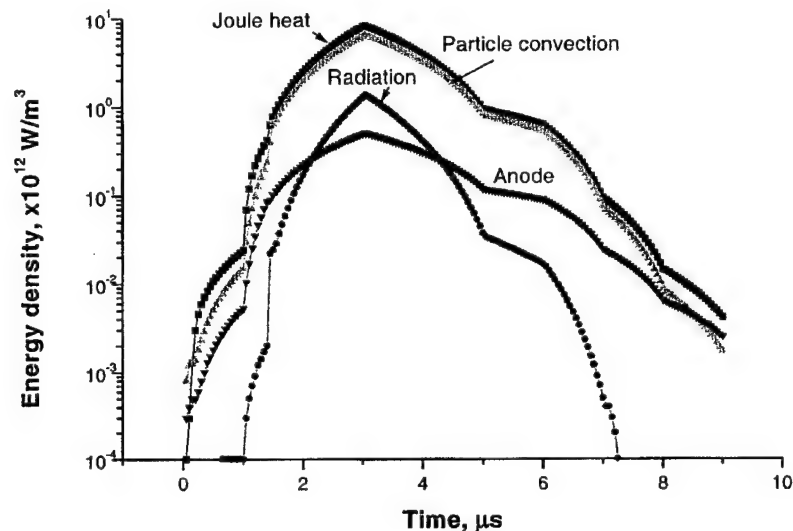
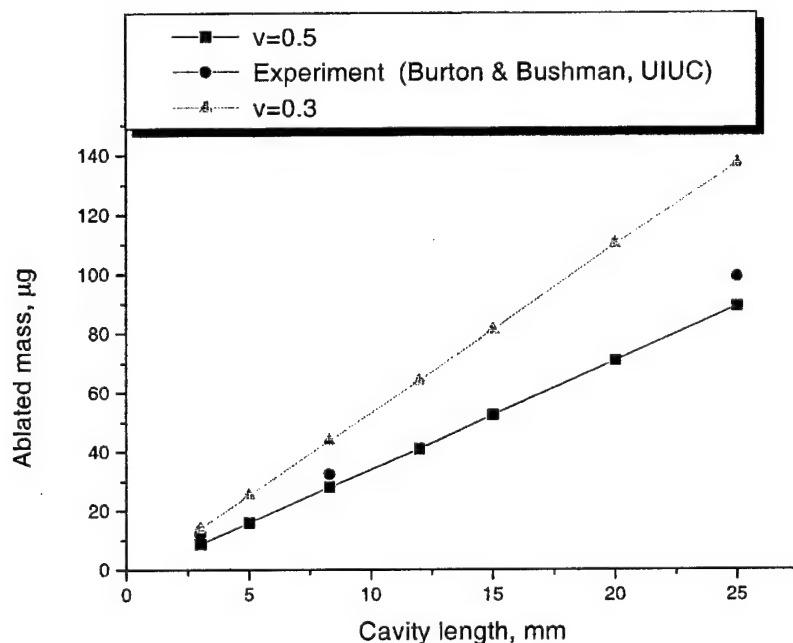Fig. 7.   Energy input and output time distribution.

Fig. 8.   Ablated mass as a function of the cavity length with velocity as a parameter. Experimental data were taken from [31].

The present approach used an ablation model based on the equilibrium vapor pressure depending on the Teflon surface temperature. This approach is similar to that used in [25]. Because equilibrium vapor pressure is sensitive to the exact value of the surface temperature, the heat transfer becomes an important issue. In general, the heat transfer to an ablated surface is a complicated nonlinear problem requiring numerical solution [18], [25]. In our model, we have used a temperature profile [17], which was found to be a fair approximation for a reacting surface. This approximation for the temperature profile is used for estimation of the temperature gradient at the Teflon surface. However, it was found that the temperature gradient on the Teflon surface has only a small effect on the surface temperature.

In order to predict the chemical composition of the plasma, the present model employed the Saha equation assuming local thermodynamic equilibrium in the plasma column. However, LTE may be established only in relatively dense plasmas $>10^{22}$ m^{-3} over a time period larger than the characteristic relaxation time for ionization and recombination in the plasma ($\sim 10^{-7}$ s). Calculation shows that during the main part of the pulse the above requirements are fulfilled. Toward the pulse end, however, the plasma density significantly decreases and the relaxation time becomes comparable to the pulse duration. In this case, the LTE approach predicts a plasma ionization degree that is much higher than it should be in the real situation. Thus, the electron density calculated after about 8 μs is overestimated and should be considered only as an upper limit.

Let us estimate the effect of possible plasma and current compression by the self-magnetic field during the discharge pulse. At the current peak ($\sim 3 \, \mu$s), the Hall parameter (ratio of electron cyclotron frequency to electron–ion collision frequency) is less than unity. Thus, the conductivity is determined by Coulomb collisions and the effect of the self-magnetic field on the current flow is small. An estimation shows that for PPT-4 conditions the ratio of the gas kinetic pressure to the magnetic pressure $P/(B_{\text{self}}^2/2\mu) \gg 1$ during the discharge pulse, except at the current peak point, where the gas kinetic pressure is slightly larger than is the magnetic pressure. However, the self-magnetic field may have substantial effect on the discharge processes in the cavity with smaller radius. Therefore, further development of the pulse discharge model may be associated with taking into account the self-magnetic field.

V. CONCLUSION

An analysis of the physical processes in the Teflon cavity of a PPT shows that the energy of the plasma column is carried off by particle convection to the dielectric and by radiation. During the pulse, the electron density peaks at about 10^{24} m^{-3} and decreases to 10^{21} m^{-3} toward the pulse end, whereas the electron temperature peaks at about 2.2 eV and decays to 1.5 eV. Teflon surface temperature peaks at about 650 K, which is above the temperature of decomposition (~ 600 K). Calculated electron temperature ablated mass were found to be in good agreement with experimental measurements. The present model allows physical time-dependent boundary conditions to be formulated for the plasma jet expansion problem.

ACKNOWLEDGMENT

REFERENCES

[1] A. A. Artsimovich, S. Yu. Luk'ynov, I. P. Podgornyi, and S. A. Chuvatin, "Electrodynamic acceleration of the plasmoid," *Sov. Phys.-JETP*, vol. 6, p. 33, 1957.
[2] L. Aronowitz and D. P. Duchs, Eds., *Characteristics of the Pinch Discharge in a Pulsed Plasma Accelerator*. New York: Academic, 1963.
[3] A. M. Andrianov, A. I. Zemskov, V. V. Prut, and V. A. Khrabrov, "Pulsed discharges in dielectric chambers," *Sov. Phys. Tech. Phys.*, vol. 14, pp. 318–321, 1969.
[4] R. J. Vondra, K. Thomassen, and A. Solbes, "Analyzes of solid teflon pulsed plasma thruster," *J. Spacecraft*, vol. 7, pp. 1402–1406, 1970.
[5] W. J. Guman and P. E. Peko, "Solid-propellant pulsed plasma microthruster studies," *J. Spacecraft*, vol. 5, pp. 732–733, 1968.
[6] I. I. Beilis and V. E. Ostashov, "Model for a high-current discharge moving between parallel electrodes," *High Temp.*, vol. 27, pp. 817–821, 1989.
[7] R. J. Vondra, "The MIT Lincoln laboratory pulsed plasma thruster,", AIAA Paper 76-998, 1976.
[8] P. J. Turchi, "Directions for improving PPT performance," in *Proc. 25th Int. Elect. Propul. Conf.*, vol. 1, Worthington, OH, 1998, pp. 251–258.
[9] R. L. Burton and P. J. Turchi, "Pulsed plasma thruster," *J. Propul. Power*, vol. 14, pp. 716–735, 1998.
[10] R. A. Spores, R. B. Cohen, and M. Birkan, "The USAF electric propulsion program," in *Proc. 25th Int. Elect. Propul. Conf.*, vol. 1, Worthington, OH, 1998, p. 1.
[11] N. A. Gatsonis and X. Yin, "Axisymmetric DSMC/PIC simulation of quasineutral partially ionized jets,", AIAA Paper 97-2535, 1997.
[12] I. D. Boyd, M. Keidar, and W. McKeon, "Modeling of a pulsed plasma thruster from plasma generation to plume far field," presented at the 35th Joint Propul. Conf., Los Angeles, CA, June 1999. AIAA Paper 99-2300. J. Spacecraft Rockets, no. 3, 2000.
[13] R. L. Burton, B. K. Hilko, F. D. Witherspoon, and G. Jaafari, "Energy-mass coupling in high-pressure liquid-injected arcs," *IEEE Trans. Plasma Sci.*, vol. 19, pp. 340–349, 1991.
[14] N. N. Ogurtsova, I. V. Podmoshenskii, and P. N. Rogovtsev, "Calculation of the parameters of an optically densse plasma obtained by a discharge with an evaporating wall," *High Temp.*, vol. 9, pp. 430–436, 1971.
[15] P. Kovitya and J. J. Lowke, "Theoretical prediction of ablation stabilised arcs confined in cylindrical tubes," *J. Phys. D*, vol. 17, pp. 1197–1212, 1984.
[16] C. B. Ruchti and L. Niemeyer, "Ablation controlled arc," *IEEE Trans. Plasma Sci.*, vol. 14, pp. 423–434, 1986.
[17] R. L. Newman, "A kinetic treatment of ablation," *J. Spacecraft*, vol. 2, pp. 449–450, 1965.
[18] B. L. Clark, "An experimental and analytical investigation of Teflon ablation heat transfer parameters by the method of nonlimear estimation," Ph.D. dissertation, Cornell Univ., Ithaca, NY, 1971.
[19] V. V. Aleksandrov, N. V. Belan, N. P. Koslov, N. A. Mashtylev, G. A. Popov, and V. I. Khvesiyk, *Pulse Plasma Accelerators*, Kharkov: KHAI, 1983. (in Russian).
[20] H. R. Griem, *Plasma Spectroscopy*. New York: McGraw-Hill, 1964.
[21] A. I. Zemskov, V. V. Prut, and V. A. Khrabrov, "Pulsed discharge in dielectric chamber," *Sov. Phys. Tech. Phys.*, vol. 17, pp. 285–289, 1972.
[22] E. C. Whipple, "Potential of surface in space," *Rep. Prog. Phys.*, vol. 44, pp. 1197–1250, 1981.
[23] Yu. Raizer, *Gas Discharge Physics*, Berlin: Springer, 1991.
[24] G. I. Kozlov, V. A. Kuznetsov, and V. A. Masyukov, "Radiative losses by argon plasma and the emissive model of a continuos optical discharge," *Sov. Phys. JETP*, vol. 39, pp. 463–468, 1974.
[25] P. G. Mikellides and P. J. Turchi, "Modeling of late-time ablation in Teflon pulsed plasma thrusters,", AIAA Paper 96-2733, 1996.
[26] M. Keidar, I. D. Boyd, and I. I. Beilis, "Particulate interaction with plasma in a Teflon pulsed plasma thruster," *J. Prop. Power*. in press.
[27] S. Dushman, *Scientifi Foundations of Vacuum Technique*. New York: Wiley, 1962.
[28] P. Kovitya, "Thermodynamic and transport properties of ablated vapors of PTFE, alumina, perspex and PVC in the temperature range 5000–30000 K," *IEEE Trans. Plasma Sci.*, vol. 12, pp. 38–42, 1984.
[29] C. S. Schmahl and P. J. Turchi, "Development of equation-of-state and transport properties for molecular plasmas in pulsed plasma thrusters—Part I: A two-temperature equation of state for Teflon," in *Proc. Inter. Electr. Propul. Conf.*, 1997, pp. 781–788.
[30] A. V. Luikov, *Analytical Heat Diffusion Theory*. New York: Academic, 1968.
[31] S. S. Bushman, "Investigations of a coaxial pulsed plasma thruster," M.S. thesis, Univ. Illinois Urbana-Champaign, May 1999.
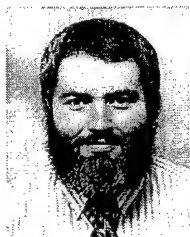
Michael Keidar (M'98) received the M.Sc. degree from the Kharkov Aviation Institute, Ukraine, in 1989, and the Ph.D. degree from Tel Aviv University, Israel, in 1997.

He was a Fulbright and Welch Postdoctoral Fellow at Lawrence Berkeley National Laboratory, Berkeley, CA, and a Research Associate at Cornell University, Ithaca, NY. Currently, he is a Research Fellow at The University of Michigan, Ann Arbor. His research interests include the plasma flow in a magnetic field, electrical discharges in vacuum interrupters and plasma thrusters, plasma-wall transition phenomena, dusty plasmas, and plasma thruster plumes. He has authored over 30 journal articles.

Dr. Keidar received a Scholarship Award by the IEEE Nuclear and Plasma Science Society in 1995.
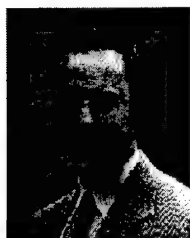
Iain D. Boyd received the B.S. degree in mathematics in 1985 and the Ph.D. degree in aeronautics and astronautics in 1988 from the University of Southampton, U.K.

He worked for four years as a contractor at NASA Ames Research Center, CA, in the area of rarefied gas dynamics. He was a faculty member in the Mechanical and Aerospace Engineering Department, Cornell University, Ithaca, NY, for six years, and recently joined the Department of Aerospace Engineering at The University of Michigan, Ann Arbor. His research interests include the development of physical models and numerical algorithms using particle methods with applications to a variety of nonequilibrium gas and plasma dynamic systems. He has authored over 60 journal articles.

Dr. Boyd is the recipient of the 1998 AIAA Lawrence Sperry Award and the 1997 AIAA Electric Propulsion Best Paper Award. He is an Associate Editor of the *Journal of Spacecraft and Rockets.*

Isak I. Beilis (M'97) received the M.Sc. degree from the Moscow Institute for Steel and Alloys, Russia, in 1966, the Ph.D. degree in 1973 and degree of Doctor of Phys. and Mathematical Sciences in 1990 from the Institute for High Temperatures (IVTAN) and Institute for High Current Electronics of the U.S.S.R. Academy of Science, Moscow.

From 1969 to 1991, he worked in the IVTAN, also holding a position of Visiting Scientist in the Institute of Mechanics of the Moscow Lomonosov University. Since January 1992, his investigations at the Faculty of Engineering at Tel Aviv University, Israel. His research interests include the electrical discharges in vacuum interrupters, MHD-generators, plasma accelerators, arc cathode and anode spots, vacuum arc plasma jet expansion in magnetic fields, plasma-wall transition (sheath and presheath), dusty plasma transport in ducts, nonstationary and nonequilibrium macroparticle charging phenomena, and processes in hot anode arcs. He was a Visiting Professor at the Max Plank Institute of Plasmaphysics, Berlin, in 1995 and the University of Minnesota, Minneapolis, in 1996 and 1998. He is coauthor of the books *MHD Energy Conversion. Physical and Technical Aspects* (Moscow: Nauka, 1982), and *Handbook of Vacuum Arc Science and Technology* (NJ: Noyes, 1995).

Modeling of a Pulsed Plasma Thruster from Plasma Generation to Plume Far Field

Iain D. Boyd[*] and Michael Keidar[†]
University of Michigan, Ann Arbor, Michigan 48103
and
William McKeon[‡]
Cornell University, Ithaca, New York 14853

Models are presented for a Teflon®-fed, pulsed plasma thruster from plasma generation to plume far field. A one-dimensional model using local thermodynamic equilibrium is developed to describe the plasma generation, Teflon ablation, and nozzle acceleration processes. A computer code that uses two different particle methods is employed to simulate the unsteady plasma plume expansion processes, including charge exchange collisions. Results are generated for a pulsed plasma thruster under development at the University of Illinois. General features of the plume reveal substantial differences in the expansion dynamics of the charged and neutral species. In addition, there is a noticeable difference between the behavior of the carbon and the fluorine ions. Direct comparisons are made between simulation results and experimentally measured data for electron number density and plasma potential. These comparisons indicate strengths and weaknesses of the models.

Introduction

PULSED plasma thrusters are receiving renewed attention because of their ability to produce small impulse bits with high reliability.[1] An accurate simulation of plumes from all electric propulsion devices is required for the assessment of spacecraft integration effects. For a pulsed plasma thruster (PPT) using solid Teflon® as a propellant, the primary integration concern is the deposition of highly condensible plume effluent on spacecraft surfaces.

The numerical investigation of PPT plumes presents many difficulties. The ablation process that leads to the acceleration of a high-density plasma is not well understood. The chemical composition of the flow exhausting from the thruster is not known. The plasma density is significantly higher than that produced by gridded ion thrusters and Hall thrusters. The neutral density at the exit places the flow in the near-continuum regime. Finally, as a result of the pulsed nature of the device, all flow processes are unsteady.

In this study, the focus is on a pulsed plasma thruster called PPT-4 that is under development at the University of Illinois.[2] The PPT-4 is unusual in that the thrust force is generated primarily by an electrothermal mechanism. In terms of modeling, this is a convenient place to start because difficulties with the modeling of the electromagnetic effects can be omitted.

Details of the PPT-4 thruster are first described. This paper reports on two modeling efforts for this device. The first is concerned with modeling the plasma generation, Teflon decomposition, and nozzle acceleration processes. A one-dimensional model is described. The main goal of this study is to provide time-varying boundary conditions for the subsequent computation of the PPT plume. The plume modeling based on particle methods is then described. Results concerning the general flow features of the plume are presented. In addition, direct comparisons are made between simulation and experiment for electron number density and plasma potential. These comparisons serve to partially validate the modeling and also indicate areas where further development is needed.

University of Illinois PPT-4

The thruster under consideration is being developed at the University of Illinois and is called the PPT-4. A schematic diagram is shown in Fig. 1. The PPT-4 has a coaxial configuration with a central anode that is 5 mm in diameter and an annular cathode that is 43 mm in diameter. The two electrodes are connected with a 30-deg half-angle nozzle. The Teflon is ablated from a cylindrical cavity with a diameter of 5 mm and a length of 3.2 mm that sits just in front of the central electrode. The measured mass ablation is 12 μg per pulse at 9 J of input energy. The pulse length is approximately 10 μs. The overall specific impulse has been measured as 1000 s. More details can be found in Ref. 2.

Modeling of Plasma Generation

Pulsed Discharge Model

In the PPT-4, plasma is generated in the Teflon cavity as a result of ionization of the Teflon ablation products. The main features of the discharge in the Teflon cavity are analogous to ablation controlled arcs.[3-5] During the pulse impulse, the plasma is heated by the joule heat and is cooled by radiation, energy losses caused by particle convection to the anode and dielectric, and ionization. This interaction of the plasma column with the walls of the cavity heats the walls rapidly. The temperature of the surface layer increases and reaches the critical temperature of decomposition. The principal mechanism of thermal degradation of the dielectric is the breaking of the bonds in the chain, which consumes the main portion of the energy transferred. As a result of heating, dissociation, and ionization of the products of decomposition, the electron density in the cavity increases. The pressure and temperature of the plasma in the cavity determine the plasma composition. In this section we briefly describe the model of the pulsed electrical discharge in the Teflon cavity. A more detailed description of the model can be found in Ref. 6.

A simplified model of the pulsed discharge in the dielectric cavity is based on the following assumptions: 1) all plasma parameters are uniform within the plasma column; that is, a diffuse type of discharge is assumed; 2) the plasma is quasineutral; and 3) the plasma column is in local thermodynamic equilibrium (LTE), and the electrons, ions, and neutrals establish a single equilibrium temperature. As a result of the foregoing considerations and assumptions, the
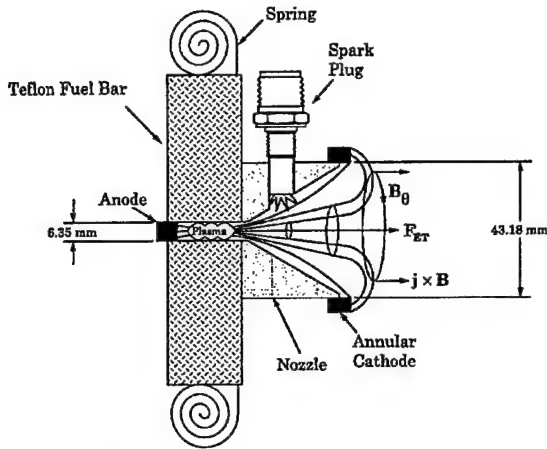
Fig. 1 Schematic diagram of the Illinois PPT-4.

following energy balance equation in the quasi-neutral plasma col-
umn can be written:

$$\frac{3}{2}n_e\frac{dT}{dt} = Q_j - Q_r - Q_d - Q_a \qquad (1)$$

where n_e is the electron density, T is the plasma temperature, Q_j is
the joule heat, Q_r is the radiative emission energy loss that depends
on plasma density and temperature, Q_d is the energy loss caused by
convection of electrons and ions to the dielectric that depends on the
plasma temperature and the potential drop in the electrostatic sheath
near the dielectric, and Q_a is the energy loss caused by electron
convection to the anode that depends on the anode sheath potential
drop.

The anode current is carried by electrons and controlled by the
potential drop in the anode sheath. The potential drop in the sheath
depends on the plasma and current density and may have spatial
variation. Assuming that the plasma column is uniform, generally,
the sheath is slightly negative in order to repel the excess of the
thermal electron current, so that the electron current to the anode
is equal to the circuit current. Similar physical reasons lead to the
appearance of the electrostatic sheath near the dielectric surface to
ensure a zero net current. The transient sheath formation near the
dielectric surface is determined by the dielectric permittivity. In the
considered range of electron density (10^{21}–10^{24} m^{-3}), the charac-
teristic charging time[7] is less than 10^{-10} s, which is much smaller
than the characteristic time of the discharge parameter changes.
Therefore we use a quasi-steady-state sheath model. Furthermore,
we assume that the plasma density is so high that the sheath thick-
ness (of the order of the Debye length) is much smaller than the
electron Larmor radius and thus the effect of the self-magnetic field
in the sheath can be neglected. As in the case of the anode sheath,
the sheath potential drop should be negative in order to repel the
excess of the thermal electron current, so that the electron current
is equal to the ion current.

In LTE, the composition of the plasma is found as a function of
the state of the plasma that is determined by the pressure and tem-
perature. The calculation of the composition of the plasma consists
of solving a set of Saha equations supplemented by a pressure bal-
ance, conservation of nuclei, and quasineutrality. It is assumed that
the plasma pressure is equal to the equilibrium vapor pressure based
on the temperature of the Teflon surface.[8] The Teflon surface tem-
perature is calculated by the solution of the heat transfer equation.
This equation is subject to the boundary conditions at the Teflon
surface accounting for heat flux from the plasma by radiation and
particle convection and heat losses caused by evaporation of the
surface. In the cavity, the plasma velocity changes from zero near
the anode up to a value equal to the local velocity of sound at the
cavity outlet. The considered plasma flow problem inside the cavity
is, in principle, two dimensional. However, in the main part of the
plasma bulk, the two-dimensional effect is small.[9] In the cavity, the

plasma velocity varies from zero near the anode up to the sound
speed at the cavity exit plane, and thus the plasma density should
decrease toward the cavity exit plane. However, if ablation is ap-
proximately uniform along the cavity, the plasma velocity increases
substantially only near the exit (at approximately 80% of the cavity
length, as shown in Ref. 9). A quasi-steady analysis[9] shows that, in
the plasma bulk, the velocity is approximately $(0.3\text{–}0.5)C_s$, where
C_s is the sound speed. Therefore the plasma velocity was used in
the model as a free parameter. It was found that the plasma veloc-
ity does not significantly affect the plasma density and temperature
distributions during the discharge pulse.

Plasma Acceleration in the Conical Nozzle

The electromagnetic thrust component of the PPT-4 is created
mainly near the thruster exit plane, where the azimuthal self-
magnetic field and the radial component of the discharge current
are maximal. However, the current pulse is essentially gone before
the main plasma cloud exits from the cavity. Thus, the main part of
the plasma generated in the cavity accelerates in the conical nozzle
by the gasdynamic mechanism. In this section we describe a quasi-
one-dimensional model of a continuum, single-fluid plasma flow in
the conical nozzle neglecting magnetic field effects.

We consider a quasi-neutral plasma in which the electrons and
ions behave as ideal gases. The plasma temperature is assumed to be
constant. This is based on the idea that the effects on the temperature
of gasdynamic expansion and plasma ohmic heating will almost
cancel. The temperatures obtained by using our approach (between
1 and 3 eV) are in good general agreement with values measured
experimentally in the plume.[2] The plasma flow is considered to be
sourceless, and plasma losses to the nozzle wall and wall evaporation
are neglected. Furthermore, we consider the situation in which all
properties vary only along the axial direction. The plasma jet cross
section $A(z)$ is determined by the nozzle geometry as follows:

$$A(z) = A_0[1 + (z/R_0)\tan\theta]^2 \qquad (2)$$

where A_0 is the initial cross section, R_0 is initial jet radius equal to
the cavity radius, and θ is the cone half-angle. Taking into account
these considerations, we find the equation for the plasma velocity
becomes

$$\frac{V^2 - C_s^2}{V}\frac{dV}{dz} = C_s^2\frac{2\tan\theta}{R_0}\frac{1}{1 + (z/R_0)\tan\theta} \qquad (3)$$

where V is the plasma jet axial velocity.

Time-Dependent Nozzle Exit Conditions

Here we present results of the calculation of the plasma parame-
ters at the exit plane of the PPT-4. To simulate the energy input dur-
ing the pulse, the experimental current waveform has been used.[2]
Linearization of the experimental current waveform causes some
perturbations in the results presented later. The calculations pre-
sented in this section correspond to the following PPT-4 design and
discharge parameters: cavity size $R_a = 3.15$ mm, $L = 8.3$ mm, noz-
zle half-angle $\theta = 30$ deg, current peak ~ 8 kA, and pulse duration
~ 10 μs.

During the discharge pulse, plasma is generated in the cavity as
a result of Teflon decomposition and then accelerates in the coni-
cal nozzle. The solution of the energy and mass balance equations
provides time dependencies of the plasma temperature and compo-
sition in the cavity. During the plasma flow in the nozzle, plasma
composition and temperature remain constant while plasma veloc-
ity increases starting from the sound speed at the cavity exit plane.
In the conical nozzle, plasma acceleration up to a Mach number of
4 is calculated.

The time evolution of the plasma component densities, tempera-
ture, and velocity are shown in Figs. 2a–2c. The chemical composi-
tion of the plasma is shown in Fig. 2a. One can see that all densities
peak at ~ 6 μs, which corresponds to the peak of the discharge cur-
rent. The fluorine (F) neutral density is larger than the carbon (C)
neutral density because Teflon has a composition of C_2F_4. However,
the difference between fluorine ion density and carbon ion density
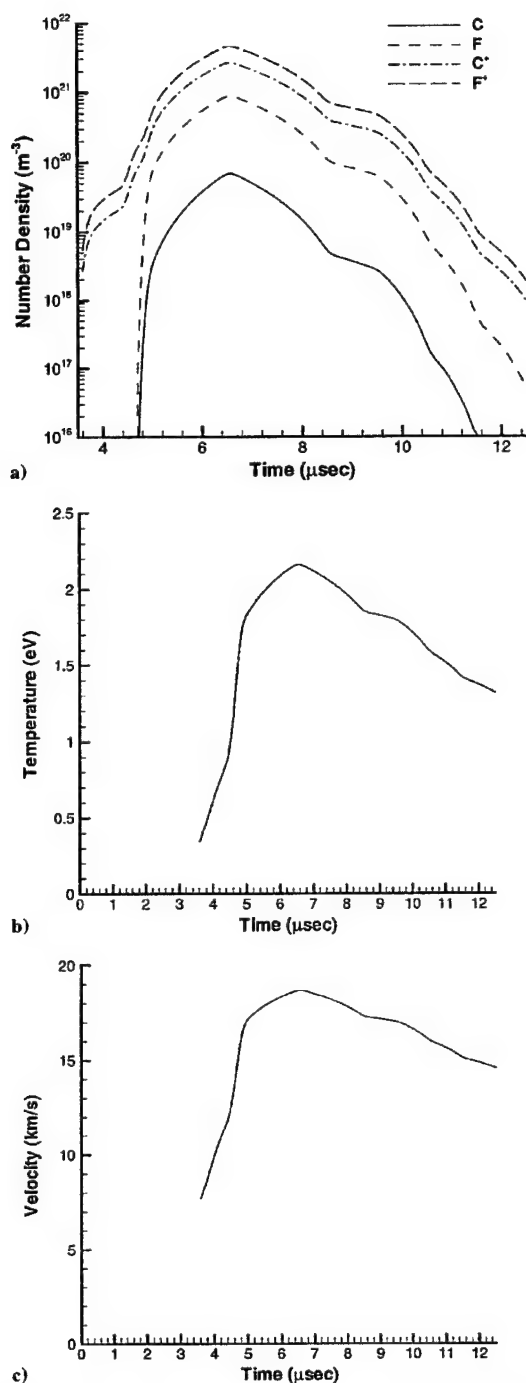is much smaller because carbon has a smaller ionization energy.

Fig. 2   Variations with time of a) species number densities, b) electron temperature, and c) velocity at the thruster exit plane.

(The first ionization energy of carbon is 11.3 eV, whereas fluorine has a corresponding ionization energy of 17.4 eV.) Initially, the plasma temperature sharply increases and peaks at ~2.3 eV. Toward the pulse end the plasma temperature decreases down to ~1.5 eV. These profiles are used as time-varying boundary conditions for the plasma plume simulations.

Plume Model

A computer model for PPT plumes has been proposed by Yin and Gatsonis.[10] A hybrid fluid–particle approach was employed.

In the present study, we employ a similar approach. Neutrals (C and F) and ions (C$^+$ and F$^+$) are modeled as particles. Particle collisions are computed by using the direct simulation Monte Carlo method (DSMC).[11] Both momentum exchange and charge exchange collisions are simulated. Momentum exchange cross sections use the model of Dalgarno et al.,[12] and the collision dynamics follows the normal DSMC procedures as described in Ref. 11. The charge exchange processes use the cross sections proposed by Sakabe and Izawa.[13] The computer code uses separate grids for the collision and plasma processes. The cells used for the collisions are sized according to the local mean free path, as is the usual case in DSMC computations. The experimental facility backpressure corresponds to a density of ~10^{18} m^{-3}. This is applied as an auxiliary condition with which particles from the thruster can collide.

Acceleration of the charged particles in self-consistent electric fields is simulated by using the particle-in-cell method (PIC).[14] The plasma potential ϕ is obtained by assuming charge neutrality to determine the electron number density from the total ion density. The electron number density n_e is then used in the Boltzmann relation to obtain the plasma potential:

$$\phi = T_e \, \ell n[n_e / n_{ref}(t)] \tag{4}$$

where the electron temperature T_e is in electron volts and n_{ref} is the electron number density at a reference point. This approach was used in our previous work on Hall thruster plumes.[15] In the case of the PPT, the reference point for the Boltzmann relation is taken as the thruster exit. It is assumed that the potential here is constant. The variation of electron number density at the thruster exit obtained in the plasma generation modeling is used to change the reference density as a function of time. A constant electron temperature of 2 eV is used in the Boltzmann relation throughout the computation. Because charge neutrality is assumed, the PIC cells do not have to be of the order of the Debye length. Instead they are chosen to be small enough to resolve in a reasonable way the gradients in the potential. The grids used in the computation are shown in Fig. 3. A single time step given by the reciprocal of the maximum plasma frequency is used throughout. All results are time dependent and are integrated over small intervals of time, which are of the order of 2×10^{-7} s.

The main difficulties in performing the computations of the PPT plume arise from the transient nature of the expansion. Because the flow conditions change as a function of time, the characteristic time and length scales of both collision and plasma phenomena continually change throughout the computational domain. In principle, the simulations should use grids that change with the local, transient flow conditions. In this first study, we have adopted the simpler approach of employing grids that should capture most of the physics most of the time. Another numerical problem related to the transient flow conditions is the fact that there are often regions of the flow where the number of simulated particles is very small. This occurs at the leading edge of the forward expansion at early times and at the trailing edge of the expansion at late times. The low number of
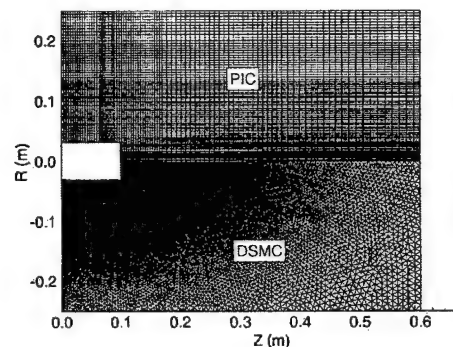

Fig. 3   Computer grids employed in the plume particle simulation.

particles in these regions leads to significant scatter in the simulation results in these regions. In the early stages of this investigation we experimented with the use of very large computations involving many millions of particles performed on parallel computers. This approach only moved the statistical scatter to lower density portions of the flowfield. As shown in the Results section, the density varies by several orders of magnitude across the jet expansions and so the statistical problem is unavoidable. It should be noted, however, that most of the results presented are unaffected by the statistical fluctuations.

Results

Particles are introduced into the flowfield through the nozzle exit plane by using the output from the plasma generation model (Fig. 2). A uniform radial profile of properties is assumed across the exit plane except that a conical distribution of flow angle is used. Ions and neutrals are assumed to have the same velocity and the same temperature. This assumption is based on the fact that the number densities are relatively high so that the frequency of charge exchange collisions inside the nozzle is high. Simulations are performed with and without the facility backpressure. It is found that the results are almost identical, indicating that, unlike some other electric propulsion devices such as Hall thrusters and ion thrusters, the PPT plume is not affected by the chamber background gas.

To illustrate some of the basic dynamics of the time evolution of the PPT plume expansion processes, Figs. 4a–4d show contours of plasma potential at four different times. In these results it is clear that the plasma potential expands very rapidly about a source that moves with the plume. The gradients in potential are such as to create

electric fields that will accelerate ions: 1) in the forward direction at the front of the expansion; 2) in the backward direction at the rear end of the expansion, which results in backflow of ions behind the thruster; and 3) in the radial direction away from the axis. Of course, these forces act only on the charged particles; thus in the results that follow, it is expected that the ions will behave quite differently from the neutral atoms.

To demonstrate the different dynamics of ions and neutrals, Figs. 5a–5d show the variation of all species densities along the axis at four different times. As shown in Fig. 5a, at 10 μs after ignition, the species densities follow the profiles shown in Fig. 2a. The ions are in a larger concentration than the neutral atoms, and fluorine is more abundant than carbon. The relative concentrations of the species do not change dramatically at later times as shown in Figs. 5b–5d. However, the shape of the profiles reveals that the charged species are spread over a larger axial region than the neutrals. The neutral atoms expand as a relatively compact puff of gas, whereas the ions are spread out both ahead of and behind the center of expansion as a result of electric field effects.

Comparisons between the computation and experimental measurement[2] of the electron number density along the axis are shown at three different locations in Figs. 6a–6c. Because charge neutrality is assumed, the computational results are obtained by summing the carbon and fluorine ion densities. When a comparison is made with the experimental data, it is expected that the data collected over the first 10 μs after ignition cannot be used. This is partly because of the noise introduced into the measurements by the operation of the spark plug igniter. In addition, there is no attempt in our modeling to simulate the behavior of the ignition plasma. With
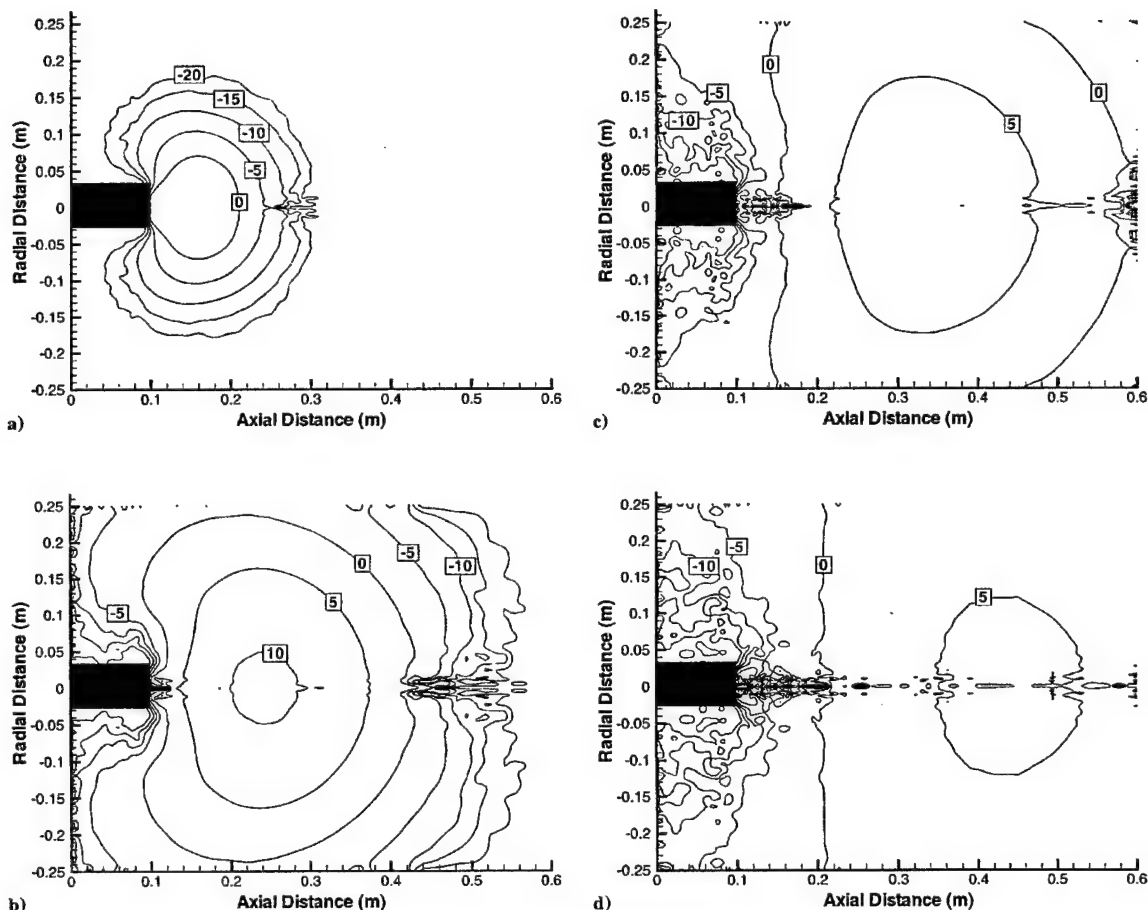

Fig. 4   Contours of plasma potential in volts: a) 10, b) 15, c) 20, and d) 25 θ s after ignition.
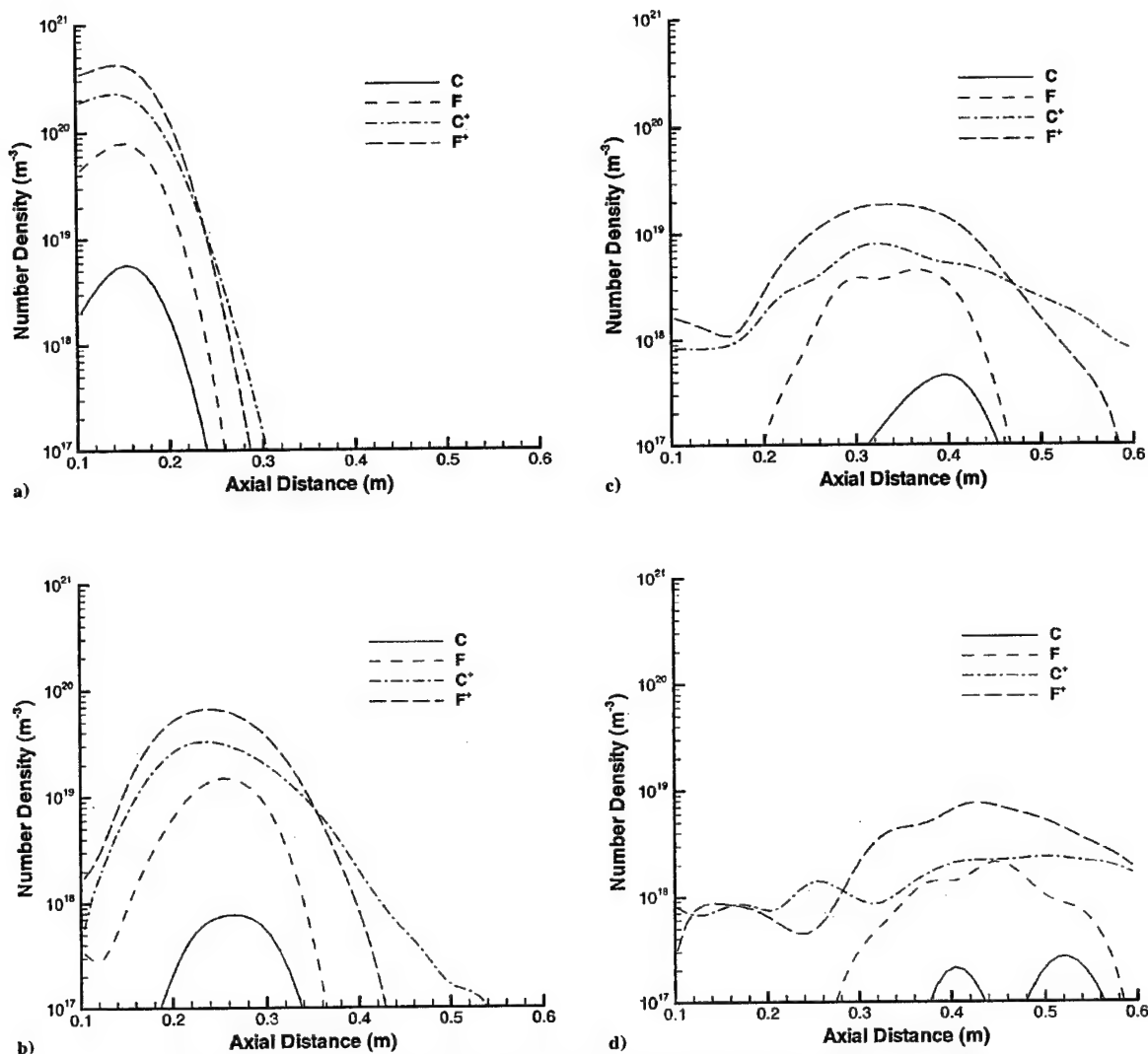
Fig. 5 Profiles of species number density along the axis: a) 10, b) 15, c) 20, and d) 25 θ s after ignition.

this in mind, we can make two clear observations about the comparisons shown in Fig. 6. The first is that there is a tendency in the simulations to overpredict the density peak. However, it should be noted that the experimental uncertainty is ±50% and the predicted peaks lie within this range. There also appears to be some indication of saturation in the experimental measurements. It is surprising to see such a small reduction in the peak density measured at 10 and 14 cm from the thruster. The second clear conclusion is that the simulation underpredicts the densities at both early and late times.

A comparison of the simulation results with experimental data shows that the main plasma plume features are captured, although the simulation underestimates the densities at long times. The underprediction of the plasma density at long times is a result of the basic assumption of the plasma generation model in considering the plasma to be uniform in the cavity. This approach means that the plasma properties are described by average plasma parameters. Thus, this model predicts that the plasma will leave the cavity after the pulse end in a time that is short compared with the pulse duration. In general, however, the problem is two dimensional, with plasma velocity and density variation in the radial and axial directions. The plasma velocity varies from zero near the central electrode up to the

sound speed at the cavity exit plane. After the pulse ends, there is a substantial reduction in the ablation rate and the plasma density in the cavity will decrease. Plasma density temporal decay in this case will be much slower than that in the present model. In the future, this effect will be included in our model by considering spatial variation in the cavity properties.

To predict the chemical composition of the plasma, the present model uses the Saha equation assuming local thermodynamic equilibrium in the plasma column. However, LTE may be established only in relatively dense plasmas with an electron number density greater than 10^{22} m^{-3} for a time period larger than the characteristic relaxation time for ionization and recombination in the plasma (of the order of 10^{-7} s; Ref. 16). Calculations show that during the main part of the pulse, these requirements are fulfilled. Toward the pulse end, however, the plasma density significantly decreases and the relaxation time becomes comparable with the pulse duration. Thus, toward the pulse end, the LTE approach predicts a plasma ionization degree that is much higher than it should be in the real situation.
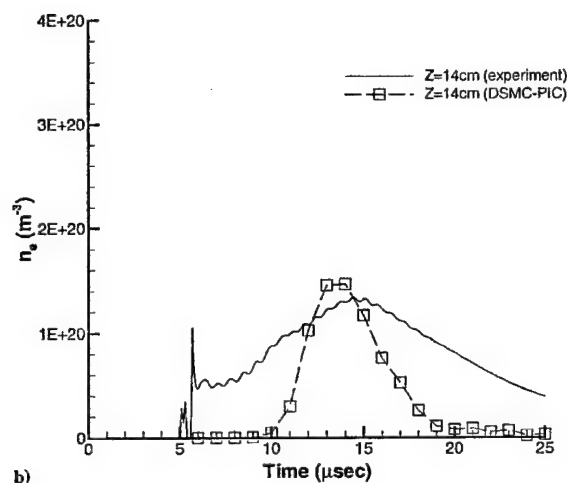
In Figs. 7a–7c a comparison is made between measurements and computations for the plasma potential on the axis at the same three
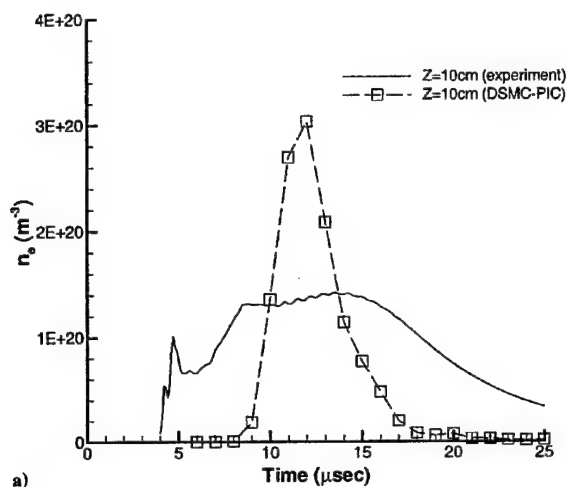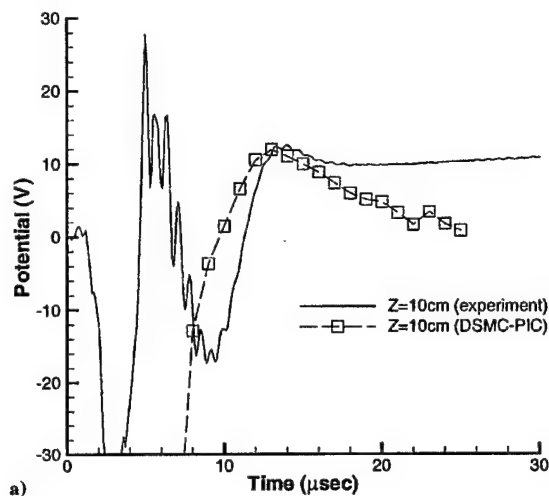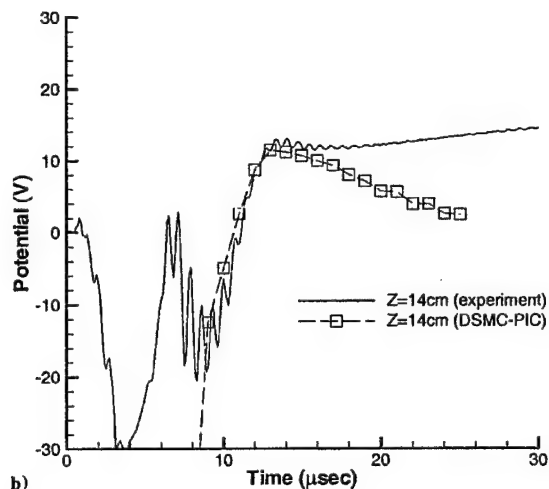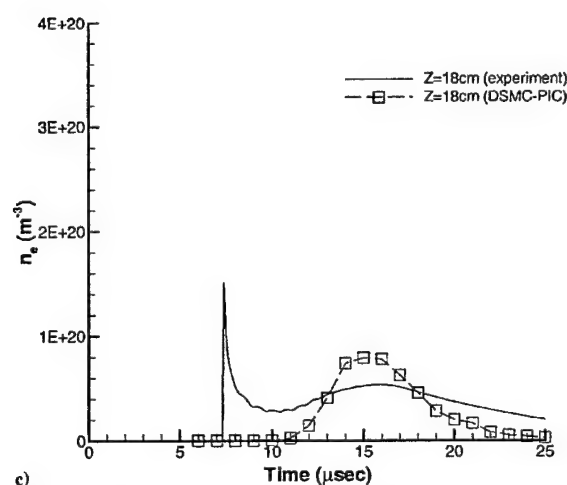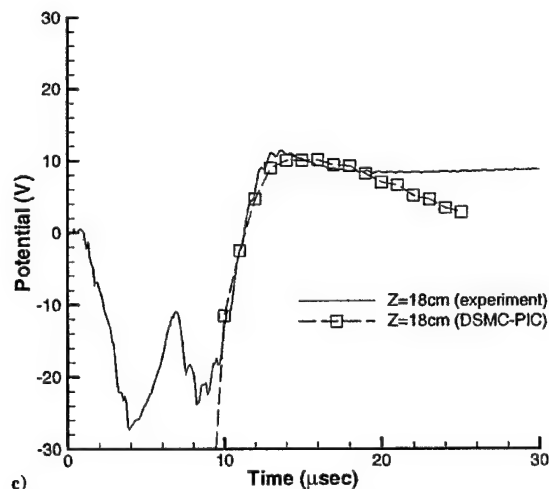
Fig. 6   Profiles of electron number density on the axis: a) 10, b) 14, and c) 18 cm from the thruster.

Fig. 7   Profiles of plasma potential on the axis: a) 10, b) 14, and c) 18 cm from the thruster.

locations as considered in Fig. 6. If we again ignore the first 10 μs, we can see that the initial rise and the actual peak of the potential data at all three locations is well predicted by the simulation. Also, consistent with the electron number density comparisons, the simulations show a more rapid decay in potential at long times after ignition. Overall, the comparisons with the experimental data shown in Figs. 6 and 7 indicate that the modeling has achieved a reasonable level of success.

As mentioned earlier, the primary reason for performing plume computations of the PPT is to assess possible spacecraft interaction effects. With this in mind, we present in Figs. 8 and 9 mass flux results as a function of time from the simulations in the radial planes at 50 cm forward of the thruster exit and above the thruster exit, respectively. The latter plane is chosen to assess the potential backflow problem. The forward contamination problem could occur if PPTs are employed on closely spaced spacecraft flying in formation. Figure 8 indicates that the mass flux at any plane changes dramatically as a function of time. As shown in Fig. 8a, the earliest flux consists of the fastest ions that are accelerated electrostatically ahead of the neutrals. Because the charge-to-mass ratio of carbon is about 50% larger than that for fluorine, it is the carbon ions that are the

first species to impact a surface forward of the thruster. Figure 8b indicates that any significant flux of neutral atoms is delayed by ~5 μs in reaching the surface and even then the flux magnitude is ~2 orders of magnitude below that of the ions. At later times, the radial acceleration of ions leads to their relative magnitudes of mass flux becoming comparable with that of fluorine atoms. The mass flux of carbon atoms remains at a lower level up until 35 μs.

The backflow contamination issue is demonstrated in Fig. 9, and this phenomenon would be of concern on any spacecraft using PPTs. Relative to ion thrusters and Hall thrusters, the potential for backflow with PPTs is significantly higher. This occurs because the carbon and fluorine ions are significantly more mobile than xenon and because the neutral and ion densities are orders of magnitude higher for the PPT, leading to increased collisional scattering. In the simulations, almost no backflow of neutral atoms is predicted. The peak mass flux occurs soon after ignition as shown in Fig. 9a, and the maximum level is only 1 order of magnitude below the maximum found in Fig. 8 for the forward fluxes. Again because of their increased mobility, carbon ions dominate the backflow flux. At later times, it can be seen that the mass flux decreases dramatically.
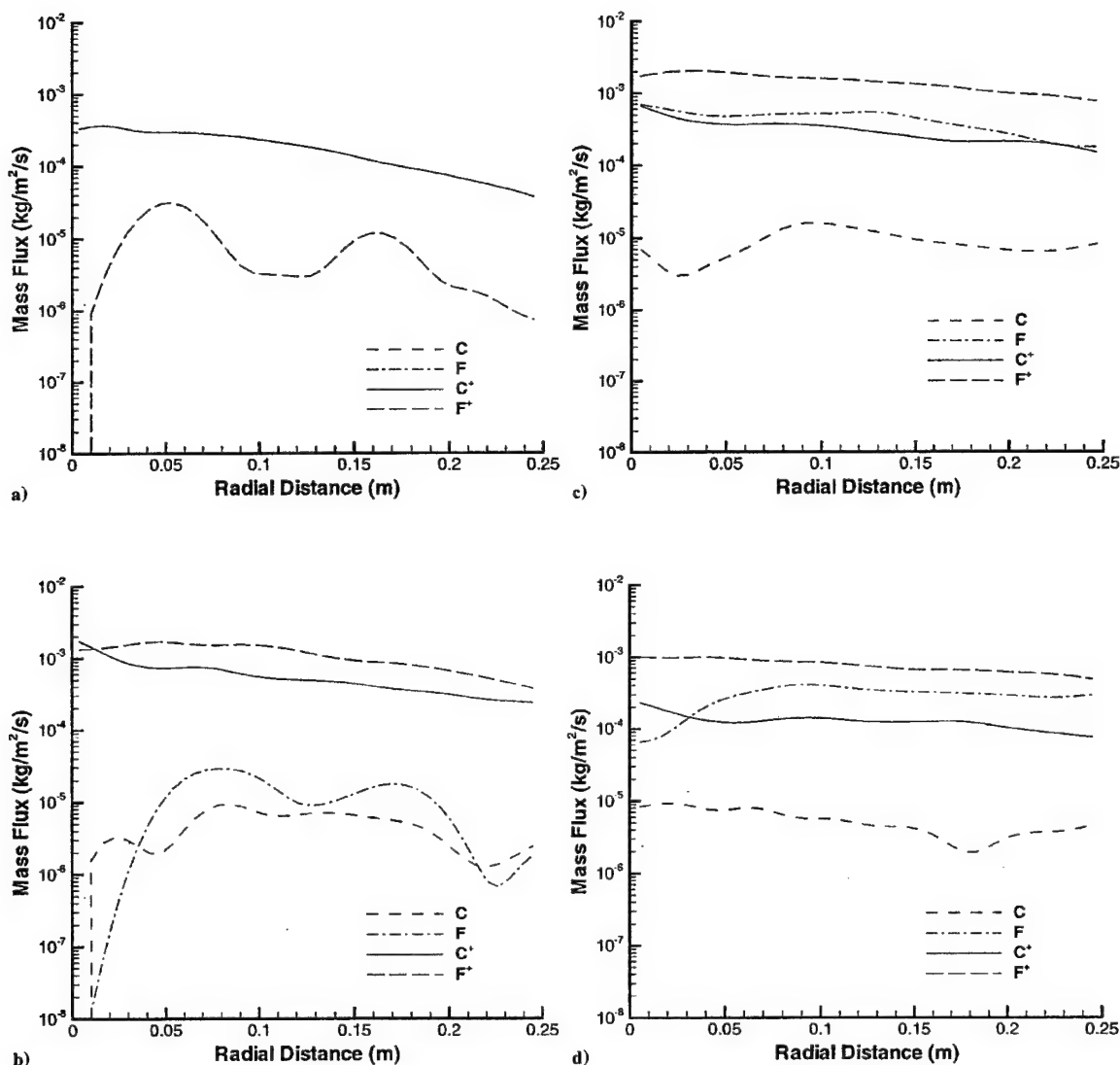

Fig. 8   Forward flow mass flux in the plane at 50 cm from the thruster exit: a) 20, b) 25, c) 30, and d) 35 θ s after ignition.
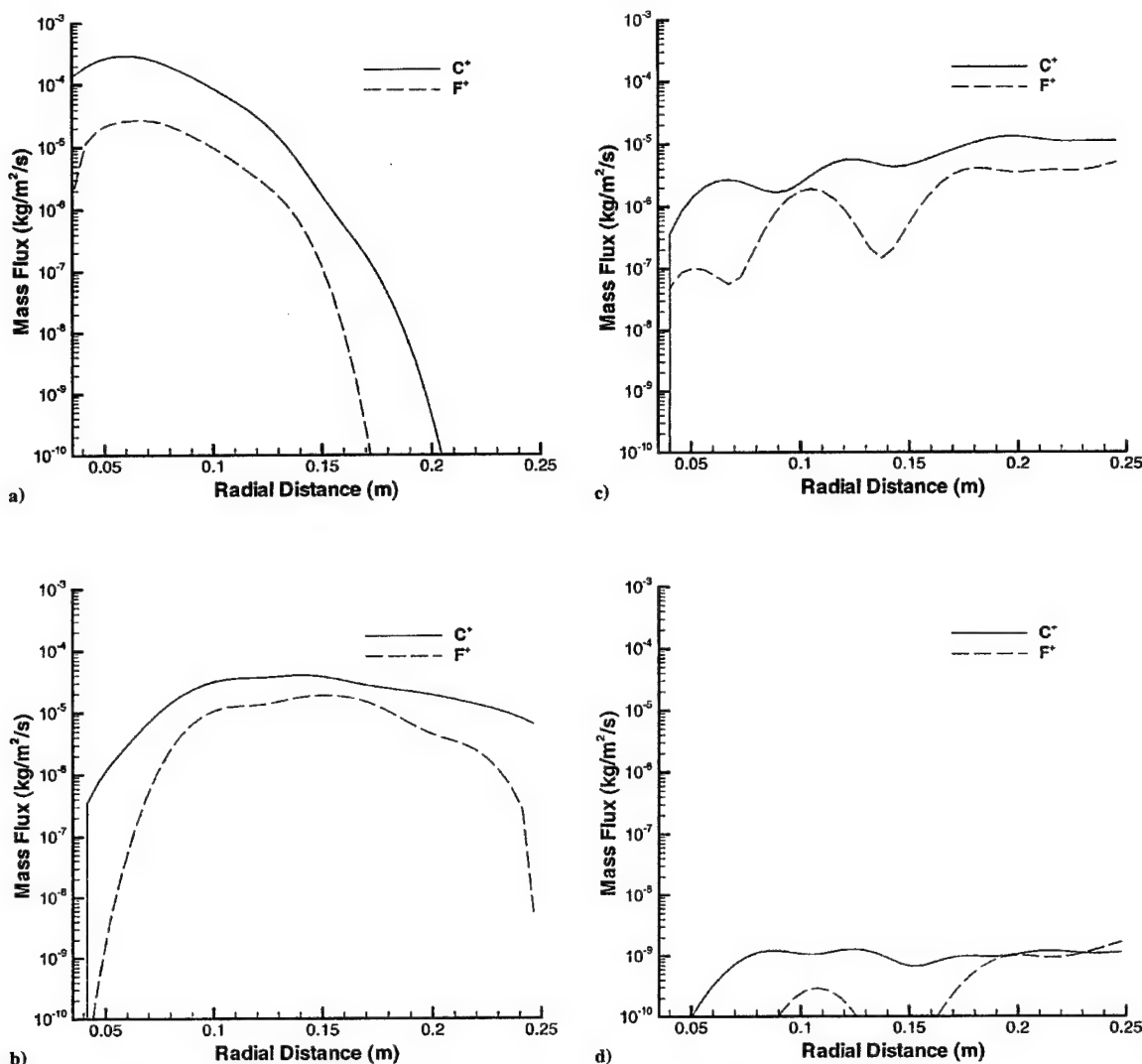
Fig. 9 Backflow mass flux in the plane above the thruster exit: a) 10, b) 15, c) 20, and d) 25 θ s after ignition.

Conclusions

A model has been developed to describe the plasma processes of a Teflon-fed pulsed plasma thruster from plasma generation to plume far field. The device considered was the PPT-4, which is being developed at the University of Illinois. From the modeling standpoint, this is an interesting thruster, as the acceleration is generated primarily by electrothermal effects.

The plasma generation, Teflon ablation, and nozzle expansion were modeled by using a one-dimensional approach. Local thermodynamic equilibrium was used to compute the chemical composition. A quasi-steady assumption was made to compute the nozzle flow. The time-dependent properties computed at the nozzle exit were used as boundary conditions for a separate plume computation.

The plume computation used a combination of the PIC and DSMC method to compute the plasma and collision phenomena in the expanding plume. The computations of plasma potential indicated that the ions are accelerated ahead of the expanding plume, radially away from the axis, and backward behind the thruster. It was found that, as a result of electric field effects, the dynamics of the ions and that of the atoms in the plume were substantially different. In addition, because of a relatively large difference in the charge-to-mass ratio, the dynamics of the carbon and that of the fluorine ions were

also perceptibly different. It was found that the primary source of backflow contamination from the thruster was carbon ions. The forward contamination was found to be time dependent, with an initial flux of ions followed by a later flux of neutral atoms.

Comparisons were made between the computations and experimental measurements taken at the University of Illinois for the plasma potential and electron number density. In general, the agreement between the data sets was very good. It was found that, at late times, the computations predicted a more rapid decay in both potential and electron number density in comparison with the measured data. This suggested improvements in the plasma generation model that will be investigated further. The good agreement obtained between predictions and measurements provides confidence in the overall modeling approach used in this study.

Acknowledgments

References

[1]Burton, R. L., and Turchi, P. J., "Pulsed Plasma Thruster," *Journal of Propulsion and Power*, Vol. 14, No. 5, 1998, pp. 716–735.

[2]Bushman, S. S., "Investigations of a Coaxial Pulsed Plasma Thruster," M.S. Thesis, Univ. of Illinois, Urbana, IL, 1999.

[3]Ogurtsova, N. N., Podmoshenskii, I. V., and Rogovtsev, P. N., "Calculation of the Parameters of an Optically Dense Plasma Obtained by a Discharge with an Evaporating Wall," *High Temperature*, Vol. 9, 1971, pp. 430–436.

[4]Kovatia, P., and Lowke, J. J., "Theoretical Prediction of Ablation Stabilised Arcs Confined in Cylindrical Tubes," *Journal of Physics D: Applied Physics*, Vol. 17, 1984, pp. 1197–1212.

[5]Ruchti, C. B., and Niemeyer, L., "Ablation Controlled Arc," *IEEE Transactions in Plasma Science*, Vol. 14, No. 4, 1986, pp. 423–434.

[6]Keidar, M., Boyd, I. D., and Beilis, I. I., "Electrical Discharge in the Teflon Cavity of a Co-Axial Pulsed Plasma Thruster," *IEEE Transactions in Plasma Science* (to be published); also International Electric Propulsion Conf., IEPC Paper 99-214, Oct. 1999.

[7]Whipple, E. C., "Potential of Surface in Space," *Report of Progress in Physics*, Vol. 44, 1981, pp. 1197–1250.

[8]Turchi, P. J., "Directions for Improving PPT Performance," International Electric Propulsion Conf., IEPC Paper 97-038, Sept. 1997.

[9]Keidar, M., Boyd, I. D., and Beilis, I. I., "Particulate Interaction with Plasma in a Teflon Pulsed Plasma Thruster," *Journal of Propulsion and Power* (to be published); also International Electric Propulsion Conf., IEPC Paper 99-213, Oct. 1999.

[10]Yin, X., and Gatsonis, N. A., "Numerical Investigation of Pulsed Plasma Thruster Plumes," International Electric Propulsion Conf., IEPC Paper 97-036, Sept. 1997.

[11]Bird, G. A., *Molecular Gas Dynamics and the Direct Simulation of Gas Flows*, Oxford Univ. Press, New York, 1994.

[12]Dalgarno, A., McDowell, M. R. C., and Williams, A., "The Mobilities of Ions in Unlike Gases," *Proceedings of the Royal Society of London*, Vol. 250, April 1958, pp. 411–425.

[13]Sakabe, S., and Izawa, Y., "Simple Formula for the Cross Sections of Resonant Charge Transfer Between Atoms and Their Ions at Low Impact Velocity," *Physical Review A: General Physics*, Vol. 45, No. 3, 1992, pp. 2086–2089.

[14]Birdsall, C. K., and Langdon, A. B., *Plasma Physics Via Computer Simulation*, Adam Hilger, Bristol, England, U.K., 1991.

[15]VanGilder, D. B., Boyd, I. D., and Keidar, M., "Particle Simulations of a Hall Thruster Plume," *Journal of Spacecraft and Rockets*, Vol. 37, No. 1, 2000, pp. 129–136; also AIAA Paper 98-3797, July 1998.

[16]Griem, H. R., *Plasma Spectroscopy*, McGraw–Hill, New York, 1964.

R. G. Wilmoth
Associate Editor

DEVICE AND PLUME MODEL OF AN ELECTROTHERMAL

PULSED PLASMA THRUSTER

Michael Keidar[*] and Iain D. Boyd[♦]

University of Michigan, Ann Arbor MI 48109

Abstract

Progress in combined device/plume modeling is presented for a Teflon-fed, pulsed plasma thruster from plasma generation to the plume far field. In this work we apply a one-dimensional unsteady model for the plasma generation and acceleration process. A new kinetic ablation algorithm is employed to calculate the Teflon ablation rate as a function of plasma parameters. A near cathode sheath model is included to calculate the plasma potential at the thruster exit plane. Results are compared with data for the electrothermal device, PPT-4. Performance characteristics of the PPT such as mass ablation and thrust impulse are calculated. Predicted plasma properties, thruster performance and plasma parameter distribution in the plume are found to be in agreement with available experimental data.

Introduction

Pulsed plasma thrusters (PPT's) have combined advantages of system simplicity, high reliability, low average electric power requirement and high specific impulse[1]. The PPT is considered as an attractive propulsion option for orbit insertion, drag makeup and attitude control of small satellites. PPT's, however, have very poor performance characteristics and an overall efficiency at the level of about 10%[2]. To improve the PPT performance several directions are being considered[3]. Accurate simulation of these devices and plumes is required for the design of PPT's with improved performances and for assessment of spacecraft integration effects.

---

[*] Research Scientist. Department of Aerospace Engineering, Member of AIAA

[♦] Associate Professor, Department of Aerospace Engineering, Senior Member of AIAA

1

In the present study we concentrate on the pulsed plasma thruster called PPT-4 that was developed recently at the University of Illinois[4]. This is an electrothermal device that derives most of its acceleration from the electrothermal or gasdynamic mechanism. This thruster is axially symmetric and a discharge occurs between the annular cathode at the thruster exit plane and the circular anode located at the far end of a cylindrical cavity made of Teflon. The plasma generated inside this cavity is accelerated in a diverging nozzle that is attached to the downstream end of the cavity. The device has a pulse length of about 10 μs, and the overall specific impulse was measured to be 850 s.

In a series of previous papers, we describe our efforts to model various aspects of this electrothermal PPT. In Ref. 5, a model of the Teflon ablation and plasma discharge processes is described. The model was calibrated against mass ablation data from the PPT-4. In Ref.6, the charging, heat and flow effects associated with large Teflon particulates in the plasma jet of the electrothermal PPT were considered. Here it was predicted that the small macro-particles are expected to decompose within the plasma jet. Finally, in Ref. 7, the results obtained in Ref. 5, at the thruster nozzle exit were used as boundary conditions to perform a particle-based PIC-DSMC computation of the electrothermal PPT plume. A significant conclusion from Ref. 7 was that almost all of the back-flow to the spacecraft from this device arises from carbon ions due to their high mobility.

The main physical processes in this type of PPT occur in the Teflon cavity. Rapid heating of a thin dielectric surface layer leads to decomposition of the material of the wall. As a result of heating, decomposition and partial ionization of the decomposition products, the total number of particles increases in the cavity. The problem of the ablated controlled discharge has a general interest since it can be used for various applications[8,9,10]. In these devices, the discharge energy is principally dissipated by ablation of wall material, which then forms the main component of the discharge plasma. The ablated vapor increases the pressure within the capillary and the plasma is expelled through the exit. Previously, discharge evolution in the PPT-4 Teflon cavity was studied by Keidar et al[11] assuming uniform plasma parameters. However, further understanding of the physical processes involved requires more detailed analyses including spatial variation of

the plasma parameter distribution along the cavity and a more sophisticated ablation model. The present model of the capillary discharge employs a recently developed ablation model[12]. These changes allow us to provide more accurate boundary conditions for the plume simulation.

The capillary discharge model

The model presented here describes the physics of the plasma generation and acceleration in a Teflon cavity for a pulsed electrical discharge as shown in Fig. 1. The main features of the model of the electrical discharge in the dielectric cavity include Joule heating of the plasma, heat transfer to the dielectric, Teflon ablation and electrothermal acceleration of the plasma up to the sound speed at the cavity exit. Mechanisms of energy transfer from the plasma column to the wall of the Teflon cavity includes heat transfer by particle convection and by radiation. The Teflon ablation is based on a recently developed kinetic ablation model[12]. It is assumed that all parameters vary in the axial direction x (see Fig. 1). Since the axial pressure and velocity gradients are much greater than the radial gradients we assume that radial variation of plasma temperature, pressure and velocity are neglegible[13],[14]. The axial component of the mass and momentum conservation equations read:

$$\partial\rho/\partial t + \partial(\rho V) = 2\Gamma(t,x)/R_a \quad\text{.. (1)}$$

$$\partial V/\partial t + V\partial V/\partial x = -\partial P/\partial x \quad\text{..(2)}$$

where ρ is the plasma density, P is the pressure, V is the plasma velocity and $\Gamma(t,x)$ is the ablation rate. The energy balance equation can be written in the form:

$$\frac{3}{2}n_e\,(\partial T/\partial t + V_z\partial T/\partial z) = Q_J - Q_r - Q_F \quad\text{..(3)}$$

where Q_J is the Joule heat, Q_r is the radiation heat and Q_F is the heat associated with particle fluxes. This equation depends on the coordinate along the cavity. However, our estimation and

previous calculations show[14] that the arc temperature varies only slightly with axial position and therefore we further assume $\partial T/\partial z=0$. The Teflon surface temperature is calculated from the heat transfer equation with boundary conditions that take into account vaporization heat and conductivity. The solution of this equation is considered for two limiting cases of substantial and small ablation rate very similar to that described in Ref. 11. For known pressure and electron temperature one can calculate the chemical plasma composition assuming LTE[11,15,16]. The Saha equations are supplemented by the conservation of nuclei and quasi-neutrality.

Electrostatic sheaths

The electrostatic sheath near the cathode provides the current continuity from the cathode to the plasma bulk as shown in Fig. 1. We assume that the cathode emission plays a small role in the current balance. The total current density in the sheath consists of electron J_e and ion J_i current densities:

$$J = J_i + J_e \dotfill (4)$$

In the case of a planar sheath in front of the cathode (the Debye radius is much less than the cathode length) J_i is determined by the Bohm relation:

$$J_i = 0.4en(kT_e/m_i) \dotfill (5)$$

where n is the plasma density at the plasma-sheath interface (see Fig. 1). The electron current is due to high energy electrons that penetrate the electrostatic barrier:

$$J_e = \frac{1}{4} en(8kT_e/m_e)\exp(-e\Delta\phi/kT_e) \dotfill (6)$$

where $\Delta\phi$ is the potential drop across the near-cathode sheath. For given current density one can calculate the potential drop:

$$\Delta\phi = T_e \ln((m_e/m_i)^{0.5} - J/en(kT_e/m_e)) \dotfill (7)$$

One can see that the potential drop depends upon current density, plasma density and electron temperature.

In the cavity near the Teflon surface, the electrostatic sheath potential drop is negative in order to repel the excess thermal electrons, so that the electron current J_e is equal to the ion current J_i. It was concluded previously that during the discharge pulse, a quasi-steady sheath structure is formed and that under typical PPT conditions this sheath is unmagnetized in the self-magnetic field generated during the pulse[11]. Under the conditions mentioned above, the potential drop in the sheath is calculated as:

$$U_d = -T \ln (J_{eth}/J_i) \dotfill (8)$$

Where J_{eth} is the random electron current density and J_i is the ion current density also determined by the Bohm condition.

Ablation model

The ablation model employed here is based on a kinetic model of the Knudsen layer near the ablated surface, which was analyzed using the distribution function moment method[17,18,19]. This method employs an approximation of the distribution function within the non-equilibrium Knudsen layer as a sum of the distribution functions before and after this layer with a coordinate dependent coefficient. In our problem of evaporation, it is only important to know the parameters on the boundaries and not their variation between the boundaries. This means that the problem is reduced to the integration of the conservation equations of mass, momentum and energy:

$$\int V_x f(V) \, dV = const$$
$$\int V_x^2 f(V) dV = const \dotfill (9)$$
$$\int V_x V^2 f(V) dV = const$$

After integration of equation (9) we obtain a set of equations in which parameters at the external boundary of the Knudsen layer depend upon velocity at the Knudsen layer edge. Applying mass and momentum conservation between the edges of the hydrodynamic layer, one can find the velocity at the outer boundary at the Knudsen layer. Velocity and density at the outer boundary of

5

the Knudsen layer determine the ablation rate. The system of equations is closed if the equilibrium vapor pressure can be specified. In the case of Teflon, the equilibrium pressure formula is used[1]:

$$P = P_c \exp(-T_c/T_o) \dots\dots\dots\dots\dots\dots\dots\dots\dots\dots\dots\dots\dots\dots\dots\dots\dots\dots\dots\dots(10)$$

where P is the equilibrium pressure, P_c and T_c are the characteristic pressure and temperature, respectively.

Nozzle and Plume models

The plasma flow through the conical nozzle is modeled by a quasi-one-dimensional continuum approach similar to that used previously (Ref. 7). We have assumed that the main part of the plasma generated in the cavity accelerates in the nozzle by the gasdynamic mechanism. We have considered the quasi-neutral plasma where ions and electrons are assumed to be ideal gases. This model also relies on the assumption that the flow is sourceless and plasma losses to the wall and wall evaporation are small and can be neglected.

The plume model is based on a hybrid fluid-particle approach similar to that used previously (Refs. 7, 20). In this model, the neutrals and ions are modeled as particles while electrons are treated as a fluid. Elastic (momentum transfer) and non-elastic (charge exchange) collisions are included in the model. The particle collisions are calculated using the direct simulation Monte Carlo (DSMC) method[21]. Momentum exchange cross sections use the model of Dalgarno et al.[22], while charge exchange processes use the cross sections proposed by Sakabe and Izawa[23]. Acceleration of the charged particles in the self-consistent electric fields is computed using Particle-In-Cell method (PIC)[24]. We have assumed quasi-neutrality that allows determination of the electron density. The plasma potential with respect to the thruster exit plane is calculated using the Boltzmann relation. The plasma potential at the thruster exit plane with respect to the cathode varies with time and is calculated using the near-cathode sheath model. The grids employed in this computation are similar to those used previously (Ref.7).

Results

In this section we present results of the calculation of the plasma parameter temporary and spatial variation in the Teflon cavity of the PPT-4 and also plume flowfield based on the boundary conditions provided by the device model. In addition, some thruster performance characteristics (thrust impulse and ablation mass) are calculated and compared with available experimental data. In this paper we also show how the improved thruster model and boundary conditions at the thruster exit plane affect the plume simulation.

Firstly, we present results for the thruster device modeling. These results later will be employed as boundary conditions for the plume simulation. All results are presented for PPT-4 with the following geometry and discharge parameters: anode radius R_a=3 mm and cavity length L=8.3 mm, current peak of about 8 kA and pulse duration of about 10 μs (Refs. 4, 25).

To illustrate the effect of the new ablation model on the ablation rate calculation, the trajectory of the ablation rate in the plasma density - Teflon surface temperature plane during the PPT-4 pulse is shown in Fig. 2. One can see that the ablation rate peaks at about 110 kg/m^{2}s at 3 μs and then rapidly decreases. It should be noted that in the experiment the average ablation rate was estimated to be about 30 kg/m^{2}s (Ref. 4).

The time evolution of the temperature and ionization degree (at the exit plane, x=L) is shown in Fig. 3. It can be seen that the electron temperature initially increases rapidly and peaks at about 3 eV and then decreases to 1 eV toward the pulse end. The model predicts that initially plasma in the cavity is strongly ionized while after about 3 μs the ionization degree decays substantially.

To demonstrate the different ion and neutral species temporal and spatial variation, their distributions are shown in Fig. 4. Both ion species peak at early times (about 3μs) while neutral species peak later. The relative concentration of the species changes along the cavity length and also during the discharge pulse.

The spatial and temporal distribution of the Teflon surface temperature is shown in Fig. 5. The temperature sharply increases during the first 2 μs of the discharge pulse and peaks at about 640 K. One can see that the temperature varies only slightly along the cavity.

To illustrate the ability of the model to predict some thruster performance characteristics, we calculate the thrust impulse bit and ablation mass per pulse as a function of cavity geometry and compare with experimental data. The gasdynamic thrust impulse is generated due to the pressure force on the anode. We integrate the pressure during the discharge to calculate the thrust impulse bit. In the case of PPT-4 nozzle with the area ratio of about 100, the nozzle may increase the thrust by a factor of 1.5 (Ref. 26). The thrust impulse bit dependence on the cavity length is shown in Fig. 6. One can see that it increases by a factor of 2.5 when L increases from 3 mm up to 25 mm. A similar trend was also found in the experiment[25]. The calculated Teflon mass ablated per pulse is shown in Fig. 7 as a function of cavity length and radius. Generally, the ablated mass increases with increasing cavity length and decreasing cavity radius. From comparison with experiment it can be shown that the model underpredicts the ablation mass by about 25%. However, it should be noted that some mass can be ablated in the form of large particulates. This effect for one particular PPT was estimated to be up to 40% of the total ablated mass[27]. The ablation in the particulate phase was not considered in the present paper.

The near-cathode sheath model allows of calculation the potential drop between the plasma at the thruster exit plane and the cathode. The plasma has a positive potential with respect to the cathode which decreases initially with time. This happens because the current pulse is essentially gone after 5 μs when the main plasma cloud arrives at the exit plane. Therefore the plasma density at the exit plane increases while the current decreases and this leads to decreasing $\Delta\phi$.

As mentioned earlier, one of the reasons for development of the 1D cavity model is to produce more accurate boundary conditions for the plume simulation. The temporal variation of the plasma density at the thruster exit plane is shown in Fig. 9. In comparison with previous results, the plasma density significantly increases at later times since plasma parameter variation along the cavity length is taken into account. These new boundary conditions are employed in the particle simulation of the plume. As expected, there is an effect on the plume structure at later

times as shown in Fig. 10. It can be seen that the simulation predicts well the initial rise and the actual peak of the potential data. To generate the results shown in Fig. 10 we assumed that the potential at the thruster exit plane is constant throughout the simulation. However, it was shown (Fig. 9) that this potential varies with respect to the cathode. The measurements of plasma potential were made with respect to the cathode[4,25] . To illustrate this effect we combine the plasma potential in the plume (Fig. 10) with variation of the plasma potential at the thruster exit plane (Fig. 8). These results are shown in Fig.11 where the electron temperature near the cathode is used as a parameter. One can see that this approach is able to predict the drop of the potential from 5 μs and the minimum before the rising part. In making this comparison with the experimental data, it is expected that the measurements collected over the first 5 μs (before main plasma cloud arrives at the thruster exit) cannot be reproduced in the frame of the present model. This is due to dependence on the ignition plasma introduced by the igniter spark, which is not modeled in present work. In the present model we assume that all plasma parameters are radially uniform while really the electron temperature near the nozzle edges may be smaller than that at the axis[28]. Therefore we introduce the electron temperature as a parameter.

The new thruster exit boundary conditions provided by the physical models presented in this study do not significantly affect the main aspects of the plume structure that were reported in Ref. 7. It is found that the overall distribution of the chemical species in the plume is almost unchanged. The main conclusion from Ref. 7 still holds, that for the PPT-4, the main component of back flow onto the spacecraft will arise from the highly mobile carbon ions.

Summary

An end-to-end device/plume model has been developed to describe plasma generation, acceleration and plume expansion for an electrothermal pulsed plasma thruster. As an example, we have studied the Teflon fed PPT-4 developed at the University of Illinois. The modeling strategy was based on a one-dimensional fluid unsteady model for the plasma generation and

acceleration processes and a particle simulation of the plume. A new kinetic ablation model was employed to calculate the Teflon ablation rate as a function of the plasma parameters. Predicted results were compared directly with data for PPT-4 performance characteristics and plume flowfield. In general, the agreement between data sets was good.

Acknowledgements

References

[1] R. L. Burton and P. J. Turchi, "Pulsed plasma thruster", *Journal of Propulsion and Power*, vol.14, 5, 1998, pp. 716-735.

[2] R. J. Vondra, The MIT Lincoln laboratory pulsed plasma thruster, AIAA Paper 76-998, 1976.

[3] P. J. Turchi, Directions for improving PPT performance, *Proceeding of the 25th International Electric Propulsion Conference*, vol. 1, Worthington, OH, 1998, pp. 251-258.

[4] R.L. Burton and S.S. Bushman, "Probe measurements in a Co-axial gasdynamic PPT", *35th Joint Propulsion Conference, Los Angeles, CA, June 1999*, AIAA Paper 99-2288.

[5] M. Keidar, I.D. Boyd and I.I. Beilis, " A model of an electrical discharge in a coaxial pulsed plasma thruster", *Proceeding of the 26th International Electric Propulsion Conference, Japan*, IEPC Paper 99-214, 1999.

[6] M. Keidar, I.D. Boyd and I.I. Beilis, " Particulate interaction with plasma in a Teflon pulsed plasma thruster", *Proceeding of the 26th International Electric Propulsion Conference, Japan*, IEPC Paper 99-213, 1999.

[7] I. D. Boyd, M. Keidar, and W. McKeon, Modeling of a pulsed plasma thruster from plasma generation to plume far field, *Journal of Spacecraft and Rockets, vol. 37, No. 3, 2000, pp. 399-407.*

[8] L. Muller, Modeling of an ablation controlled arc, J. Phys. D: Appl. Phys., 26 1993 pp. 1253-1259.

[9] E. Domejean, P. Chevrier, C. Fievet and P. Petit, Arc-wall interaction modeling in a low-voltage circuit breaker, J. Phys.D: Appl. Phys., 30, 1997, pp. 2132-2142.

[10] S.V. Kukhlevsky, J. Kaiser, O. Samek, M. Liska, and J. Erostyak, stark spectroscopy measurements of electron density of ablative discharge in Teflon-$(CF_2)_n$ capillaries, J. Phys. D: Appl. Phys., 33 (2000) 1090-1092.

[11] M. Keidar, I.D. Boyd and I.I. Beilis, Electrical discharge in the Teflon cavity of a co-axial pulsed plasma thruster, IEEE Trans. Plasma Sci., 28, 2000, pp. 376-385.

[12] M. Keidar, I.D. Boyd and I.I. Beilis, " A model of Teflon ablation in a pulsed plasma thruster", 27th IEEE International Conference on Plasma Science, New Orleans, LA, June 3-7, 2000; (IEEE Conference Record-Abstracts, IEEE Catalog No. 00CH37087, p. 241)

[13] C. B. Ruchti and L. Niemeyer, Ablation controlled arc, IEEE Trans. Plasma Sci., 14 1986, pp. 423-434.

[14] P. Kovatya and J. J. Lowke, Theoretical prediction of ablation stabilized arcs confined in cylindrical tubes, J. Phys. D: Appl. Phys., 17, 1984, pp. 1197-1212.

[15] P. Kovatya, Thermodynamic and transport properties of ablated vapors of PTFE, alumina, perspex and PVC in the temperature range 5000-30000 K, IEEE Trans. Plasma Sci., 12, 1984 pp. 38-42.

[16] C.S. Schmahl and P.J. Turchi, Development of equation-of-state and transport properties for molecular plasmas in pulsed plasma thrusters. Part I: A two-temperature equation of state for Teflon, Proc. Inter. Electr. Propul. Conf. Pp. 781-788, 1997.

[17] S.I. Anisimov, Vaporization of metal absorbing laser radiation, Sov. Phys., JETP, 27, No. 1, 1968, pp. 182-183.

[18] I.I. Beilis, Parameters of the kinetic layer of arc-discharge cathode region, IEEE Trans. Plasma Sci., Vol.PS-13, No.5, 1985, pp. 288-290.

[19] M. Keidar, I.D. Boyd and I.I. Beilis, IEEE Trans. Plasma Sci., 2000 (submitted).

[20] N. A. Gatsonis and X. Yin, Axisymmetric DSMC/PIC simulation of quasineutral partially ionized jets, AIAA paper 97-2535, 1997.

[21] G.A. Bird, "Molecular gas dynamics and the direct simulation of gas flows" (Clarendon Press, Oxford, 1994).

[22] A. Dolgarno, M.R.C. McDowell and A. Williams, The modilities of ions in unlike gases, Proc. Of Royal Soc. Of London, Vol. 250, April 1958, pp. 411-425.

[23] S. Sakabe and Y. Izawa, Simple formula for the cross sections of resonant charge transfer between atoms and their ions at low impact velocity, Physical Rev. A: General Physics, v. 45, No. 3, 1992, pp. 2086-2089.

[24] C.K. Birdsall and A.B. Langdon, Plasma Physics via Computer Simulation, Adam Hilger Press, 1991.

[25] S. S. Bushman, Investigations of a coaxial pulsed plasma thruster, Master Thesis, University of Illinois Urbana-Champaign, May 1999.

[26] A. Shapiro, "*The dynamics and thermodynamics of compressible fluid flow*", John Wiley & Sons, New York.

[27] G. G. Spanjers, J. S. Lotspeich, K.A. McFall, and R. A. Spores, Propellant losses because of particulate emission in a pulsed plasma thruster, *Journal of Propulsion and Power*, Vol. 14, 4, 1998, pp. 554-559.

[28] I.D. Boyd, "Monte Carlo simulation of nonequilibrium flow in a low-power hydrogen arcjet", Phys. Fluids 9 (10) 1997, 3086-3095.
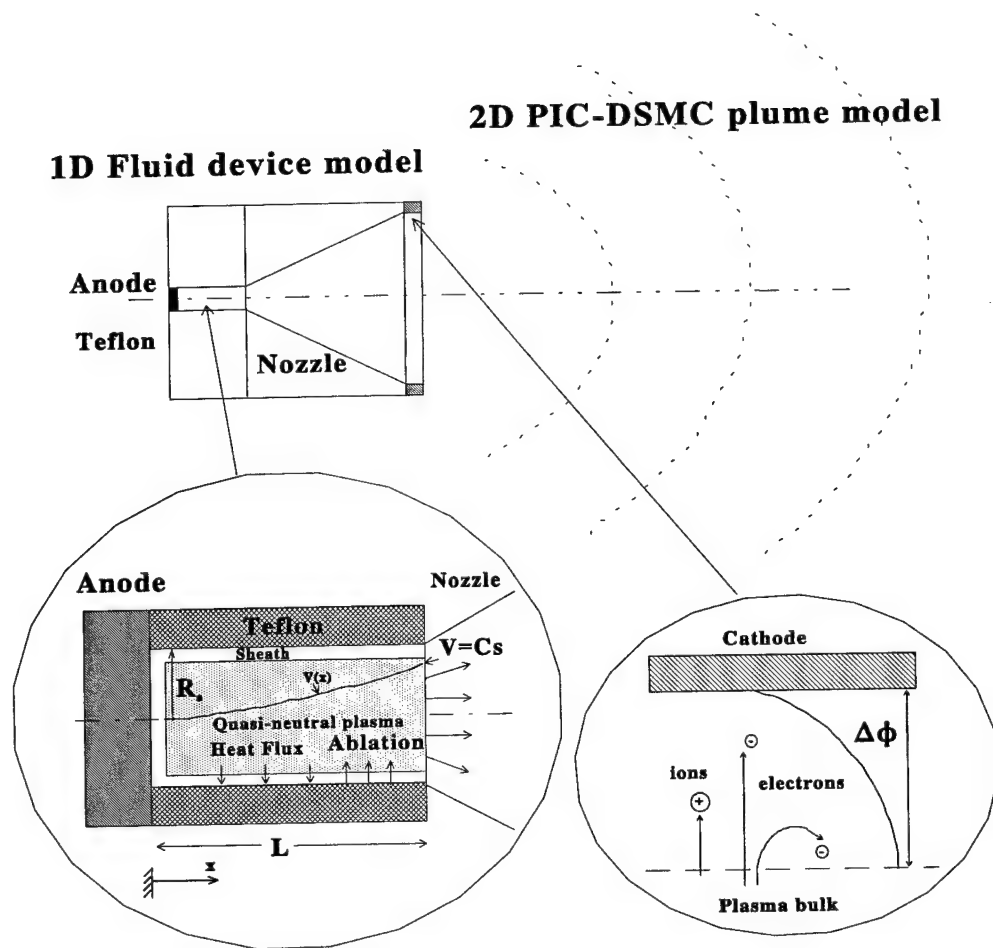
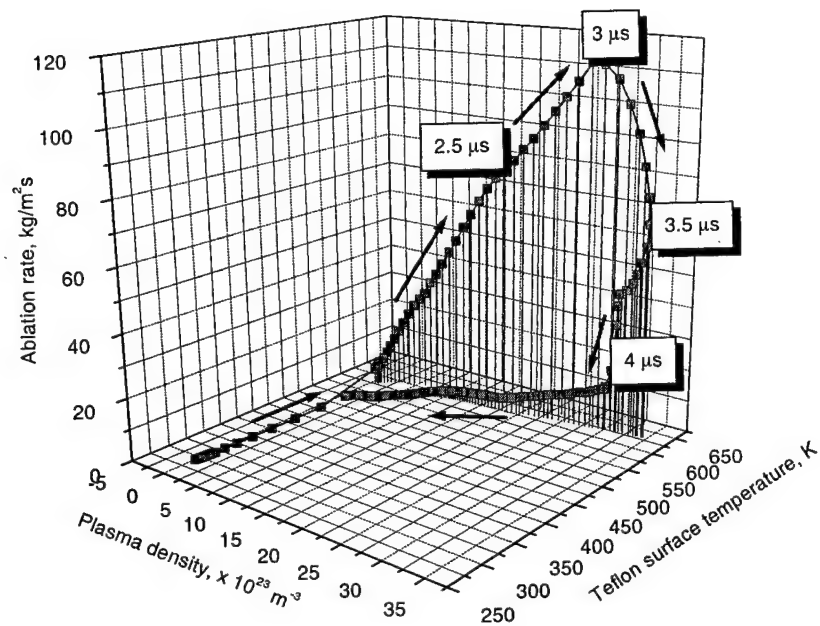**Figure 1.** Schematic diagram of the PPT-4 and plume

Figure 2. The ablation rate as a function of plasma density and Teflon surface temperature. The arrow indicates the direction of ablation rate evolution during the pulse.
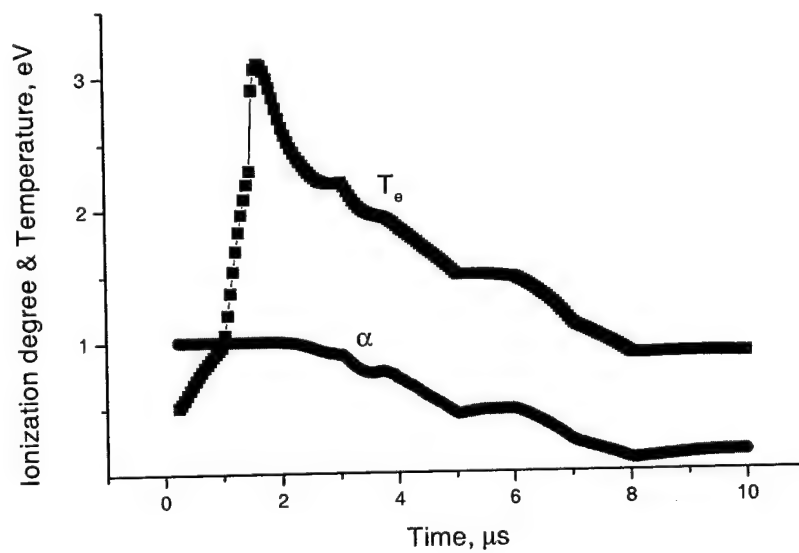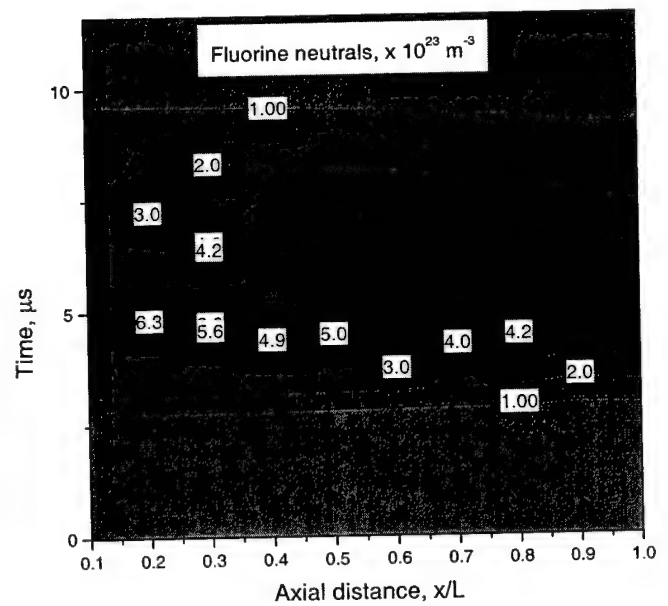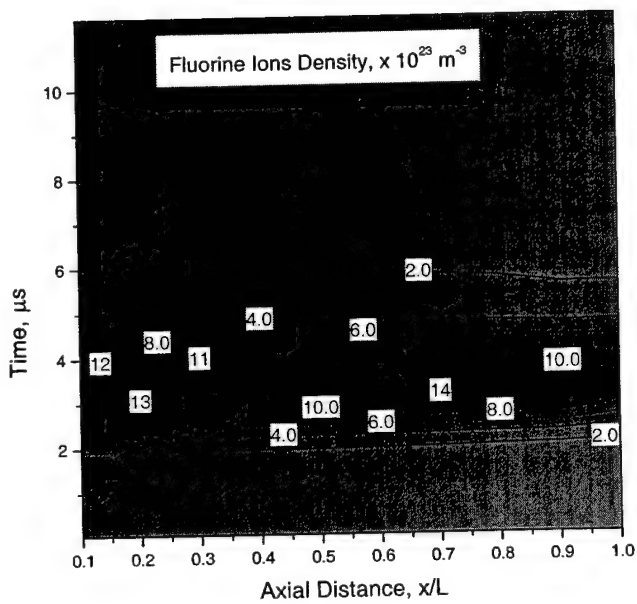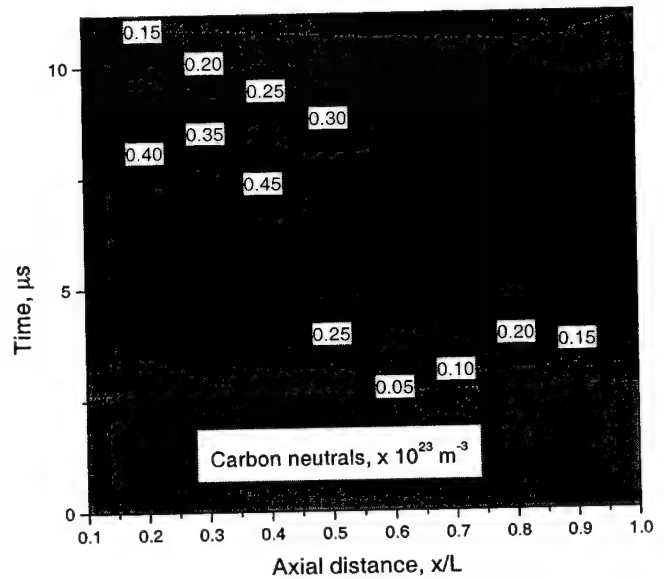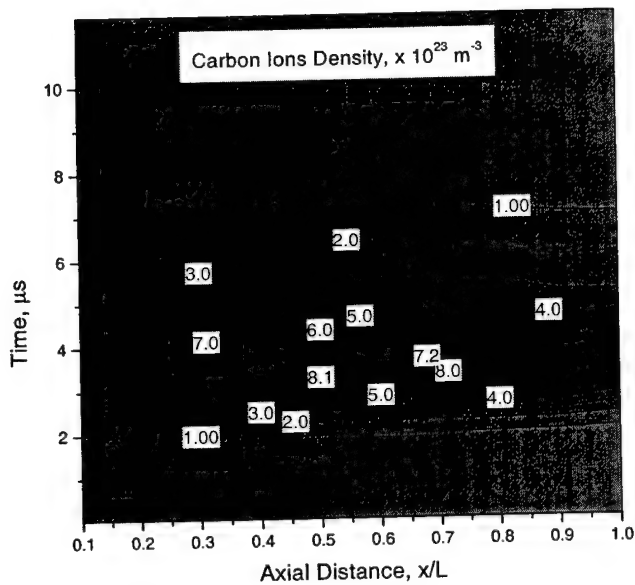

Figure 3. Variation with time of electron temperature and ionization degree in the cavity

Figure 4. Temporal and spatial variation of the chemical species during the discharge pulse
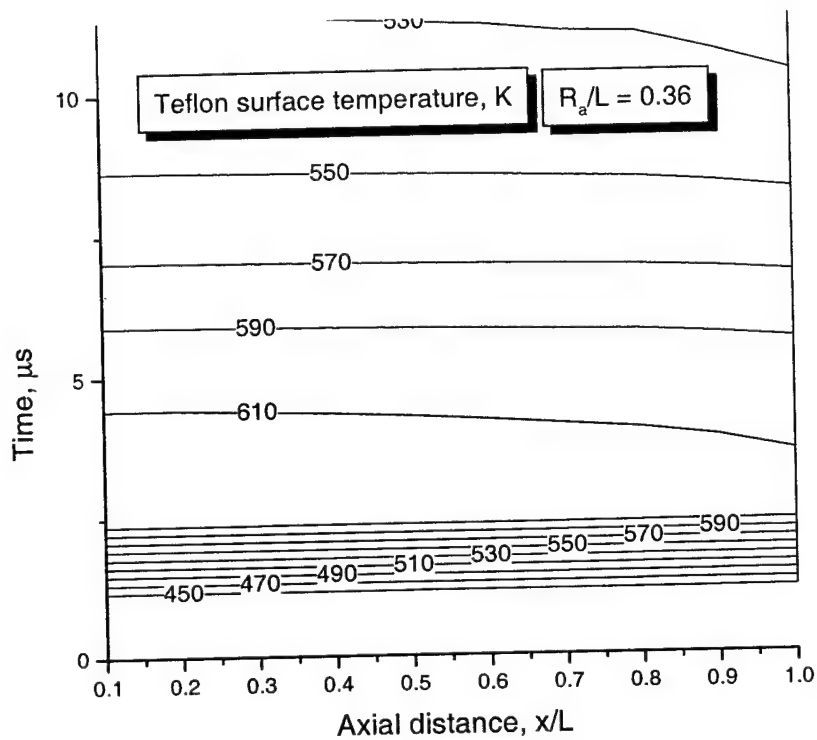
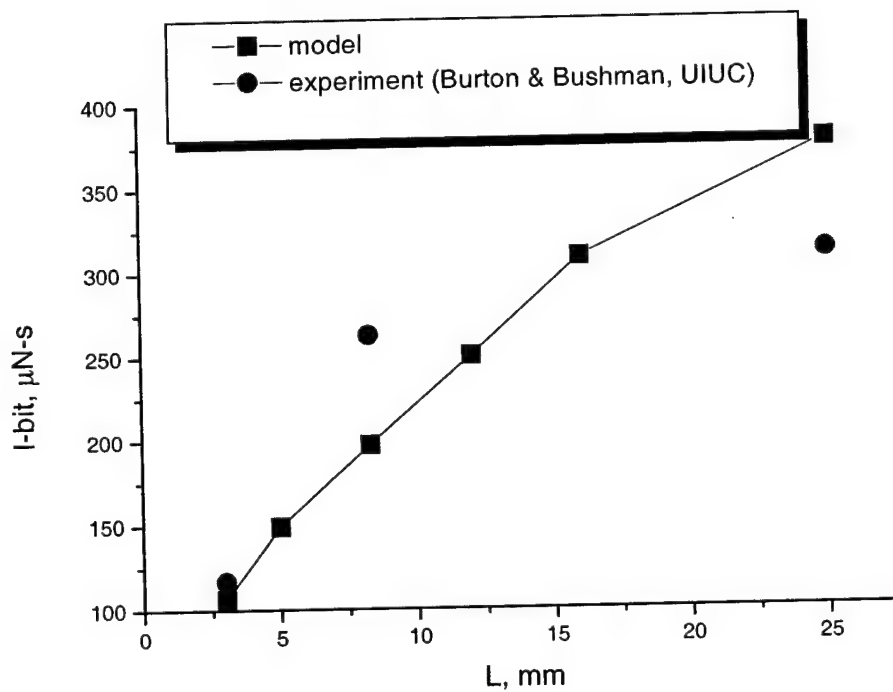**Figure 5.** Temporal and spatial variation of the Teflon surface temperature

Figure 6. Thrust impulse bit variation with cavity length and comparison with experiment
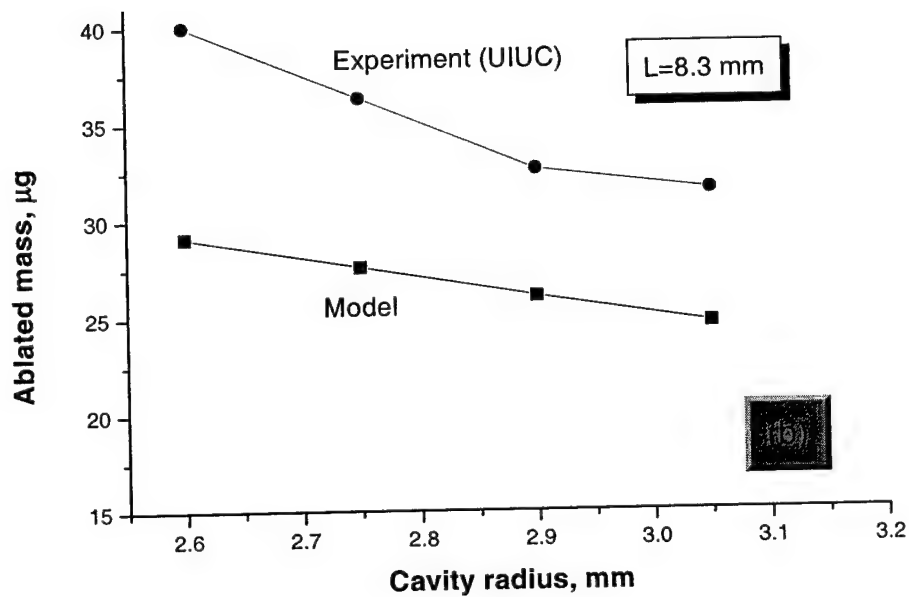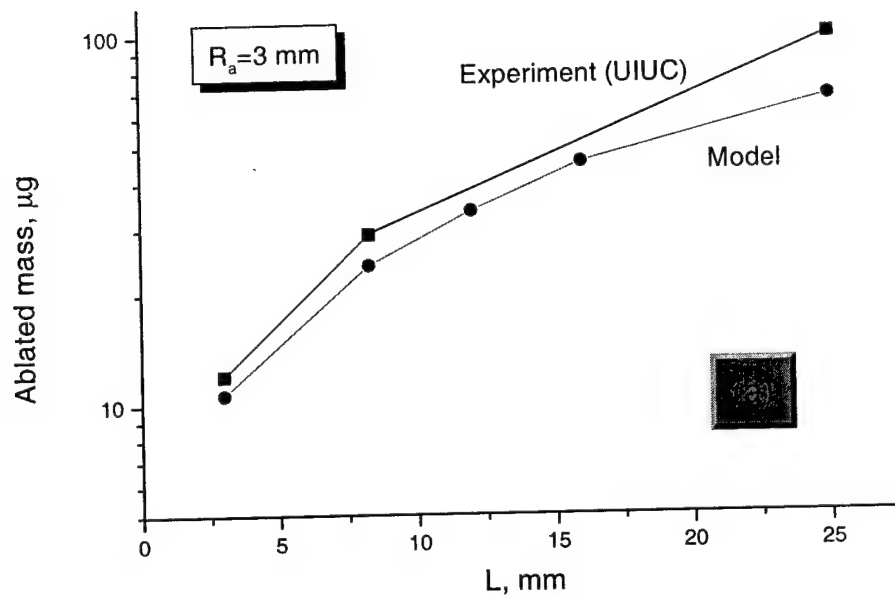
Figure 7. Ablated mass as a function of cavity geometry and comparison with experiment. a) constant cavity radius R_a; b) constant cavity length L.
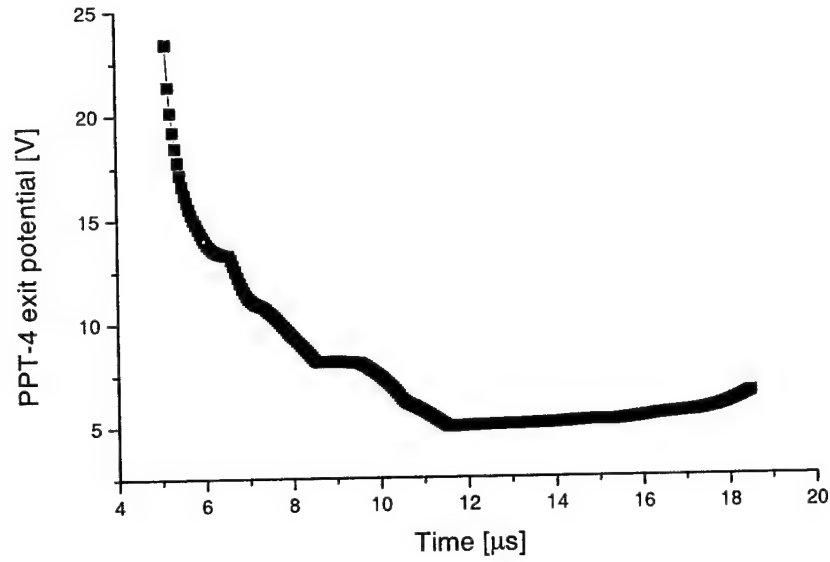
Figure 8. Temporal variation of the plasma potential at the thruster exit plane with respect to the cathode

Figure 9. Variation with time of electron density and comparison with previous results

Figure 10. Variation of the plasma potential on the plume centerline at 10 cm from the thruster exit plane and comparison with experiment

Figure 11. Variation with time of the plasma potential in the plume at 10 cm from the PPT-4 exit plane with electron temperature near the cathode as a parameter

Vaporization of heated materials into discharge plasmas

Michael Keidar,[a] Jing Fan, and Iain D. Boyd
Department of Aerospace Engineering, University of Michigan, Ann Arbor, Michigan 48109
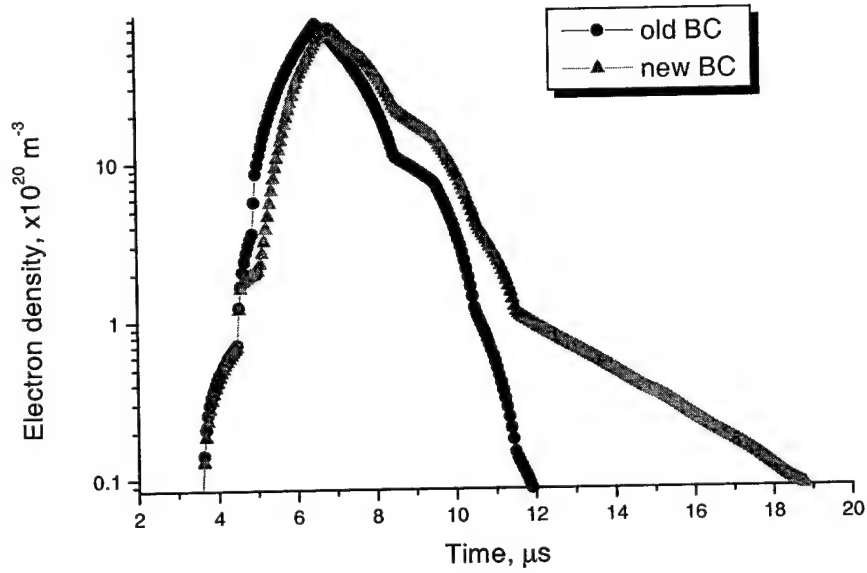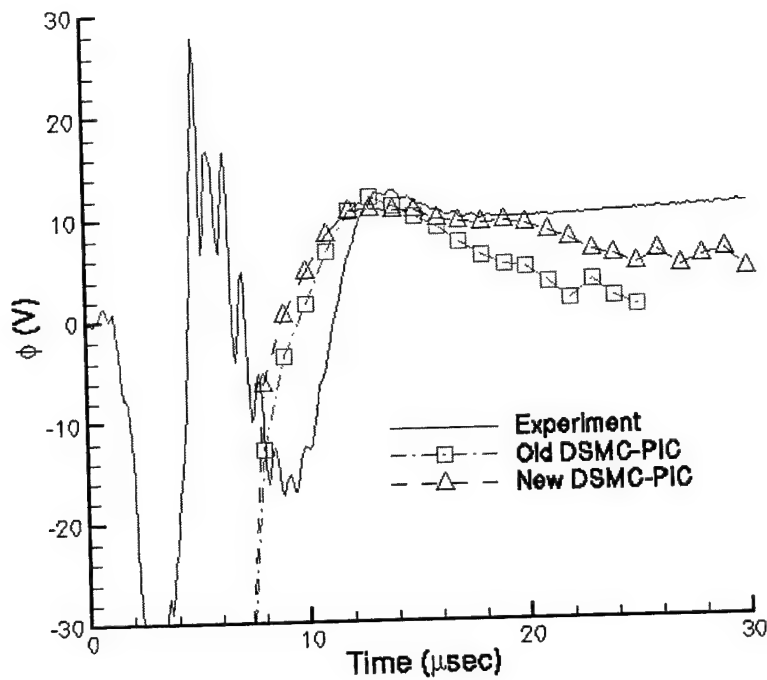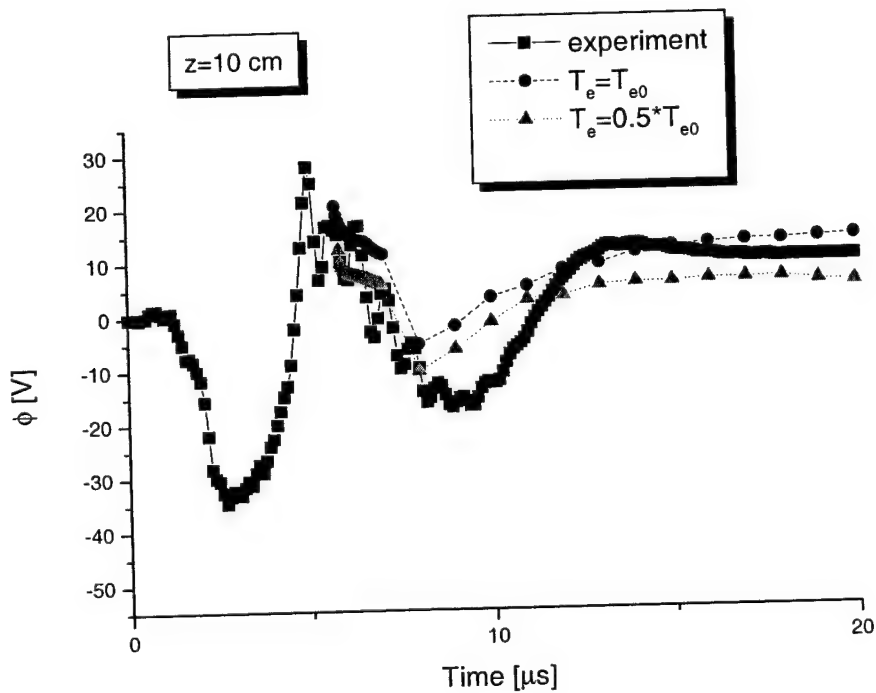
Isak I. Beilis
Electrical Discharge and Plasma Laboratory, Fleischman Faculty of Engineering, Tel Aviv University, P.O.B. 39040, Tel Aviv 69978, Israel

The vaporization of condensed materials in contact with high-current discharge plasmas is considered. A kinetic numerical method named direct simulation Monte Carlo (DSMC) and analytical kinetic approaches based on the bimodal distribution function approximation are employed. The solution of the kinetic layer problem depends upon the velocity at the outer boundary of the kinetic layer which varies from very small, corresponding to the high-density plasma near the evaporated surface, up to the sound speed, corresponding to evaporation into vacuum. The heavy particles density and temperature at the kinetic and hydrodynamic layer interface were obtained by the analytical method while DSMC calculation makes it possible to obtain the evolution of the particle distribution function within the kinetic layer and the layer thickness. © *2001 American Institute of Physics.* [DOI: 10.1063/1.1345860]

I. INTRODUCTION

The vaporization of a heated surface interacting with discharge plasmas has a great interest for different applications such as ablation controlled arcs,[1] pulsed plasma thrusters,[2,3] high-pressure discharges,[4] vacuum arcs,[5] electroguns,[6] and metal evaporation by laser radiation action.[7] In most models, the rate of evaporation is calculated using the Langmuir relationship[8] that is, however, limited to the case of vaporization into vacuum.

Anisimov[9] considered a case of vaporization of a metal exposed to laser radiation using a bimodal velocity distribution function in the nonequilibrium (kinetic) layer. The main result of this work is the calculation of the maximal flux of returned atoms to the surface, which was found to be about 18% of the flux of vaporized atoms. This result was obtained under the assumption that the atom flow velocity is equal to the sound velocity at the external boundary of the kinetic layer. In many physical situations, however, the expansion of the vapor is not by the sound speed since there is a dense plasma in the volume discharge. Beilis[10,11] analyzed metal vaporization into discharge plasmas in the case of a vacuum arc cathode spot. He concluded that the parameters at the outer boundary of the kinetic layer are close to their equilibrium values and that the velocity at the outer boundary of the kinetic layer is much smaller than the sound velocity. In both the analyses mentioned above, no information is provided about the change of the particle velocity distribution function from a nonequilibrium state to an equilibrium state inside the kinetic layer.

In the present article we study the nonequilibrium layer close to the evaporating surface using the particle method known as direct simulation Monte Carlo (DSMC).[12] It will determine the thickness of the nonequilibrium layer and the

evolution of the particle distribution function within the layer. The numerical simulation results will be compared with the analytical results for the case when the vapor velocity at the outer boundary of the kinetic layer is given as a parameter.

II. MODEL OF THE NONEQUILIBRIUM LAYER

In this section we will present two different kinetic models (particle simulation and analytical approach) for the nonequilibrium layer near the evaporating surface.

A. Particle simulation

In the nonequilibrium layer near the surface there are collisions between particles that eventually lead to a change of the distribution function. The DSMC method uses particle motion and collisions to perform a simulation of gas dynamics under nonequilibrium conditions. Each particle has spatial and velocity coordinates. The collision approach between particles is based on a probability model developed from the kinetic theory and commonly used in DSMC.[12]

To perform the DSMC simulation we have to specify conditions at two boundaries (see Fig. 1). At the evaporating surface with density n_0 and temperature T_0, the velocity distribution function for emitted particles is in the equilibrium form[9,10]

$$f_0(\mathbf{V}) = n_0 \left(\frac{m}{2\pi k T_0} \right)^{3/2} \exp\left(-\frac{mV^2}{2kT_0} \right), \quad V_x > 0. \quad (1)$$

At the outer boundary of the kinetic layer the distribution function for particles is assumed to be

$$f_1(\mathbf{V}) = n_1 \left(\frac{m}{2\pi k T_1} \right)^{3/2} \exp\left(-m \frac{(V_x - V_1)^2 + V_y^2 + V_z^2}{2kT_1} \right), \quad (2)$$
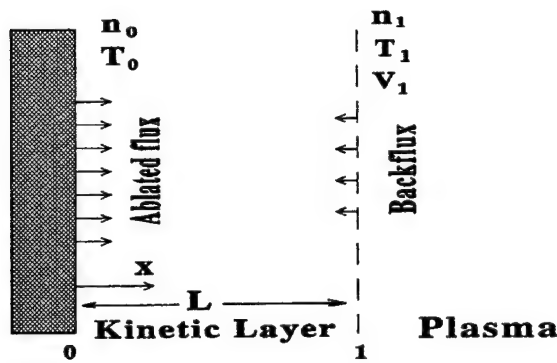
[a] Electronic mail: keidar@engin.umich.edu

FIG. 1. Schematic representation of the near surface layer.

where V_1 is the velocity, n_1 is the density, and T_1 is the temperature. These boundary conditions are supplemented by using an empirical relation between T_0 and n_0. As an example, we have used the equilibrium vapor pressure for the case of Teflon in the form[2]

$$P_0 = P_c \exp(-T_c/T_0) \quad \text{and} \quad n_0 = P_0/kT_0, \tag{3}$$

where P_0 is the equilibrium pressure, $P_c = 1.84 \times 10^{20} \, \text{N/m}^2$ and $T_c = 20\,815 \, \text{K}$ are the characteristic pressure and temperature obtained empirically. The physical meaning of the characteristic pressure and temperature is that the equilibrium pressure equals P_c when vapor reaches the temperature of T_c. The calculations are performed assuming that vapor consists of CF_2 molecules at a surface temperature in the range 550–650 K that is typical for an electrothermal pulsed plasma thruster.[3]

The DSMC model employed in the present article has the following strategy. Uniform cells 0.5 λ in size are employed, and time step $\Delta t = 0.3\lambda/V_{m,s}$ (Ref. 13) where λ and $V_{m,s} = (2kT_0/m)^{0.5}$ are the molecular mean free path and the most probable thermal speed at the ablated surface. Molecules enter the flow field successively from the surface due to evaporation, and from the outer boundary due to Maxwellian velocity distribution that allows particle velocities in the negative direction. Using the assumption about the distribution function at the surface and at the external boundary Eqs. (1) and (2) we can calculate the flux of molecules entering from the surface, G_s, and from the outer boundary of the layer, G_b, as follows:

$$G_s = n_0(2kT_0/m)^{0.5}/2\pi^{0.5} \tag{4}$$

and

$$G_b = n_1(2kT_1/m)^{0.5} \times [\exp(-\alpha^2) - \pi^{0.5}\alpha\{1 - \text{erf}(\alpha)\}]/2\pi^{0.5}, \tag{5}$$

where $\alpha = V_1/(2kT_1/m)^{0.5}$. The molecular interaction is described by the variable hard-sphere (VHS) model.[12] The VHS model is employed to select molecular collision pairs from cells and to distribute the postcollision velocities. This model assumes that the scattering from molecular collision is isotropic in the center of mass frame of reference.[12] Both boundaries (wall and outer boundary of the kinetic layer) are assumed to be perfectly absorbing. The flow will arrive at a

steady state when the sum of G_s and G_b is exactly balanced by the flux of molecules leaving from the outer boundary or sticking on the surface:

$$G_s + G_b = G_r + G_f, \tag{6}$$

where G_r is the flux of the particles returned to the surface during the time step and G_f is the flux of the particles crossing the outer boundary of the layer.

In the DSMC approach, in order to calculate the evolution of the distribution function inside the kinetic layer, we have to specify the thickness of the layer in units of λ. The parameters at the outer boundary of the kinetic layer (n_1 and T_1) and the flux of returned particles are calculated as a function of the distance of the location of the outer boundary of the layer and of the velocity at this boundary V_1.

B. Analytical approach

Let us consider the analytical approach developed in Refs. 9–11, where the vapor parameters T_1 and n_1 at the outer boundary can be obtained without information about the layer thickness. This means that the problem is reduced to integration of the conservation equations of mass, momentum, and energy across the layer.[9] We consider a nonequilibrium layer (thickness of about a mean free path λ) adjacent to the surface (as shown in Fig. 1), where the velocity distribution function of the evaporated molecules reached equilibrium by the rare-field collisions with the background heavy particles and furthermore the vapor flow is described by a hydrodynamic approach. Using Anisimov's assumption[9] that the velocity distribution function for the returned particles ($V_x < 0$) is $\beta f_1(\mathbf{V})$, where β is the proportionality coefficient, the relation of the heavy particle parameters at the outer boundary of the kinetic layer in the case of an arbitrary velocity is obtained from the model[10] and reads as follows:

$$\frac{n_0}{2(\pi d_0)^{0.5}} = n_1 V_1 + \beta \frac{n_1}{2(\pi d_1)^{0.5}} \times \{\exp(-\alpha^2) - \alpha\pi^{0.5}\text{erfc}(\alpha)\},$$

$$\frac{n_0}{4d_0} = \frac{n_1}{2d_1}\{(1 + 2\alpha^2) - \beta[(0.5 + \alpha^2)\text{erfc}(\alpha) - \alpha\exp(-\alpha^2)/\pi^{0.5}]\}, \tag{7}$$

$$\frac{n_0}{(\pi d_0)^{1.5}} = \frac{n_1}{(d_1)^{1.5}}\pi^{-1}[\alpha(\alpha^2 + 2.5) - 0.5\beta\{(2.5 + \alpha^2)\alpha \times \text{erfc}(\alpha) - (2 + \alpha^2)\exp(-\alpha^2)/\pi^{0.5}\}],$$

where $d_0 = m/2kT_0$, $d_1 = m/2kT_1$, $\text{erfc}(\alpha) = 1 - \text{erf}(\alpha)$, and $\text{erf}(\alpha)$ is the error function. The equation system (7) is obtained using the boundary conditions (1)–(3) and the conservation laws of mass, momentum, and energy across the layer.[9,10] By calculating the parameters at the outer boundary of the kinetic layer we can obtain the flux of returned particles:
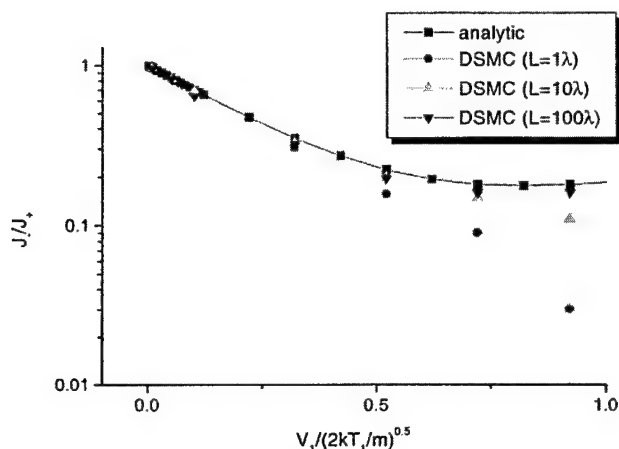
FIG. 2. Comparison of the analytic and DSMC return flux as a function of velocity V_1 with the distance of location of the outer boundary of the kinetic layer L as a parameter.

$$J_- = \int_{-\infty}^{0} \beta f_1(V) V dV$$

$$= \beta N_1 \left(\frac{kT_1}{2\pi m} \right)^{0.5} \{\exp(-\alpha^2) - \alpha \pi^{0.5} \operatorname{erfc}(\alpha)\}. \qquad (8)$$

The system of equations (7) has four unknowns and therefore the solution can be found having one unknown as a parameter, which is the velocity V_1 at the outer boundary of the kinetic layer in our case.

III. RESULTS

DSMC calculations and a comparison with the analytical predictions for the flux of returned atoms is shown in Fig. 2 where the thickness of the kinetic layer is used as a parameter. One can see that in the case of small velocity ($\alpha \leqslant 0.5$) at the outer boundary all results agree well. This is the case when the thickness of the nonequilibrium layer is about one mean free path. In the case when evaporation occurs at about the sound velocity at the outer boundary, the DSMC calculations approach the analytical value at a layer thickness of ~ 10–20 mean free paths.

The calculation of the backflux dependence with distance inside the layer when $\alpha=1$ is presented in Fig. 3. It can be seen that in the case when V_1 is about the sound velocity, the flux of the returned molecules depends upon the distance from the evaporating surface where the external boundary is placed. Thus up to a layer thickness of about 20 mean free paths, the flux changed strongly and then it is weakly saturated. The DSMC calculation predicts a 16% flux of returned particles, which is very close to the analytical result of 18%. The reason for this difference can be understood by analyzing the velocity distribution function of returned particles in the DSMC calculation.

Results of the DSMC calculation of the velocity distribution function and comparison with the analytic approximation $\beta f_1(V)$ are shown in Fig. 4(a) for the case of sound velocity at the outer boundary. One can see that the distribution functions remain different in the case of a 100λ kinetic
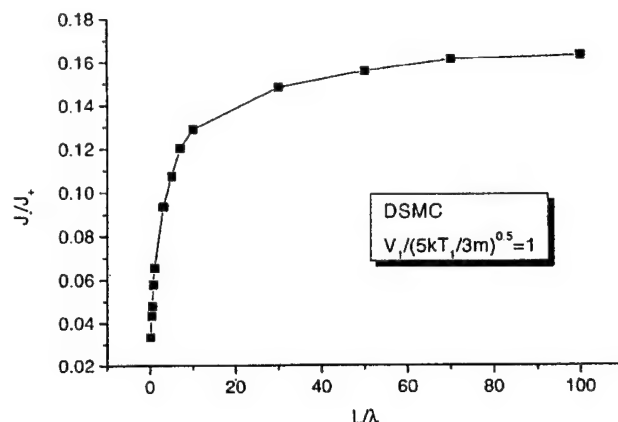

FIG. 3. The DSMC calculated return flux as a function of the distance of location of the outer boundary of the kinetic layer L in the case of sound velocity at the boundary 1.

layer thickness. This is not the case when the velocity at the outer boundary of the kinetic layer is small as shown in Fig. 4(b), where the DSMC distribution function agrees well with the analytic approximation. Therefore it is not surprising that the calculated flux of returned particles is also found to be in good agreement with the analytical result. It should be noted
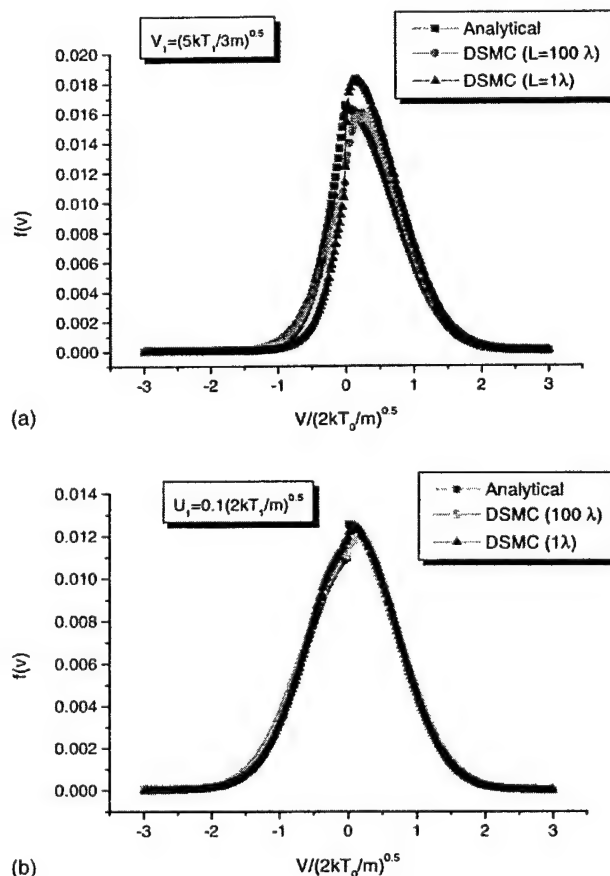

FIG. 4. Variation of the velocity distribution function of the returned particles near the wall with the distance of location of the outer boundary of the kinetic layer L as a parameter. (a) $V_1 = (5kT_1/3m)^{0.5}$ and (b) $V_1 = 0.1(2kT_1/m)^{0.5}$.
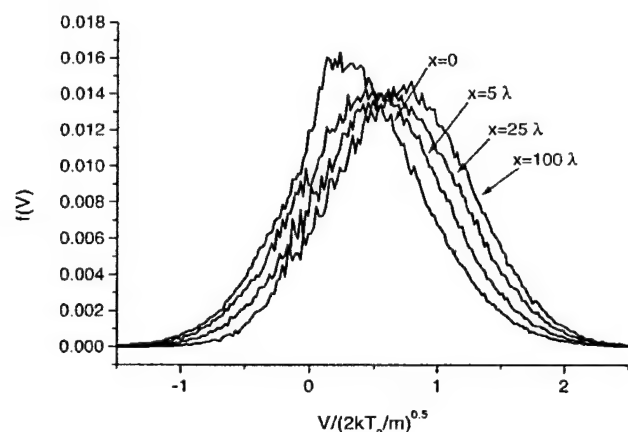
FIG. 5. Variation of the velocity distribution function (normal to the surface component) with the distance from the evaporated surface as a parameter. The thickness of the kinetic layer $L = 100\lambda$ and $V_1 = (5kT_1/3m)^{0.5}$.

that the discontinuity in the analytical distribution function [Fig. 4(b)] is the result of the definition of the distribution function of the returned particles (Sec. II B).

The evolution of the particle distribution function within the Knudsen layer is shown in Fig. 5 for the case $V_1 = (5kT_1/3m)^{0.5}$. One can see that the velocity distribution function approaches a drifted Maxwellian at a distance of several mean free paths from the surface. The drift velocity slightly increases with further distance from the evaporating surface.

The results of calculation of the analytic system of equations (7) are presented in Fig. 6 with the normalized velocity V_1 as a parameter. The temperature T_1, density n_1, and the flux of returned particles J_- all decrease as the velocity at the outer boundary of the kinetic layer increases. In the limiting case of the sound velocity, the flux of returned particles is equal to 18% as was obtained by Anisimov.[9] In this case the analytically predicted flux of returned particles is larger than that obtained by numerical simulations (16%, see Fig. 3). It should be pointed out that the dependence of the flux of
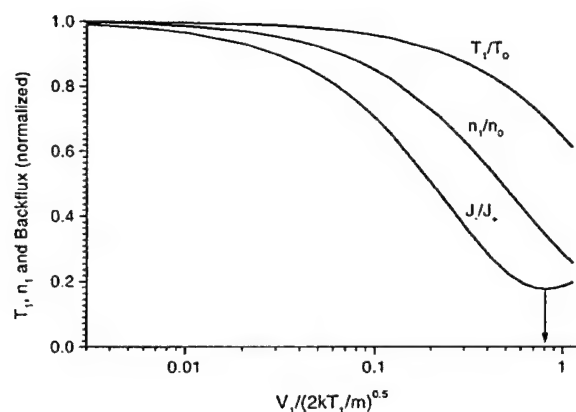
returned particles J_- on the velocity V_1 has a minimum near the sound speed (see Fig. 6). The minimum corresponds to the sound speed with adiabatic index 1.3. This fact as well as the overestimate of the returned particle flux is connected with the assumption in the analytical approach of the form of the particle velocity distribution for the particles returned to the evaporating surface, i.e., that the distribution function of the returned particles is proportional to the distribution function at the outer boundary of the kinetic layer.[9]

IV. SUMMARY

Two kinetic approaches, namely the particle method (DSMC) and bimodal distribution function approach were employed to describe the parameters in the nonequilibrium kinetic layer near the evaporating surface. DSMC calculation makes it possible to establish the thickness of the kinetic layer and the evolution of the particle distribution function within the layer. The thickness of the kinetic layer and the vapor density and temperature in the kinetic layer adjacent to the evaporating surface depend upon the velocity at the outer boundary of the layer. We have found that the thickness of the kinetic layer increases from a few mean free paths λ in the case of small velocity up to about 10–20 λ in the case of the evaporation with sound speed at the outer boundary of the layer. Comparison of the DSMC and analytical results indicates that the analytical model predicts correctly the flux of returned particles over a wide range of velocity at the outer boundary of the layer. The present model can be used for calculation of the rate of evaporation of the heated surface interacting with a plasma. The free parameter of this model, the velocity at the outer boundary of the layer, can be determined by coupling this model with a model of the hydrodynamic layer and the plasma bulk.

FIG. 6. Parameters (temperature, density, and returned flux) at the outer boundary of the kinetic layer as a function of velocity V_1 calculated from Eq. (7).

[1] C. B. Ruchti and L. Niemeyer, IEEE Trans. Plasma Sci. **14**, 423 (1986).
[2] R. Burton and P. Turchi, J. Propul. Power **14**, 716 (1998).
[3] M. Keidar, I. D. Boyd, and I. I. Beilis, IEEE Trans. Plasma Sci. **28**, 376 (2000).
[4] M. I. Boulos, P. Fauchais, and E. Pfender, *Thermal Plasmas: Fundamentals and Applications, Vol. 1* (Plenum, New York, 1995).
[5] *Vacuum Arc Science and Technology*, edited by R. L. Boxman, P. Martin, and D. Sanders (Noyes, Park Ridge, NJ, 1995).
[6] L. L. Raja, P. L. Varghese, and D. E. Wilson, J. Thermophys. Heat Transfer **11**, 353 (1997).
[7] L. V. Zhigilei, P. B. S. Kodali, and B. J. Garrison, J. Phys. Chem. B **102**, 2845 (1998).
[8] I. Langmuir, Phys. Rev. **2**, 329 (1913).
[9] S. I. Anisimov, Sov. Phys. JETP **27**, 182 (1968).
[10] I. I. Beilis, IEEE Trans. Plasma Sci. **13**, 288 (1985).
[11] I. I. Beilis, Theoretical Modeling of Cathode Spot Phenomena, in *Vacuum Arc Science and Technology*, edited by R. L. Boxman, P. Martin, and D. Sanders (Noyes, Park Ridge, NJ, 1995).
[12] G. A. Bird, *Molecular Gas Dynamics and the Direct Simulation of Gas Flows* (Clarendon, Oxford, 1994).
[13] E. S. Oran, C. K. Oh, and B. Z. Cybyk, Annu. Rev. Fluid Mech. **30**, 403 (1998).

On the model of Teflon ablation in an ablation-controlled discharge

Michael Keidar[1], Iain D Boyd[1] and Isak I Beilis[2]

[1] Department of Aerospace Engineering University of Michigan, Ann Arbor, MI 48109, USA
[2] Electrical Discharge and Plasma Laboratory, Fleischman Faculty of Engineering,
Tel Aviv University, POB 39040, Tel Aviv 69978, Israel

Abstract
A kinetic model is developed of Teflon ablation caused by a plasma.
The model takes into account the returned atom flux that forms in the
non-equilibrium layer during the ablation. This approach makes it possible
to calculate the ablation rate for the case when the Teflon surface
temperature and the density and temperature in the plasma bulk are known.

The problem of the ablation controlled discharge has a common general interest in a number of applications such as electric fuses, circuit breakers, soft x-ray, pulsed plasma thrusters and extreme ultraviolet sources [1–5]. In these devices, the discharge energy is principally dissipated by ablation of wall material, which then forms the main component of the discharge plasma. The ablated vapour increases the pressure within the capillary and the plasma is expelled through the exit.

Previously, most of the plasma models of the ablated controlled discharge employed the Langmuir relationship [6], which is limited to the case of material ablation into a vacuum. For the conditions of a pulsed plasma thruster (PPT) this approach was also recently used [7, 8]. However, the process of ablation in the ablation controlled discharge should be described taking into account the fact that in the Teflon cavity the vapour does not expand into vacuum but rather into a volume discharge. For application to the vacuum arc discharge, a kinetic model of the cathode vapourization in the non-equilibrium plasma layer was developed by Beilis [9, 10]. It was shown that the flux of returned atoms toward the surface can become comparable to the flux of vaporizing atoms. It was also concluded [9, 10] that the parameters at the outer boundary of the kinetic layer are close to their equilibrium values and that the velocity at the outer boundary of the kinetic layer is much smaller than the sound velocity. Therefore, it was found that the cathode erosion rate in an arc discharge by vapourization is much smaller than the solid body evaporation rate into vacuum. In the present work we employ a kinetic approach similar to that used for the cathode vacuum arc evaporation to calculate Teflon ablation parameters. As an example, the conditions typical for an electrothermal PPT are considered [4, 7].

The problem starts by considering the non-equilibrium kinetic layer near the evaporating surface. Let us consider the structure of the near surface layers in detail as shown in figure 1. One can distinguish two different layers between
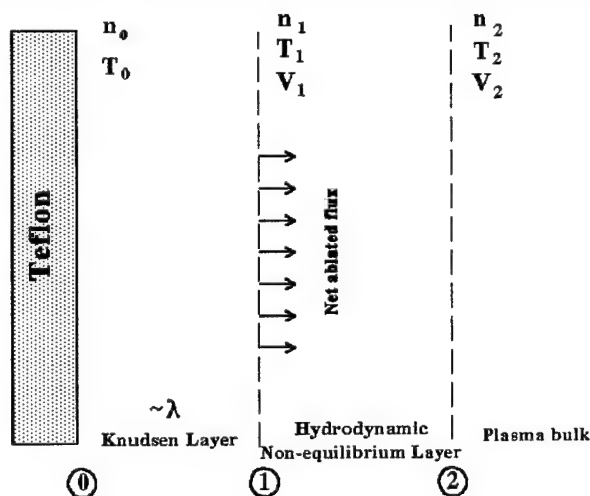

Figure 1. Schematic representation of the layer structure near the ablated surface.

the surface and the plasma bulk: (1) a kinetic non-equilibrium layer adjusted to the surface with a thickness of a few mean free paths (the Knudsen layer), (2) a collision-dominated non-equilibrium layer, where the electron and heavy particle temperatures differ. It is assumed that at the right edge of the second layer, all species (ions, neutrals and electrons) reach thermal equilibrium. The basic idea of the present model consists in combining the model for the kinetic layer [9–11] with hydrodynamic layer analyses in the second layer. Use of the general plasma model [7] in the equilibrium region provides the electron temperature T_2 and plasma density n_2. Firstly, we briefly introduce the kinetic model of the non-equilibrium layer. According to the approach of the work in [9] and [10] (using Anisimov's [11] assumption that the velocity distribution function for the returned particles is

$\beta f_1(V)$, where β is a proportionality coefficient and $f_1(V)$ is the Maxwellian distribution function shifted by V_1, V is the velocity vector) the relation of the heavy particle parameters at the outer boundary of the kinetic layer in the case of arbitrary velocity V_1 are as described by the following set of equations:

$$\frac{n_0}{2(\pi d_0)^{0.5}} = n_1 V_1 + \beta \frac{n_1}{2(\pi d_1)^{0.5}} \{\exp(-\alpha^2) - \alpha \pi^{0.5} \mathrm{erfc}(\alpha)\}$$

$$\frac{n_0}{4d_0} = \frac{n_1}{2d_1}\{(1 + 2\alpha^2) - \beta[(0.5 + \alpha^2)\,\mathrm{erfc}(\alpha)$$

$$-\alpha \exp(-\alpha^2)/\pi^{0.5}\}$$

$$\frac{n_0}{(\pi d_0)^{1.5}} = \frac{n_1}{(d_1)^{1.5}} \pi^{-1}[\alpha(\alpha^2 + 2.5)$$

$$-(\beta/2)\{(2.5 + \alpha^2)\alpha\,\mathrm{erfc}(\alpha) - (2 + \alpha^2)\exp(-\alpha^2)/\pi^{0.5}]$$

$$\tag{1}$$

where $d_0 = m/2kT_0$, $d_1 = m/2kT_1$, $\alpha = V_1/(2kT_1/m)^{0.5}$, $\mathrm{erfc}(\alpha) = 1 - \mathrm{erf}(\alpha)$, $\mathrm{erf}(\alpha)$ is the error function, T_0 is the surface temperature and n_0 is the equilibrium density.

Very recently it was shown that the velocity at the outer boundary of the kinetic layer V_1 strongly affects the kinetic layer parameters [12]. To find the velocity V_1 we apply the mass and momentum conservation equations for heavy particles in the hydrodynamic region (assuming a single fluid model) between boundaries 2 and 3. Assuming weakly ionized plasma in the hydrodynamic layer, the integration of the mass and momentum conservation equations yields the following relations between parameters at boundaries 2 and 3:

$$n_1 V_1 = n_2 V_2 \tag{2}$$

$$n_1 kT_1 + mn_1 V_1^2 = n_2 kT_2 + mn_2 V_2^2. \tag{3}$$

Combination of these two equations yields the following expression for the velocity at the outer boundary of the kinetic (Knudsen) layer:

$$V_1^2/(2kT_1/m) = (T_2 n_2/2T_1 - n_1/2)/(n_1 - n_1^2/n_2). \tag{4}$$

This equation makes it possible to calculate the velocity at boundary 1 and therefore to calculate the ablation rate that is proportional to $V_1 n_1$. The system of equations is closed if the equilibrium vapour pressure can be specified. In the case of Teflon, the equilibrium pressure formula is used:

$$P = P_c \exp(-T_c/T_0) \tag{5}$$

where $P = n_0 kT_0$ is the equilibrium pressure, $P_c = 1.84 \times 10^{20}$ N m^{-2} and $T_c = 20\,815$ K are the characteristic pressure and temperature, respectively [4].

The solution of the problem depends upon plasma density n_2, plasma temperature T_2 and surface temperature T_0. The parameters n_2, T_2 are determined by the bulk plasma flow. It was estimated from various experiments that, under typical PPT operation conditions, the plasma density near the Teflon surface is about 10^{21}–10^{24} m^{-3}, the plasma temperature is about 1–4 eV and the Teflon surface temperature T_0 is about 600–650 K [4, 7, 8, 13]. In the present paper we present solutions with n_2, T_2 and T_0 as parameters in the ranges mentioned above.
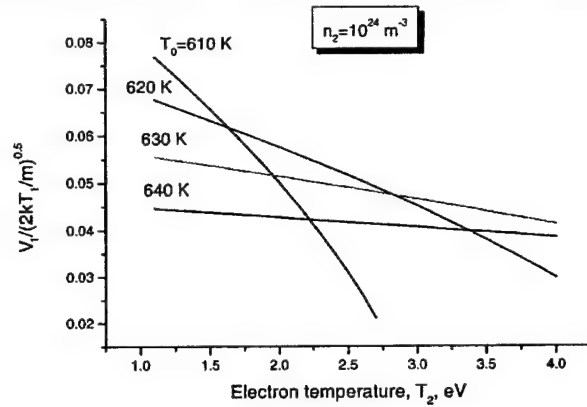

Figure 2. The velocity V_1 as a function of plasma temperature with Teflon surface temperature as a parameter.
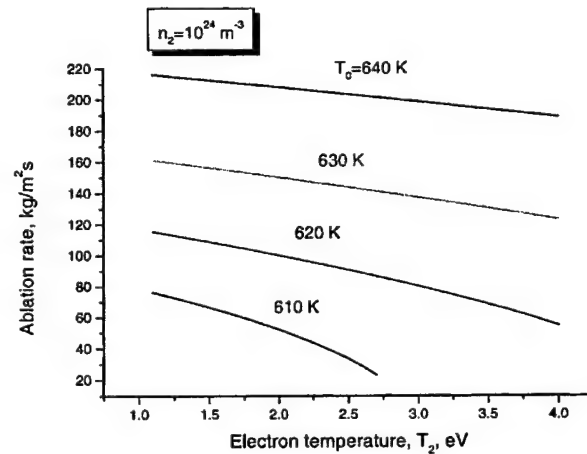

Figure 3. The ablation rate as a function of plasma temperature with Teflon surface temperature as a parameter.

The dependence of the velocity V_1 on the electron temperature T_2 is shown in figure 2 with surface temperature T_0 as a parameter for given n_2. One can see that the velocity V_1 remains small over the entire range of plasma temperature and generally decreases with temperature increase. The velocity V_1 is very sensitive to the plasma temperature variation in the case of relatively small surface temperature. As a result of this dependence, the ablation rate also decreases with increasing electron temperature as shown in figure 3.

Ablation rate contours in the plane with the plasma density and Teflon surface temperature as the coordinates are displayed in figure 4. The same ablation rate that can be found in the high and low density range corresponds to the solution of the problem with small and large velocity at the outer boundary of the kinetic layer, respectively. There is no solution for the ablation rate in regions above the curve with ablation rate equal to zero. This region in the n_2–T_0 plane corresponds to the case when the right-hand side in equation (4) is negative. The physical meaning of these results can be explained as follows. In the ablation-controlled discharge, the plasma density in the bulk is determined by the rate of ablation from the surface. In the case of small surface temperature one can expect a smaller ablation rate and therefore high plasma densities in the discharge cannot be generated.
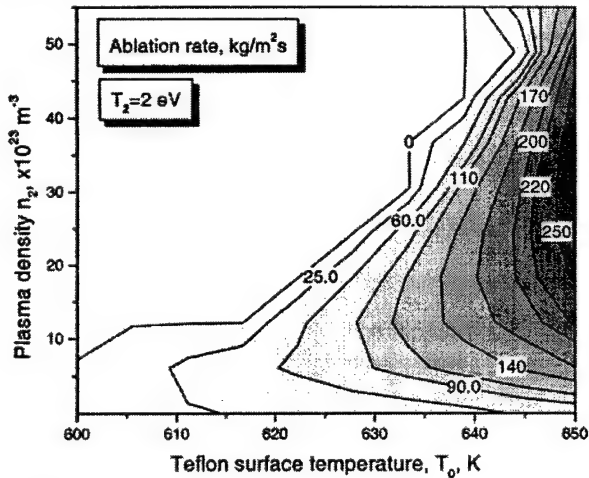
Figure 4. Contours of ablation rate in the plasma density (n_2)–Teflon surface temperature (T_0) plane.

It is important to note that the present model predicts the dependence of the ablation rate on the plasma bulk density, electron temperature and the surface temperature. It is also found that the flow velocity at the outer boundary of the kinetic layer (that determines the ablation rate) is smaller than the sound velocity under typical PPT conditions. In this sense the present model is different from previously used approaches [7, 8], where the ablation rate was determined by the surface temperature only and the sonic velocity was assumed at the outer boundary of the kinetic layer.

In the typical range of PPT parameters considered the maximum ablation rate was calculated to be about $300 \ \mathrm{kg \ m^{-2} \ s^{-1}}$. It should be noted that the average ablation rate measured in experiments is in the range $1\text{--}40 \ \mathrm{kg \ m^{-2} \ s^{-1}}$ depending on the parameters n_2, T_2 for different thruster types [4, 13]. During the discharge pulse, the plasma parameters vary so that near the current peak one can expect an ablation rate higher than average while towards the end of the pulse the ablation rate decreases. The time-averaged ablated mass calculated using this model for baseline PPT-4 is about

$24 \ \mathrm{kg \ m^{-2} \ s^{-1}}$, which is close to that measured in the experiment ($\sim 29 \ \mathrm{kg \ m^{-2} \ s^{-1}}$, [13]).

In summary, we have developed a kinetic model of the material ablation in an ablated controlled discharge with application to a pulsed plasma thruster. The model accounts for the case when the velocity at the outer boundary of the kinetic layer is smaller than the sound velocity due to the presence of a high-density discharge plasma. The present model can be coupled with a plasma discharge model to describe the electrical discharge self-consistently.

Acknowledgments

References

[1] Muller L 1993 *J. Phys. D: Appl. Phys.* **26** 1253
[2] Domejean E, Chevrier P, Fievet C and Petit P 1997 *J. Phys. D: Appl. Phys.* **30** 2132
[3] Kukhlevsky S V, Kaiser J, Samek O, Liska M and Erostyak J 2000 *J. Phys. D: Appl. Phys.* **33** 1090
[4] Burton R L and Turchi P J 1998 *J. Prop. Power* **14** 716
[5] Hong D, Dussart R, Cachoncinlle C, Rosenfeld W, Gotze S, Pons J, Viladrosa R, Fleurier C and Pouvesle J M 2000 *Rev. Sci. Instrum.* **71** 15
[6] Langmuir I 1913 *Phys. Rev.* **2** 329
[7] Keidar M, Boyd I D and Beilis I I 2000 *IEEE Trans. Plasma Sci.* **27** 376
[8] Mikellides Y G 1999 Theoretical modeling and optimization of ablation-fed pulsed plasma thruster *PhD Thesis* The Ohio State University
[9] Beilis I I 1985 *IEEE Trans. Plasma Sci.* **13** 288
[10] Beilis I I 1995 Theoretical modeling of cathode spot phenomena *Vacuum Arc Science and Technology* ed R L Boxman, P Martin and D Sanders (Park Ridge, NJ: Noyes)
[11] Anisimov S I 1968 *Sov. Phys.–JETP* **27** 182
[12] Keidar M, Fan J, Boyd I D and Beilis I I 2001 *J. Appl. Phys.* **89** 3095
[13] Burton R L and Bushman S S 1999 *AIAA Paper* 99-2288

Model of Particulate Interaction with Plasma in a Teflon Pulsed Plasma Thruster

Michael Keidar* and Iain D. Boyd†
University of Michigan, Ann Arbor, Michigan 48109
and
Isak I. Beilis‡
Tel Aviv University, Tel Aviv 69978, Israel

The presence of particulates [referred to as macroparticles (MPs)] in the plume of a pulsed plasma thruster (PPT) may affect interaction with the spacecraft. Possible particulate related effects depend on particulate properties. The MPs emitted into the plasma during the discharge may be charged, accelerated, and heated by the ion, electron, and neutral fluxes depending on the MP residual time. Different aspects of MP–plasma interaction in the experimentally observed range of MP radii (0.1–100 μm) are analyzed. It is found that the charging time is smaller whereas the steady-state potential is larger in the case of a large MP. A 1-μm MP is found to have a charge of about 10^5 electrons in the case of an electron density of about 10^{23} m^{-3}. The two primary forces acting on the MP in the PPT discharge are a drag force due to collision with neutral atoms and ions and an electric force due to the presence of the electric field in the current carrying plasma. The calculation of the MP velocity shows that the maximum possible velocity of a 1-μm MP is about 230 m/s, which is close to that estimated experimentally. Only small MPs ($\sim$ 0.1 μm) can be entrained by the plasma jet, whereas large MPs are generally slower and flow substantially behind the plasma jet. MP temperature and decomposition rates are calculated by solving a heat balance equation. It is found that small MPs (<1 μm) may completely decompose during a 1-μs pulse.

Nomenclature

C	=	specific heat
C_s	=	sound speed
E	=	electric field
F_d	=	total drag force
g	=	Teflon® ablation rate
I	=	discharge current
$J_e(r)$	=	electron current density in the sheath around microparticle (MP)
J_{e0}	=	electron thermal flux at the plasma–sheath interface
$J_i(r)$	=	ion current density in the sheath around MP
J_{i0}	=	ion flux in the absence of a field at the plasma–sheath interface
j	=	current density
L	=	cavity length
L_D	=	Debye length
M_p	=	MP mass
m_a	=	atom mass
N	=	plasma density at the plasma–sheath interface
N_a	=	plasma density near the anode, that is, where $z=0$
Nu	=	Nusselt number
n	=	plasma density normalized by N_a
P_0	=	equilibrium pressure
Q_d	=	cooling rate due to decomposition of material
$Q_{i,e}$	=	heat rate due to ion and electron flux
Q_n	=	neutral atom heat flux
Q_p	=	MP charge
Q_r	=	radiation cooling rate
R_p	=	MP radius
R_{p0}	=	initial MP radius
r_a	=	radius of cavity
T	=	neutral gas temperature
T_e	=	electron temperature
T_i	=	ion temperature
T_p	=	MP temperature
U_p	=	MP potential with respect to the plasma
U_s	=	potential drop in the near spacecraft surface sheath
V	=	plasma velocity
V_d	=	MP ablation rate
V_p	=	MP velocity
V_{pn}	=	normal component of the MP velocity
v	=	plasma velocity normalized by the sound speed
z	=	coordinate in the axial direction normalized by cavity length
α	=	heat transfer coefficient
ΔH	=	ablation heat
ΔT	=	temperature difference between the plasma and the MP
Δt	=	residual time of MP in discharge
ε	=	dielectric permittivity of Teflon®
ε_0	=	permittivity of vacuum
λ_C	=	mean free path
ξ	=	particle emissivity
ρ	=	specific density
σ	=	plasma conductivity
σ_r	=	Stefan–Boltzmann constant
τ	=	dimensionless time, L_D/C_s
ϕ	=	normalized MP potential, eU_p/kT_e

*Associate Professor, Department of Aerospace Engineering. Senior Member AIAA.

†Research Fellow, Department of Aerospace Engineering. Member AIAA.

‡Professor, Electrical Discharge and Plasma Laboratory, P.O. Box 39040.

I. Introduction

THE pulsed plasma thruster (PPT) has been reconsidered recently as an attractive spacecraft propulsion option.[1,2] This has happened mainly due to a greater emphasis being placed on the development of satellites with reduced size for many applications. PPTs are expected to provide exact impulse bits to be used for accurate attitude control. The principal advantage of PPTs is their simple design, which provides high reliability. In particular, the higher reliability of the PPT is achieved through the use of solid propellant, which eliminates design and operation complexity connected with using liquid and gas propellants.

Unfortunately, the PPT has a very poor performance characteristic. For instance, a flight-qualified PPT design had an efficiency of about 8% (Ref. 3). One of the factors leading to low efficiency is the late neutral ablation.[4] Another factor that may significantly reduce the efficiency is the particulate emission. Estimates have shown that the particulate emission consumes about 40% of the total propellant mass, albeit contributing only 1% to the total thrust.[5]

Particulates, sometimes referred to as macroparticles (MPs), are emitted during the pulse and may interact with the surrounding plasma. Various experimental and theoretical aspects of MP interaction with plasma have been studied in different systems such as plasma assisted chemical vapor deposition,[6] plasma etching,[7] rf and glow discharge,[8,9] cathodic vacuum arc deposition,[10,11] and in-space plasma.[12] The MPs are subjected to charging, heating, and momentum transfer.[6-12] It may be concluded that in spite of many common features of MP–plasma interaction, the MP charge, velocity, and temperature depend on properties of the plasma and MP related to each specific system. Recently, results for the MP size distribution in a PPT have been presented by Spanjers et al.[5] Particulates were observed to have characteristic diameters ranging from about 0.1 μm to over 100 μm. The PPT plasma has a weak degree of ionization.[1] Thus, one can expect an important role of the neutral component in the momentum and energy transfer to MPs. No analyses of MP interaction with the PPT plasma have been reported previously. The present work has the primary objective of removing this deficiency by analyses of different aspects of MP behavior of a PPT, such as charging, acceleration, heating, and decomposition. This work will provide additional information about MPs to help mission planners in estimating the particulate contamination potential.

II. Model of MP–Plasma Interaction

In the present section we will develop the model of MP interaction with plasma, including MP charging, transport, and heating in a pulsed discharge. As a working example, we will concentrate on a specific type of PPT, developed at the University of Illinois, the so-called PPT-4 (Ref. 1). This PPT has a coaxial configuration in which Teflon® is ablated from a cylindrical cavity sitting in front of the central electrode of 6-mm diam and an annular electrode of 43-mm diam. The two electrodes are connected with a 30-deg half-angle nozzle. The typical PPT-4 pulse duration is about 10 μs with a current peak of about 8 kA. The main physical process in this type of thruster occurs in the Teflon cavity. Rapid heating of a thin dielectric surface layer leads to decomposition of the material of the wall. As a result of heating, decomposition, and partial ionization of the decomposition products, the total number of particles increases in the cavity.

At the same time, nonuniformities in the discharge distribution across the Teflon surface may cause overheating followed by phase change of propellant.[1] High plasma pressure in the PPT channel may lead to Teflon MP generation. However, the mechanism of such MP generation from the propellant is not understood sufficiently. Another possible source of MPs is the spot attachment at electrodes that is a typical phenomenon in the early stages of discharge.[13] Several scenarios leading to particle generation from the electrodes are possible: action of the plasma pressure on the liquid pool in the quasi-steady regime may form droplets, similar to that occurring in the vacuum arc cathode spot[14]; growth of the perturbation of the liquid surface due to the Rayleigh–Taylor instability may result in liquid jet fragmentation and small droplet generation, as it occurs in liquid-metal ion sources[15]; solid-particle generation due to a wave of thermoelastic stresses may also be caused by local overheating.[16]

In the experiment, basically two populations of MPs were found.[5] One population of MPs is characterized by a diameter less than 1 μm and by a spherical shape. It was concluded that these MPs come from the steel PPT electrodes[5] due to discharge attachment. The second population has a more random shape and size with maximal size up to 200 μm. The second population is concluded to be originated from the Teflon propellant.[5] In PPT-4, where copper electrodes were used, tracks of discharge attachment at the electrodes were not observed, as was noted in a private communication with R. L. Burton. However, Teflon macroparticles may still be generated that have a sig-
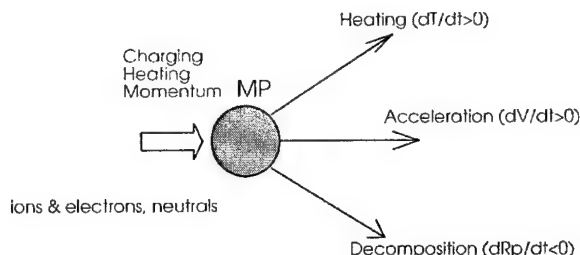

Fig. 1 Schematic presentation of MP–plasma interaction.

nificant effect on propellant losses. Thus, as we consider the PPT-4 configuration in the present paper, we will concentrate on these MPs.

The MPs emitted into the plasma during the discharge may be charged, accelerated, and heated by the ion, electron, and neutral fluxes, depending on the MP residual time. It is assumed in the model that the MP may be emitted at any point of time during to the discharge pulse. This implies that MPs generated at the later stage of discharge will have less time for interaction with plasma. The scheme of MP–plasma interaction is shown in Fig. 1. The present model is based on the assumption that during the MP flight the plasma parameters do not change significantly, that is, the following condition is fulfilled: $V_p \Delta t \ll (\partial \ln X / \partial z)^{-1}$, where X is any of the plasma parameters (velocity, density, and temperature). This model of plasma–MP interaction is approximation to the more complex reality in which plasma parameters vary during the MP residual time. In the present model, we will analyze the plasma–MP interaction having plasma density and velocity that lie in the range of their possible variation during the discharge pulse, as free parameters of the problem.

A. Quasi-Steady-State Plasma Model

The main features of the electrical discharge in the dielectric cavity include joule heating of the plasma, heat transfer to the Teflon, decomposition followed by ionization, and acceleration of the plasma up to the sound speed at the cavity exit. In this section, we will present a simple quasi-stationary model of the plasma flow in the Teflon cavity. A quasi-steady-state approach to the PPT flow has numerous limitations.[17] It requires that the propellant ablation must supply material to the discharge chamber in times shorter than the characteristic flow convection time, which, in turn, should be less than the characteristic time of discharge parameter variation. However, this approach may provide some useful information about the possible range of density in the discharge chamber and the spatial plasma density and velocity distribution along the cavity length. In the present model the plasma velocity and density will be used in the MP–plasma interaction model as parameters.

We apply a one-dimensional hydrodynamic model for the plasma under the assumption that the Teflon evaporates uniformly. Products of Teflon evaporation are partially ionized in the cavity. Partially ionized plasma conducts the current, which is carried in the direction parallel to the plasma flow. Therefore, for simplicity, we omit effects connected with electric and self-magnetic fields. Partially ionized plasma accelerates in the axial direction due to the pressure gradient and achieves the sound speed at the cavity exit plane.[18] Note that this is a dominant acceleration mechanism in the electrothermal PPT-4 device, whereas traditional PPT has predominant electromagnetic acceleration mechanism. Teflon evaporation is the origin of the source term in the mass conservation equation. In this case, the governing equations in dimensionless form are

$$\frac{dv}{dz} = \frac{\beta}{n(1 - v^2)} \qquad (1)$$

$$\frac{dn}{dz} = -\frac{n}{v}\frac{dv}{dz} + \frac{\beta}{v} \qquad (2)$$

where $\beta = g/(N_a C_s m_a \pi r_a^2)$ and $C_s = ([kT_e + kT_i]/m_i)^{0.5}$. The following boundary conditions are used for Eqs. (1) and (2): $n(z = 0) = 1$ and $dv/dz = 0$.
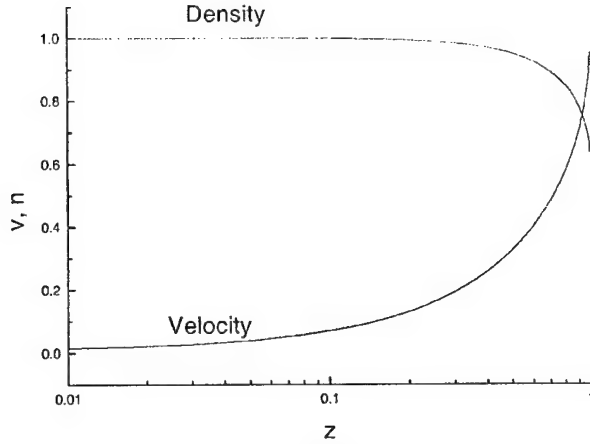
Fig. 2 Plasma density and velocity spatial distribution in the cavity, $\beta = 0.6$.

The plasma density and velocity distribution are shown in Fig. 2. Note that the plasma is significantly accelerated toward the cavity exit. Burton et al. obtained similar flowfield development in a liquid-injected capillary discharge[19] when the plasma flow approaches steady-state conditions. Taking into account that the plasma velocity should be sonic at the exit ($z = 1$), it is found that $\beta = 0.6$. In one PPT-4 design it was measured that the ablation rate is about 30 μg per 10-μs pulse.[20] One can estimate that the plasma density near the central electrode should be $\sim 10^{24}$ m^{-3} using this experimental value for g. Note, however, that the aforementioned estimated number density of the plasma in the cavity represents the low limit. This is because it was assumed that, in the framework of a quasi-steady-state model, the characteristic time is equal simply to the pulse duration. Under the assumption that the characteristic discharge time is about the acoustic time (L/C_s, which is typically a few microseconds) the plasma density near the central electrode may be substantially higher (up to an order of magnitude) than the preceding estimation.

B. MP Charging

An experimental investigation of the MP size distribution showed a variation from 0.1 up to 100 μm (Ref. 5). It was also found that some MPs have a spherical shape, whereas generally MPs have a rather random shape distribution.[5] To make it possible to develop a model quantitatively, we will assume that all MPs have a spherical shape with radii in the experimentally observed range. Under the typical conditions of PPT-4 operation, the electron density in the cavity during the pulse is about 10^{21}–10^{24} m^{-3}, which corresponds to a debye length of about 10^{-6}–10^{-7} m. It is known that the thickness of the sheath around a MP is about the Debye length.[21,22] Therefore, one can see that there are basically two cases: small MPs for which the Debye length is less than or about the MP radius, and large MPs for which the Debye length is much less than the MP radius. These two cases may be handled using different approaches for modeling the charging process. The second case is more straightforward and corresponds to that of a plane probe. The MP charging in the first case was developed in detail in Ref. 22.

In both cases, the MP charging process is modeled with the aid of the following assumptions: 1) The plasma consists of two species of charged particles. For PPT-4 conditions, thermal equilibrium between all species is achieved and, therefore, we assume that $T = T_e = T_i$. 2) The plasma jet flow is not substantially obstructed in the sheath around the MP, and, thus, spherical symmetry of the plasma density relative to the MP is assumed. 3) Self-magnetic field effects are neglected because PPT-4 has predominantly electrothermal acceleration mechanism.

The kinetics of the MP charging is controlled by the ion and electron fluxes to the MP, which depend on the potential distribution in the sheath. Using Maxwell's equation and assumption 3, the electric field $E(r)$ changes with time according to the relation

$$\varepsilon \frac{\partial E(r)}{\partial t} = -[J_i(r) + J_e(r)] \tag{3}$$

The time derivative of the electric field is a function of the radius r. An estimation indicated[22] that the characteristic time for the electric field to reach steady state decreases with radius and has its maximum value at the MP surface, that is, where $r = R_p$. Thus, Eq. (3) will be solved at the radius R_p. The electron and ion current densities are required to solve Eq. (3). The electron current density is calculated according to the following relation:

$$J_e = J_{e0} \exp(-eU_p/kT_e) \tag{4}$$

The ion current density depends on the ratio of Debye length to the MP radius and, thus, will be different for small and large MPs.

1. Small MPs

This case corresponds to the low limit of the measured MP size distribution function. In the case of a spherical sheath around an MP and $L_D > R_p$, the ion flux may be calculated using the orbital motion limit[23,24]:

$$J_i = J_{i0}(1 + eU_p/kT_i) \tag{5}$$

This expression is exact for an infinite L_D/R_p ratio. By considering different ion trajectories around the MP, it is possible to calculate the ion flux for a finite L_D/R_p ratio. An influence of this effect was examined in detail in Ref. 22.

In the general case, the capacitance of the MP in the plasma is given by $C = Q_p/U_p = 4\pi R_p \varepsilon_0 G(R_p/L_D)$. The function $G(R_p/L_D)$ is presented in Ref. 22, and, for the case $R_p/L_D \approx 1$, this function is $G(R_p/L_D) \approx 1.8$, whereas in the orbital motion limit this function is equal to 1.

When we take into account the preceding expression for MP capacitance and combine Eqs. (3–5), the kinetics of MP charging may be described by the following dimensionless equation (in the orbital motion limit):

$$\frac{d\phi}{d\tau} = \frac{R_p}{L_D} \frac{1}{\sqrt{2\pi}} \left(1 + \phi - \sqrt{\frac{m_i}{m_e}} e^{-\phi}\right) \tag{6}$$

2. Large MPs

In this case, the sheath model near the planar electrode can be used. Because in the cavity the plasma velocity is less than the sound speed (see Sec. II.A), the ion flux can be calculated from the Bohm expression[25]:

$$J_i = 0.4eNC_s \tag{7}$$

The capacitance in this case reads[26]

$$C = 4\pi R_p^2 \varepsilon_0 (1/R_p + 1/L_D) \sim 4\pi\varepsilon_0 \left(R^2/L_D\right) \tag{8}$$

When we take into account the expression for MP capacitance, the kinetics of MP charging may be described by the following dimensionless equation:

$$\frac{d\phi}{d\tau} = \left(0.4 - \sqrt{\frac{m_i}{2\pi m_e}} e^{-\phi}\right) \tag{9}$$

The time variation of the dimensionless MP potential is shown in Fig. 3 for two limiting cases of $R_p/L_D \gg 1$ and $R_p/L_D \ll 1$. Note that the charging time is smaller, whereas the steady-state potential is larger in the case $R_p/L_D \gg 1$. The steady-state potential increases from about 3.5 in the case of $R_p/L_D \ll 1$ up to about 5 in the case of $R_p/L_D \gg 1$. All possible cases realized in a typical PPT are placed between the limits of these two curves. Thus, in the PPT plasma with $T = 2$ eV, MP has a negative potential of about $-(7 \div 10)$ V with respect to the plasma.
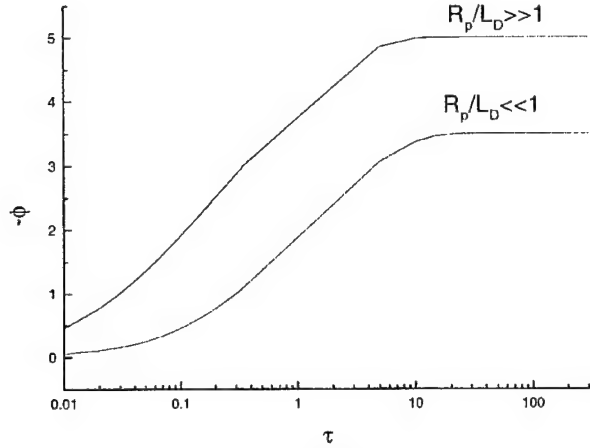
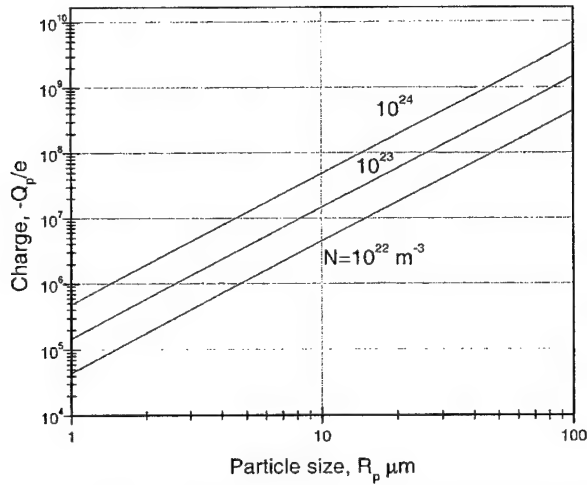Fig. 3 Temporal behavior of dimensionless MP potential with R_p/L_D as a parameter.

Fig. 4 MP charge dependence on the radius with electron density as a parameter, $T_e = 1.5$ eV.

3. MP Charge

To calculate possible values of the charge accumulated on the MP, we will convert from the dimensionless parameters. The MP charge (in the large MP limit) may be connected with the dimensionless potential as follows:

$$Q_p = 4\pi R_p^2 L_D N\phi \qquad (10a)$$

In the small MP limit, the corresponding expression for the MP charge reads

$$Q_p = 4\pi \varepsilon_0 R_p \phi kT_e/e \qquad (10b)$$

The calculated steady-state MP charge as a function of MP radius is shown in Fig. 4 with electron density as a parameter for the large MP limit ($R_p > 1\ \mu$m). Note that the 1-μm MP has a charge of about 10^5 electrons in the case of $N = 10^{23}$ m^{-3}. One can see that, in this case, MP charge increases with electron density unlike the other case (small MP with $R_p < 1\ \mu$m) when Q_p is independent of the plasma density. In the latter case, the MP charge is a linear function of R_p and can be estimated as $Q_p = 2.4 \cdot 10^3 \times R_p$ (micrometers) where Q_p is in electrons.

C. Momentum Transfer

There are two primary forces acting on the MP in the PPT discharge: 1) a drag force due to collision with neutral atoms and ions and 2) a force due to the presence of the electric field in a current

carrying plasma. To predict the MP velocity, we simply integrate the equation of motion from some starting point. We assumed that MPs have zero initial velocity. Given the solution for plasma density and velocity distribution in the cavity, we evaluate the forces that act on an individual MP. The equation of motion of an individual MP may be written as

$$\frac{d(M_p V_p)}{dt} = F_d + Q_p E \qquad (11)$$

The mass M_p of the MP traveling in the plasma may be changed as a result of MP ablation (see next section).

The first term is the total drag force and the second term is the electric force, which depends on the electric field in the plasma and the MP charge. An average electric field E in the plasma may be calculated from Ohm's law for known current density j, namely, $E = j/\sigma$. We will consider a diffuse discharge on the anode and, therefore, $j = I/\pi r_a^2$. The current density was estimated at the current peak of about 8 kA and plasma conductivity was calculated for electron temperature of about 2 eV (see Ref. 20).

In partially ionized plasmas, there are coulomb collisions of the MP with ions because the MP is charged. These collisions contribute to the drag and may result in a force called ion drag.[27] In low-density plasmas with large ratio of Debye length to MP radius (small MPs, see preceding section), it was found that the momentum transfer due to ions that are collected by a MP cross section is much less than that due to ions scattered but not collected.[21] Note that if the Debye length is much less than or about the MP size (large MPs), the momentum transfer is determined by the MP cross section.[28] In general, the neutral drag force is also determined by the MP cross section. Analyses of the MP size distribution and range of possible plasma densities (10^{21}–10^{24} m^{-3}) shows that both free molecular and continuum regimes for the drag force can be realized.

1. Small MP (Free Molecular Regime)

In the free molecular regime, that is, $R_p \ll \lambda_c$, the drag force can be written as[29]

$$F_d = \left(\sqrt{\pi}\rho R_p^2/2\beta\right)\left\{[s + (1/2s)\exp(-s^2)]\right.$$
$$\left. + (s^2 + 1 - 1/4s^2)\sqrt{\pi}\,\text{erf}(s)\right\} \qquad (12)$$

where $\beta = m/2kT$ and $s = 2V_p/[\sqrt(\pi)(V - V_p)]$.

### 2. Large MP (Continuum Regime)

In this case the drag force that acts on the isolated MP placed into a plasma moving with velocity V is determined by the expression[30,31]

$$F_d = C_D \pi R_p^2 \rho (V - V_p)^2/2 \qquad (13)$$

where C_D is the drag coefficient that depends on the Reynolds number. For instance, in the case of $Re \leq 1$, coefficient $C_D = 24.8/Re$ (Refs. 30 and 31). Estimation shows that in the PPT plasma, the Reynolds number is about 10^{-3} V, where V is the plasma velocity in meters per second.

The calculation of the MP velocity in the continuum regime as a function of time with normalized plasma velocity as a parameter is plotted in Fig. 5a for the case $R_p = 1\ \mu$m. Note that the maximum possible MP velocity is about 230 m/s. In experiments it was found that some MPs have a velocity of about 200 m/s (Ref. 5). Smaller MPs may have a larger velocity as shown in Fig. 5b for the case of $R_p = 0.1\ \mu$m, calculated in the free molecular regime. One can see that the MP velocity depends on the residual time in the discharge. Thus, those MPs generated toward the end of the pulse are expected to have a smaller velocity.

The ratio of MP velocity to the plasma velocity dependence on the MP radius is shown in Fig. 6 with plasma density as a parameter. These calculations are performed for the case of MP residual time
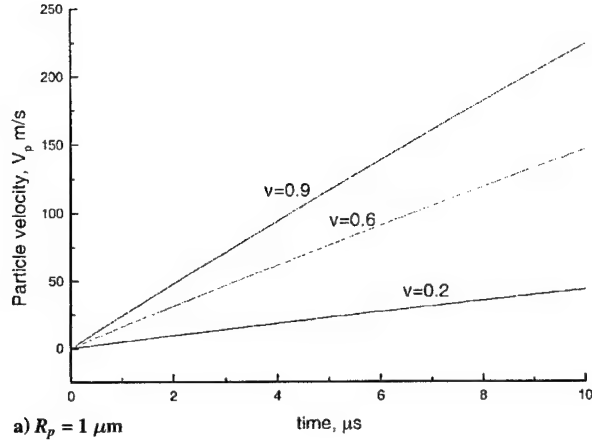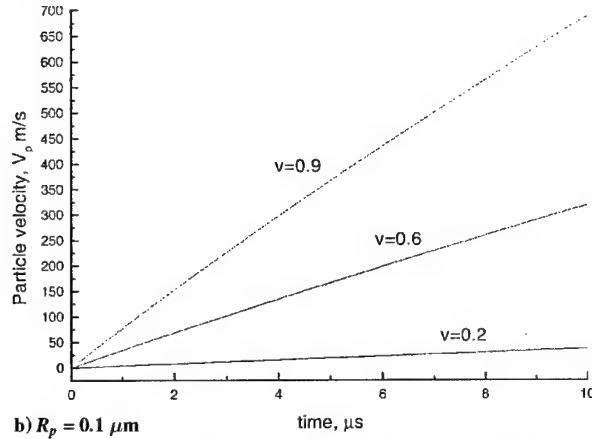
Fig. 5 Temporal behavior of the MP velocity with dimensionless plasma velocity as a parameter, $T_e = 1.5$ eV and $N = 10^{23}$ m^{-3}.
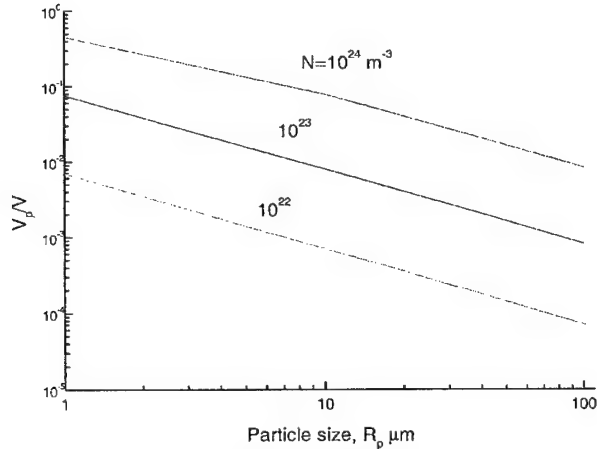
Fig. 6 Normalized MP velocity dependence on the MP radius with plasma density as a parameter, $T_e = 1.5$ eV and $\Delta t = 10$ μs.

equal to the discharge pulse, that is, for $t = 10$ μs. One can see that small MPs in the dense plasma can approach the plasma velocity and can be entrained by the plasma jet. However, the large MPs are generally slower and flow substantially behind the plasma jet.

Note that, due to ablation, the MP radius decreases in the course of interaction with the plasma, and, thus, MP-plasma interaction may change from initially continuum to free molecular. An effect of MP ablation is considered in the next section.

D.   Heat Transfer

As the particle moves through the plasma, it is heated by neutral, electron, and ion fluxes and is cooled by radiation. An additional cooling mechanism is due to decomposition of the dielectric material under high temperature. We will consider the situation where the thermal time constant is much shorter than the MP residual time. In this case, the MP has a uniform temperature throughout its volume and inward heat conduction from the surface may be neglected. The resulting energy balance reads

$$\frac{4}{3}\pi R_p^3 \rho C \frac{dT_p}{dt} = 4\pi R_p^2 (Q_{i,e} + Q_n - Q_r - Q_d) \quad (14)$$

According to the charging model (see Sec. II.B) the ion and electron fluxes are equal after the MP reaches steady-state charge. Therefore, the gross energy input by ions and electrons to the MP is given by the current density and the sum of the energy carried by each species:

$$Q_{i,e} = j_i(R_p)[2kT_e + kT_e + eU_p(t)] \quad (15)$$

where $U_p(t)$ is the time-dependent MP potential (see Sec. II.A).

The neutral atoms' heat transfer may be calculated using the Newtonian model

$$Q_n = \alpha \Delta T \quad (16)$$

In the general case, the coefficient of heat transfer is a complex function of MP size, gas flow temperature and velocity, heat conductivity, specific heat, and density. The relation between the coefficient of heat transfer and the preceding parameters was determined by a similarity law.[30] For the convective heat transfer between a body and gas flow, the following similarity can be used:

$$Nu = \alpha R_p / \lambda \quad (17)$$

Considering plasma–MP interaction in the PPT-4 cavity, one can estimate Nusselt number in the case when the particle is not moving relative to the plasma. In this case the Nusselt number Nu equals 2 (Ref. 30). The dependence of atomic thermal conductivity on temperature is given by: $\lambda = 2.4 \times 10^{-4} T^{3/4}$ W/mK (Ref. 30).

The radiative flux is given by the Stefan–Boltzmann law:

$$Q_r = \sigma_r \xi T^4 \quad (18)$$

The heat flux associated with material decomposition can be calculated as

$$Q_d = V_d \Delta H \quad (19)$$

The ablation rate can be estimated at equilibrium using Knudsen's law:

$$V_d = P_0/\rho \sqrt{m_a/(2\pi kT)} \quad (20)$$

where P_0 is the equilibrium pressure of Teflon (see Refs. 1 and 4).

The rate of the MP radius change is determined by the ablation rate V_d:

$$\frac{dR_p}{dt} = -V_d \quad (21)$$

The initial condition is $R_p(t = 0) = R_{p0}$.

The calculated temporal variation of the MP temperature is shown in Fig. 7 with MP radius as a parameter. It can be seen that small MPs are heated substantially up to 1000 K during a short time period, whereas large MPs are only slightly affected by the plasma. Heating of the MP leads to significant ablation as plotted in Fig. 8. Note that small MPs (~1 μm) completely ablate if their residual time is larger than 0.5 μs.
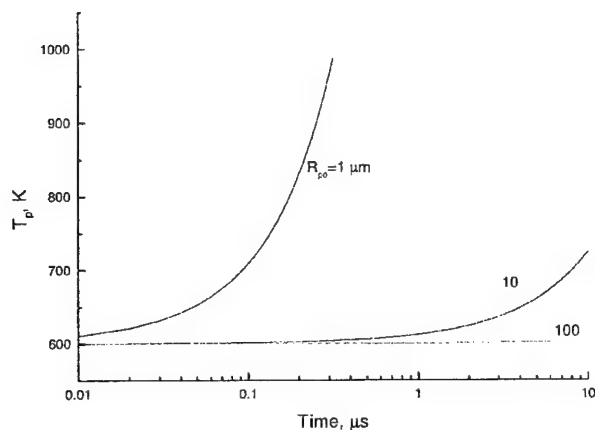
Fig. 7   Temporal dependence of the MP temperature with the MP radius as a parameter, $T_e = 1.5$ eV and $N = 10^{23}$ m^{-3}.
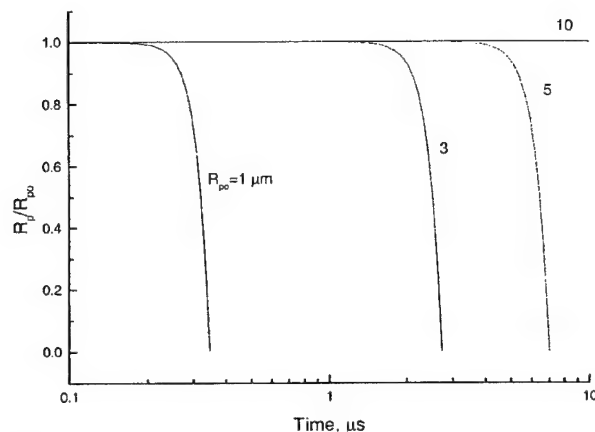

Fig. 8   MP radius vs time with the initial MP radius as a parameter, $T_e = 1.5$ eV and $N = 10^{23}$ m^{-3}.

III.   Discussion

One of the important possible applications of the PPT is for attitude control of small satellites that are part of a group of close-flying satellites. In this case, interaction of the integrated plasma plume from the PPT with another spacecraft becomes an important issue. An experimental investigation has shown that the plasma plume contains a substantial fraction of MPs that originated from the dielectric as well as from the electrodes. The presence of such particles in the interacting plume may be a source of local damage to the spacecraft. The potential for MP damage on their collision with spacecraft surfaces depends on the MP directed velocity. The present calculation shows that the MP velocity depends mainly on MP size and residual time in the discharge. It was assumed that MP–plasma interaction occurs mainly during the discharge pulse. This is because the plasma density and temperature that control the interaction drop substantially after the pulse. Therefore, the maximum MP residual time considered in this model was equal to the pulse duration. Those small MPs emitted at the beginning of the discharge pulse may have a velocity of 200 m/s. Thus, one can expect a relatively broad range of MP velocity from zero up to a few hundred meters per second depending on the point of MP formation and the MP size. Another useful outcome from the MP velocity calculation is the possibility to estimate some characteristic time of MP flux ejection. Because MP velocity is generally smaller than the plasma velocity, and due to the broad range of MP velocities, the effective time of MP ejection from the thruster is much larger than the pulse duration. For instance, our estimation shows that the large MPs ($\sim$100 μm) exhaust from the thruster only after several seconds.

Because of the possible electrostatic nature of MP interaction with a spacecraft, the MP charge may play an important role. A spacecraft interacts with a plasma jet so as to become electrically charged to ensure zero net current, just like the MP. Thus, because the spacecraft has some negative potential with respect to the plasma, the MP may interact with the electric field in the thin sheath around the spacecraft. In some cases, the MP may be reflected in the sheath without mechanical collision with the surface. This effect has a positive role because the electrostatic nature of MP interaction with surfaces in space is not then connected with any mechanical damage. Thus, it is important to estimate the possibility of such MP–surface interactions. Previously, this effect was studied for the case of vacuum arc-generated MPs.[10,11] It was obtained both theoretically and experimentally for typical conditions that the electrostatic nature of the MP interaction with surfaces (without mechanical touching) is possible. It occurs in those cases when an MP approaches the surface with a grazing angle such that the MP kinetic energy will be smaller than the potential electrostatic energy. The possibility of this effect may be estimated using the following integral expression:

$$Q_p U_s > M_p V_{pn}^2 / 2$$

For instance, if the spacecraft potential U_s is about 10 V, a 1-μm MP may be electrostatically reflected if its normal velocity component is less than 4 m/s.

Another important outcome from the present study is prediction of the MP complete or partial decomposition due to interaction with the plasma during the discharge pulse. It was found that MPs with size less than 10 μm may totally decompose during 10 μs. However, large MPs may be still be present in the plasma plume. This means that the size distribution of MPs exhausted from the PPT is different from the original MP distribution. According to our calculation, the difference is more significant in the range of small MPs. Thus, any measurements of the MP flux in the plasma plume involve some combination of the original MP distribution and that from MP–plasma interaction rather than the size distribution of MPs emitted from the Teflon.[32] Note also that the MP decomposition may be a substantial volume source of the neutral component of the discharge plasma. However, because there is an uncertainty in the original MP size distribution, the significance of the last effect cannot be estimated accurately. One can also conclude that the increase in MP residence time leads to MP decomposition and, therefore, may have some effect on increasing propellant efficiency.

Note that in this paper the MP–plasma interaction was considered for the conditions typical for the electrothermal PPT-4 device. This device is fundamentally different from the usual LES 8/9 class PPT with dominant electromagnetic acceleration mechanism. It appears that the basic features of the present model should be same for electromagnetic PPT. The main difference is a much higher plasma velocity realized in this PPT due to $J \times B$ acceleration. It implies that the effective MP residual time may decreases, and, therefore, the MP charging, acceleration, and heating may be affected. Higher plasma velocity will increase the ion flux to the MP that may lead to increase MP charge in the steady state. However, because the MP steady-state charge depends logarithmically on the ion flux, one would expect only small changes. Small (submicrometer) MPs have the potential for acceleration when they interact with a high-velocity plasma jet.

IV.   Conclusion

We have shown that the plasma may affect particulate contamination from the plume of a PPT. During flight, a MP may become charged, heated, and accelerated. It was found that the charging time depends on MP size and is generally smaller in the case of small MPs. We have found that a 1-μm MP has a charge of about 10^5 electrons in the case of an electron density of about 10^{23} m^{-3}. There are two primary forces acting on the MP in the PPT discharge: a drag force due to collision with neutral atoms and ions and an electric force due to the presence of the electric field in a current carrying plasma. The maximum possible velocity of a 1-μm MP is about 230 m/s, which is close to that estimated experimentally. Only small

MPs ($\sim$0.1 μm) can be entrained by the plasma jet, whereas large MPs are generally slower and flow substantially behind the plasma jet. Small MPs (<1 μm) may completely decompose during a 1-μs pulse.

Acknowledgments

References

[1]Burton, R. L., and Turchi, P. J., "Pulsed Plasma Thruster," *Journal of Propulsion and Power*, Vol. 14, No. 5, 1998, pp. 716–735.

[2]Spores, R. A., Cohen R. B., and Birkan, M., "The USAF Electric Propulsion Program," *Proceedings of the 25th International Electrical Propulsion Conference*, Electric Rocket Propulsion Society, Worthington, OH, 1997, pp. 1–8.

[3]Vondra, R. J., "The MIT Lincoln Laboratory Pulsed Plasma Thruster," AIAA Paper 76-998, July 1976.

[4]Mikellindes, P. G., and Turchi, P. J., "Modeling of Late-Time Ablation in Teflon Pulsed Plasma Thruster," AIAA Paper 96-2733, July 1996.

[5]Spanjers, G. G., Lotspeich, J. S., McFall, K. A., and Spores, R. A., "Propellant Losses Because of Particulate Emission in a Pulsed Plasma Thruster," *Journal of Propulsion and Power*, Vol. 14, No. 4, 1998, pp. 554–559.

[6]Roth, R. M., Spears, K. G., Stein, G. D., and Wong, G., "Spatial Dependence of Particle Light Scattering in an of Silence Discharge," "Spatial Dependence of Particle Light Scattering in an rf Silane Discharge," *Applied Physics Letters*, Vol. 46, No. 3, 1985, pp. 253–255.

[7]Hwang, H., Keiter, E. R., and Kushner, M. J., "Consequences of Three-Dimensional Physical and Electromagnetic Structures on Dust Particle Trapping in High Plasma Density Material Processing Discharges," *Journal Vacuum Science Technology*, Vol. A 16, No. 4, 1998, p. 2454.

[8]Selwyn, G. S., Heidenreich, J. E., and Haller, K. L., "Particle Trapping Phenomena in Radio Frequency Plasmas," *Applied Physics Letters*, Vol. 57, No. 18, 1990, pp. 1876–1878.

[9]Barnes, M. S., Keller, J. H., Forster, J. C., O'Neil, J. A., and Coultas, D. K., "Transport of Dust Particles in Glow-Discharge Plasmas," *Physical Review Letters*, Vol. 68, No. 3, 1992, pp. 313–316.

[10]Keidar, M., Beilis, I. I., Boxman, R. L., and Goldsmith, S., "Transport of Macroparticles in Magnetized Plasma Ducts," *IEEE Transactions on Plasma Science*, Vol. 26, No. 2, 1996, pp. 226–234.

[11]Keidar, M., Beilis, I. I., Aharonov, Arbilly, R. D., Boxman, R. L., and Goldsmith, S., "Macroparticle Distribution in a Quarter-Torus Plasma Duct of a Filtered Vacuum Arc Deposition System," *Journal Physics D: Applied Physics*, Vol. 30, Nov. 1997, pp. 2972–2978.

[12]Gatsonis, N. A., Erlandson, R. E., and Meng, C. I., "Simulation of Dusty Plasmas Near Surfaces in Space," *Journal of Geophysical Research*, Vol. 99, No. A5, 1994, pp. 8479–8489.

[13]Aleksandrov, V. V., Belan, N. V., Koslov, N. P., Mashtylev, N. A., Popov, G. A., and Khvesiyk, V. I., "Pulse Plasma Accelerators," KHAI, Kharkov, 1983 (in Russian), p. 55.

[14]Boxman, R. L., Martin, P. J., and Sanders, D. (eds.), *Handbook of the Vacuum Arc Science and Technology*, Noyes, Park Ridge, NJ, pp. 1995.

[15]Vladimirov, V. V., Badan, V. E., and Gorshkov, V. N., "Microdroplet Emission and Instabilities in Liquid-Metal Ion Sources," *Surface Science*, Vol. 266, April 1992, p. 185.

[16]Parkus, H., *Thermoelasticity*, Blaisdell, Waltham, MA, 1968, pp. 70–100.

[17]Turchi, P. J., "Direction for Improving PPT Performance," *Proceedings of the 25th International Electrical Propulsion Conference*, Electric Rocket Propulsion Society, Worthington, OH, 1997, pp. 251–258.

[18]Ogurtsova, N. N., Podmoshenskii, I. V., and Rogovtsev, P. N., "Calculation of the Parameters of an Optically Dense Plasma Obtained by a Discharge with an Evaporating Wall," *High Temperature*, Vol. 9, 1971, pp. 430–436.

[19]Burton, R. L., Hilko, B. K., Witherspoon, F. D., and Jaafari, G., "Energy-Mass Coupling in High-Pressure Liquid-Injected Arcs," *IEEE Transactions on Plasma Science*, Vol. 19, No. 2, 1991, pp. 340–349.

[20]Bushman, S. S., "Investigation of a Coaxial Pulsed Plasma Thruster," M.S. Thesis, Univ. of Illinois, Urbana-Champaign, IL, May 1999.

[21]Kilgore, M. D., Daugherty, J. E., Porteous, R. K., and Graves, D. B., "Ion Drag on an Isolated Particulate in a Low-Pressure Discharge," *Journal Applied Physics*, Vol. 73, No. 11, 1993, pp. 7195–7202.

[22]Keidar, M., Beilis, I. I., Boxman, R. L., and Goldsmith, S., "Non-Stationary Macroparticle Charging in an Arc Plasma Jet," *IEEE Transactions on Plasma Science*, Vol. 25, No. 6, 1995, pp. 902–908.

[23]Mott-Smith, H. M., and Langmuir, I., "Collectors in the Gaseous Discharges," *Physics Review*, Vol. 28, 1926, p. 727.

[24]Laframboise, J. G., and Parker, L. W., "Probe Design for Orbit-Limited Current Collection," *Physics of Fluids*, Vol. 16, No. 5, 1973, pp. 629–636.

[25]Swift, J. W., and Schwar, M. J. R., *Electrical Probes for Plasma Diagnostics*, Iliffe, London, 1970.

[26]Whipple, E. C., "Potential of Surfaces in Space," *Reports on Progress in Physics*, Vol. 44, 1981, pp. 1197–1250.

[27]Kilgore, M. D., Daugherty, J. E., Porteous, R. K., and Graves, D. B., "Transport and Heating of Small Particles in High Density Plasma Sources," *Journal Vacuum Science and Technology*, Vol. B 12, No. 1, 1994, pp. 486–493.

[28]Boxman, R. L., and Goldsmith, S., "The Interaction Between Plasma and Macroparticles in a Multi-Cathode Spot Vacuum Arc," *Journal of Applied Physics*, Vol. 52, No. 1, 1981, pp. 151–161.

[29]Baines, M. J., Williams, I. P., and Asebiomo, A. S., "Resistance to the Motion of a Small Sphere Moving Through a Gas," *Monthly Notices of the Royal Astronomical Society*, Vol. 130, Sept. 1965, pp. 63–74.

[30]Dresvin, S. V. (ed.), *Physics and Technology of Low-Temperature Plasmas*, Iowa State Univ. Press, Ames, IA, 1977.

[31]Crowe, C. T., "Drag Coefficient of Particles in a Rocket Nozzle," *AIAA Journal*, Vol. 5, May 1967, pp. 1021, 1022.

[32]Newman, R. L., "A Kinetic Treamment of Ablation," *Journal of Spacecraft*, Vol. 3, May–June 1965, pp. 450, 451.

Electromagnetic Effects in the Near Field Plume Exhaust
of a Pulsed Plasma Thruster

Michael Keidar♦ and Iain D. Boyd*

University of Michigan, Ann Arbor, MI 48109

Abstract

In this work we present a model of the near field plasma plume of a Pulsed Plasma Thruster (PPT). As a working example we consider a micro-PPT developed at the Air Force Research Laboratory. This is a miniaturized design of the axisymmetric PPT with a thrust in the 10 μN range that utilizes Teflon[TM] as a propellant. The plasma plume is simulated using hybrid fluid-PIC-DSMC approach. The plasma plume model is combined with Teflon ablation and plasma generation models that provide boundary conditions for the plume. This approach provides a consistent description of the plasma flow from the surface into the near plume. The magnetic field diffusion into the plume region is also considered and plasma acceleration by the electromagnetic mechanism is studied. Teflon ablation and plasma generation analyses show that the Teflon surface temperature and plasma parameters are strongly non-uniform in the radial direction. The plasma density near the propellant surface peaks at about 10^{24} m^{-3} in the middle of the propellant face while the electron temperature peaks at about 4.5 eV near the electrodes. The model predicts ablated mass per pulse of about 1 μg that is close to that measured in experiment. The plume simulation shows that a dense plasma focus is developed at a few mm from the thruster exit plane at the axis. This plasma focus exists during the entire pulse, but the plasma density in the focus decreases from about 2×10^{22} m^{-3} at the beginning of the pulse down to 0.3×10^{22} m^{-3} at 5 μs. The velocity phase is centered at about 30 km/s in the axial direction. At later stages of the pulse there are two ion populations with positive and negative radial velocity. An ion population having negative axial velocity up to about 10 km/s is predicted. This is a significant finding in terms of backflow contamination onto a spacecraft.

♦ *Research Scientist, Department of Aerospace Engineering, Member of AIAA*
* *Associate Professor, Department of Aerospace Engineering, Senior Member of AIAA*

1. Introduction

The pulsed plasma thruster (PPT) was among the first of various electrical propulsion concepts accepted for space flight mainly due to its simplicity and hence high reliability[1]. However, the PPT has an efficiency that is generally low[2] at about 10% leaving open the opportunity for considerable improvement[3]. Currently, PPT's are considered as an attractive propulsion option for stationkeeping and drag makeup purposes of mass and power limited satellites[4,5]. Guaranteeing successful operation of spacecraft using a PPT requires a complete assessment of the spacecraft integration effects. The PPT plume contains various ion and neutral species due to propellant decomposition and possible electrode erosion. Some attempts of PPT plume modeling using particle simulations were performed recently[6,7,8]. In Refs. 7,8 we have considered the plume flowfield exhaust from an electrothermal PPT and therefore electromagnetic effects in the plume were neglected. Different variations of electromagnetic PPTs are also candidates for various missions[9]. Recently, a micro-PPT has being designed at AFRL for delivery of very small impulse bit[10]. This is a simplified miniaturized version of a conventional PPT designed to provide attitude control and stationkeeping for microsatellites. We will use the AFRL micro-PPT as a working example for several reasons. Firstly, electromagnetic ($j \times B$) acceleration is the primary mechanism in this thruster; and secondly, there is no internal flow in this device and therefore the near-field plasma plume is an essential part of the thrust generation process. Therefore careful modeling of the acceleration is needed to understand the characteristics of the device as a whole in addition to being a pre-cursor to accurate estimation of contamination issues. Since in this device there is no separation between the main plasma acceleration region and the plume expansion, both regions must be simulated in one model. Because the plasma acceleration is external, the plasma is sufficiently rarefied so that an MHD approach such as MACH2 (Ref. 11) cannot be used.

An accurate model of the PPT plume relies on the boundary and initial conditions. These conditions can be formulated by consideration of the Teflon ablation process. The Teflon ablation computation is based on a recently developed kinetic ablation model[12,13]. In this model the detailed physics of the Teflon evaporation is studied by consideration of the distribution function of the particles in the kinetic layer adjacent to the surface.

Another important effect related to the plasma plume exhaust from an electromagnetic PPT is the magnetic field diffusion into the near plume. Previously, we have modeled the effect of the magnetic field on the near-field plume for Hall thrusters[14] under steady state conditions. It was found that the magnitude of the magnetic field at the thruster exit has an important effect on the plasma potential distribution in the plume. In the present research, it is proposed to include the electromagnetic effects on the near field plume of unsteady plasma flow. The computational domain is shown in Fig. 1. The model is based on a hybrid approach involving a DSMC description of neutrals, a PIC model for ions and a fluid description of the electrons. In these methods, the potential distribution is usually calculated by reducing the electron momentum equation to the Boltzmann relation in the absence of a magnetic field. In the plasma plume domain where the magnetic field exists, i.e. the near field, it is necessary to include the magnetic field effects in the electron momentum equation.

2. The model of the plasma layer

The model presented here describes the plasma layer near the Teflon surface as shown in Fig. 2. The model of the plasma layer includes Joule heating of the plasma, heat transfer to the Teflon, and Teflon ablation. Mechanisms of energy transfer from the plasma column to the wall of the Teflon include heat transfer by particle convection and by radiation. The Teflon ablation computation is based on a recently developed kinetic ablation model[12]. It is assumed that within

3

the plasma layer all parameters vary in the radial direction r (see Fig. 2). The energy balance equation can be written in the form:

$$\frac{3}{2}n_e \, dT_e/dt \; = \; Q_J - Q_r - Q_F \dots\dots\dots\dots\dots\dots\dots\dots\dots\dots\dots\dots\dots\dots\dots\dots\dots\dots\dots\dots\dots(1)$$

where Q_J is the Joule heat, Q_r is the radiation heat and Q_F is the heat associated with particle fluxes. This equation depends on the coordinate along the propellant face. For known plasma density and temperature the heat flux to the surface is calculated. The Teflon surface temperature is calculated from the heat transfer equation with boundary conditions that take into account vaporization heat and conductivity. The solution of this equation is considered for two limiting cases of substantial and small ablation rate very similar to that described in Ref. 8. The density at the Teflon surface is calculated using the equilibrium pressure for Teflon. The plasma density in the layer is determined in the framework of the kinetic ablation model (see next section). For known pressure and electron temperature one can calculate the chemical plasma composition assuming LTE[8,15,16]. The Saha equations are supplemented by the conservation of nuclei and quasi-neutrality.

3. Ablation model

The Teflon ablation is modeled in the framework of the approximation[13] based on a kinetic model of the material evaporation into discharge plasmas[12]. The model couples two different layers between the surface and the plasma bulk as shown in Fig. 2b: (1) a kinetic non-equilibrium layer adjusted to the surface with a thickness of about one mean free path; and (2) a collision-dominated layer with thermal and ionization non-equilibrium. The velocity at the edge of the kinetic layer U_1 can be determined from the coupling solution of the hydrodynamic layer and the

quasi-neutral plasma. For known velocity and density at this interface, it is possible to calculate the ablation rate. In the hydrodynamic layer the relation between the velocities, temperatures and densities at the boundaries 1 and 2 as well as the ablation rate are formulated according to Ref. 13 in the form:

$$\Gamma = mU_1N_1 = N_1[(2kT_1/m)\cdot(T_2N_2/2T_1 - N_1/2)/(N_1 - N_1^2/N_2)]^{0.5} \dots\dots (2)$$

The system of equations is closed if the equilibrium vapor pressure can be specified that determines parameters (N_o and T_o) at the Teflon surface. The full self-consistent solution of this problem can be obtained when the ablation is coupled with the plasma plume expansion. In the present work in order to simplify the problem, we will assume that the plasma accelerates up to the sound speed near the boundary 2. This assumption can be justified by the fact that due to significant electrodynamic acceleration in this type of PPT, the plasma density will quickly decrease therefore providing solution of the ablation problem close to that ablation into the vacuum. In this case the plasma density at the edge of the kinetic layer will be equal to $0.34 \cdot N_o$ and the temperature is $0.7 \cdot T_o$. The flux returned to the surface is equal to 16% of the ablated flux (Ref. 12).

4. Plasma plume electrodynamics

The general approach for the plume model is based on a hybrid fluid-particle approach that was used previously (Refs. 7). In this model, the neutrals and ions are modeled as particles while electrons are treated as a fluid. Elastic (momentum transfer) and non-elastic (charge exchange) collisions are included in the model. The grids employed in this computation are also similar to those used previously (Ref.7). The particle collisions are calculated using the direct simulation

Monte Carlo (DSMC) method[17]. Momentum exchange cross sections use the model of Dalgarno et al.[18], while charge exchange processes use the cross sections proposed by Sakabe and Izawa[19]. Acceleration of the charged particles is computed using the Particle-In-Cell method (PIC)[20]. The plasma velocity distribution depends upon the magnetic field distribution and ion dynamics is calculated as follows:

$$dV/dr = -C_s^2 \nabla \ln(n) + \mathbf{j} x \mathbf{B}/mn \dots\dots\dots(3)$$

where C_s is the sound speed, n is the plasma density, j is the current density and B is the magnetic field.

The electron dynamics is very important in the plasma plume. Previously our model was based on the assumption that electrons rapidly reach the equilibrium distribution and in the absence of the magnetic field can be described according to the Boltzmann distribution. While this was a satisfactory assumption in the case of an electrothermal thruster plume this is not suitable for the near field of an electromagnetic thruster. In the presence of a strong magnetic field, the electron density distribution deviates from that according to Boltzmann[21]. In the case of a magnetic field the electron momentum equation reads (neglecting electron inertia):

$$0 = -e^2 n_e(\mathbf{E} + \mathbf{V_e} \times \mathbf{B}) - e\nabla P_e - \nu_{ei} m_e \mathbf{j} \dots\dots\dots(4)$$

We have assumed quasi-neutrality therefore $n_e = n_I = n$. The electric and magnetic field distributions in the plume are calculated from the set of Maxwell equations. We further assume that the magnetic field has only an azimuthal component and also neglect the displacement

current. The combination of the Maxwell equations and electron momentum conservation gives the following equation for the magnetic field:

$$\partial \mathbf{B}/\partial t = 1/(\sigma\mu)\nabla^2 \mathbf{B} \ - \nabla\times(\mathbf{j}\times\mathbf{B}/(en)) + \nabla\times(\mathbf{V}\times\mathbf{B}) \dots\dots\dots\dots\dots\dots\dots\dots\dots\dots\dots(5)$$

where σ is the plasma conductivity, μ is the permittivity, n is the plasma density, $\mathbf{j}$ is the current density and $\mathbf{V}$ is the plasma velocity. A scaling analysis shows that the various terms on the right hand side of Eq. 5 may have importance in different regions of the plasma plume and therefore general end-to-end plasma plume analysis requires keeping all terms in the equation. In the case of the near plume of the micro-PPT with a characteristic scale length of about 1 cm the magnetic Reynolds number $Re_m \ll 1$ and therefore the last term can be neglected. Taking this into account in the dimensionless form, Eq. 5 can be written as:

$$Re_m\frac{\partial B}{\partial t} = \nabla^2 B \ - (\omega\tau)\cdot\left\{\frac{\partial}{\partial r}\left(\frac{Br}{r\cdot n}\right)\frac{\partial(Br)}{\partial z} - \frac{\partial}{\partial z}\left(\frac{Br}{r\cdot n}\right)\frac{\partial(Br)}{\partial r}\right\} \dots\dots\dots\dots\dots\dots\dots\dots\dots(6)$$

where $(\omega\tau)$ is the Hall parameter that measures of the Hall effect. Therefore, depending on the plasma density, the Hall effect may be important for the magnetic field evolution. One of the first calculations of the plasma flow with Hall effect were performed by Brushlinski and Morozov (see Ref. 22 and references therein). They considered isothermal flow. The plasma density becomes high at the cathode and lower at the anode. The Hall effect has a particularly noticeable influence on the magnetic field distribution. The field near the anode increases and near the cathode decreases. As a result the current is deflected to the side and grazes the anode.

Our estimations show that the Hall parameter $\omega\tau \ll 1$ if the plasma density near the Teflon surface $N > 10^{23}$ m^{-3}. This case is realized in the micro-PPT (see the next section) so the Hall effect is

7

expected to be small for this particular case. Having the magnetic field distribution one can calculate the current density distribution from Ampere's law:

$$\mu \mathbf{j} = \nabla \times \mathbf{B} \dotfill (7)$$

The magnetic field and current distributions calculated from this model are used in PIC to evaluate the ion dynamics according to Eq. 3.

5. Boundary conditions

The boundary conditions for the magnetic field calculations are shown in Fig. 1. We have assumed that the current is uniform on both electrodes that allows us to estimate the current density on the cathode j_c and on the anode j_a. The magnetic field is assumed to vary as $1/r$ on the upstream boundary. At the lateral boundary we have assumed that the normal current $j_n=0$. The downstream boundary is considered to be far enough away that B=0 can be assumed. Along the centerline the magnetic field B=0.

The boundary conditions for the plume are generated through solution of the Teflon ablation problem as will be presented in the Results section. These are time and radial dependent variations of the plasma (including Carbon and Flourine ions and neutrals) density and electron temperature.

The results are presented for a 3.6 mm diameter micro-PPT which has a 0.9 mm diameter central electrode, 3.1 mm propellant diameter and 0.24 mm anode wall (Ref. 10). In these simulations,

the experimental current waveform was used, that is described in a first approximation as an underdamped LRC circuit current:

$$I(t) = I_p \cdot \sin(\alpha t) \exp(-\beta t)$$

where $I_p = \sqrt{\dfrac{2E}{L}}$; $\quad \alpha = \sqrt{\dfrac{1}{LC}}$; $\quad \beta = \dfrac{R}{2L}$; L is the effective inductance in the circuit, C is the capacitance, R is the total circuit resistance, and E is the pulse energy. The best fit with the experimental waveform (frequency) corresponds to $\alpha = 3 \cdot 10^6$ s^{-1}. For C=0.3 μF we can estimate that L in the circuit is about $3.6 \cdot 10^{-7}$ H. Results presented below correspond to the 15.2 J (Ref.10).

6. Results

The spatial and temporal variation of the Teflon surface temperature is shown in Fig. 3a. The Teflon temperature sharply increases during the first 1-2 μs of the pulse and peaks at about 635 K. One can see that the temperature is generally non-uniform in the radial direction and has a minimum at radial distances of 1.1-1.3 mm. Since the Teflon ablation is approximately exponentially proportional to the surface temperature, the model predicts a lower rate of ablation in the areas where the surface temperature has a minimum. Taking this into account, the effect of the temperature distribution may be related to the preferential charring of the Teflon surface observed experimentally [Ref. 10]. A detailed study of the Teflon surface charring and its relation to the non-uniform ablation will be presented in a parallel paper [23].

The plasma density and electron temperature distribution are also shown in Fig. 3. The plasma density peaks at about 10^{24} m^{-3} midway between the electrodes. The electron temperature is strongly non-uniform radially with peak near the electrodes of about 4.5 eV. The reason for

9

higher electron temperature near the electrodes is due to current spreading in the space between the electrodes and current focusing near the electrodes (see below results on current distribution). As was mentioned earlier, the ablation rate is also non-uniform radially. This effect is shown in Fig. 4. One can see that the ablation rate peaks near the electrodes at about 120 kg/m^{2}s, while in the middle of the propellant face it is about 80-100 kg/m^{2}s. The calculated total ablated mass per pulse was about 1 μg that is close to the measured value of 1.3 μg [10].

A region of magnetic field diffusion in the near field outside the micro-PPT is shown in Fig. 5a. The magnetic field drops by an order of magnitude at about 1.5 mm that is equal to the thruster radius. This is the region where also the most of the current is concentrated as shown in Fig. 5b. One can see that the current density is high near the central electrode and near the outer electrode. This is a reason for the increasing Teflon surface temperature and electron temperature in these regions. According to the model presented in Sec. 4 the electromagnetic acceleration of the plasma is also expected to occur in this region.

Figure 6 shows evolution of the Carbon ion (C+) component of the plasma plume during the main part of the pulse. One can see that a dense plasma focus is developed at a few mm from the thruster exit plane. This plasma focus exists during the entire pulse as shown in Fig. 6, but the plasma density in the focus decreases from about 2×10^{22} m^{-3} at the beginning of the pulse down to 0.3×10^{22} m^{-3} at 5 μs. At the beginning (first 2 μs) the C+ density mainly develops a gradient in the radial direction that is a result of high directed velocity in the axial direction. Later, during the pulse, the axial density gradient becomes comparable to the radial one.

The Flourine ions (F+), due to their larger mass, have different dynamics as shown in Fig.7. They have smaller acceleration in the axial direction even at the beginning of the pulse and therefore

both axial and radial density gradients are developed. The F+ density in the plume and in the plasma focus is larger than that of C+, because originally Teflon has composition C_2F_4 with F density twice larger than that of C. Additionally F ions experience less acceleration in the plume because of their mass that also contribute to their relative density increase.

The micro-PPT is essentially an electromagnetic accelerator as shown in the velocity phase plots (Figs. 8,9). The phase plot of the Carbon ions at 1 μs is centered at 30 km/s in the axial direction. Ions experience also radial expansion in both directions due to the magnetic field structure and the temperature expansion. The radial velocity in the negative direction is related to the focus formation along the axis, as shown in Figs. 6,7. The Flourine ions have generally smaller both axial and radial velocities due to their higher mass. At a later stage of the pulse (see Fig. 9) clearly there are two ion populations with positive and negative radial velocities. This is due to the annular plasma injection corresponding to the thruster geometry (see Figs. 1,2).

During the entire pulse there is a population of ions having a negative axial velocity with the magnitude up to about 10 km/s (see Figs. 8,9). This population creates the backflow contamination that is an important issue of concern for a spacecraft using the PPT. The Carbon ions have a larger negative velocity due to their higher mobility that results in their domination in the backflux.

7. Summary

In this paper, a self-consistent description of an electromagnetic pulsed plasma thruster from plasma generation into the near plume is presented. A micro-PPT developed at AFRL is considered as a working example. In this device, no separation exists between the main plasma acceleration region, which usually occurs in an internal flow, and the external plasma plume field. Therefore, a single end-to-end model is necessary for accurate simulations. A kinetic Teflon ablation model is incorporated in order to provide the boundary conditions for the plasma plume. This model predicts an ablated mass per pulse of about 1 µg that is close to that measured in experiment. The phenomena in the plasma plume related to the electromagnetic effects are studied. The plume simulation shows that a dense plasma focus is developed at a few millimeters from the thruster exit plane at the axis. This plasma focus exists during the entire pulse, but the plasma density in the focus decreases from about 2×10^{22} m^{-3} at the beginning of the pulse down 0.3×10^{22} m^{-3} at 5 µs. The velocity phase is centered at about 30 km/s in the axial direction demonstrating that the micro-PPT is essentially an electromagnetic accelerator. At a later stage of the pulse there are two ion populations with positive and negative radial velocity. It is predicted that there is a population of ions having a negative axial velocity magnitude up to about 10 km/s. This population relates to the backflow contamination that is an important issue of concern for a spacecraft using the PPT.

Acknowledgements
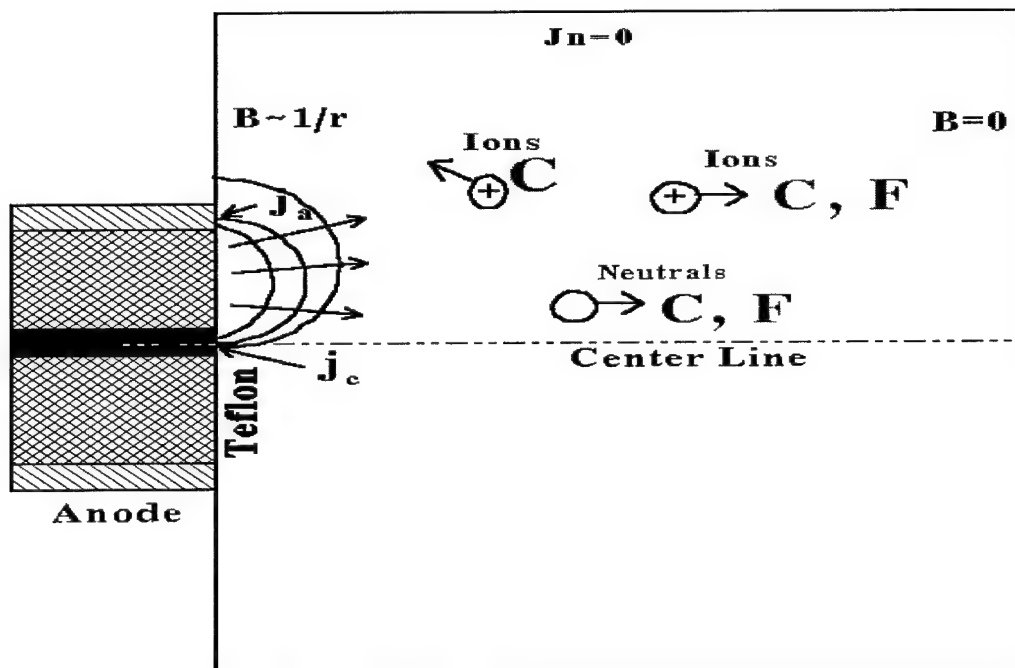
Figure 1. Schematic diagram of micro-PPT plume and boundary conditions
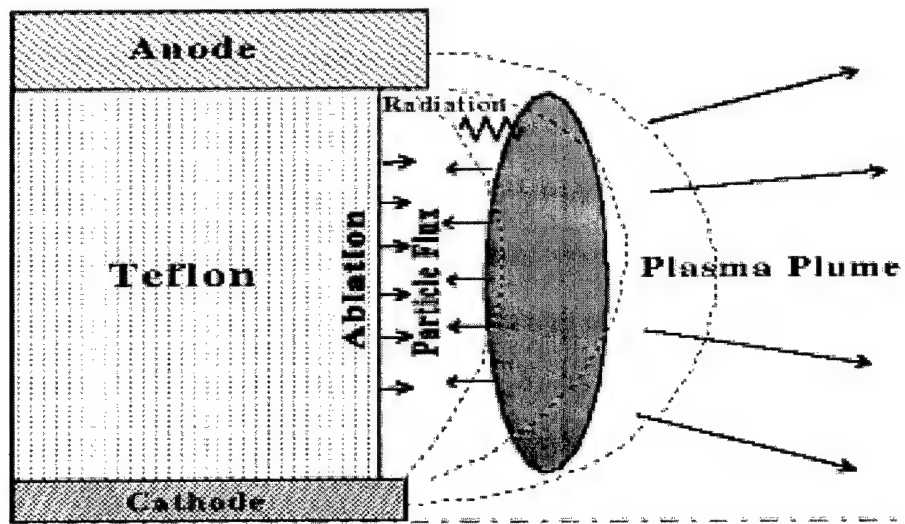
(a)
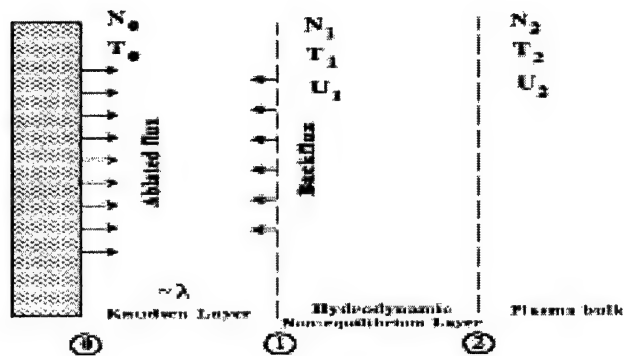
(b)

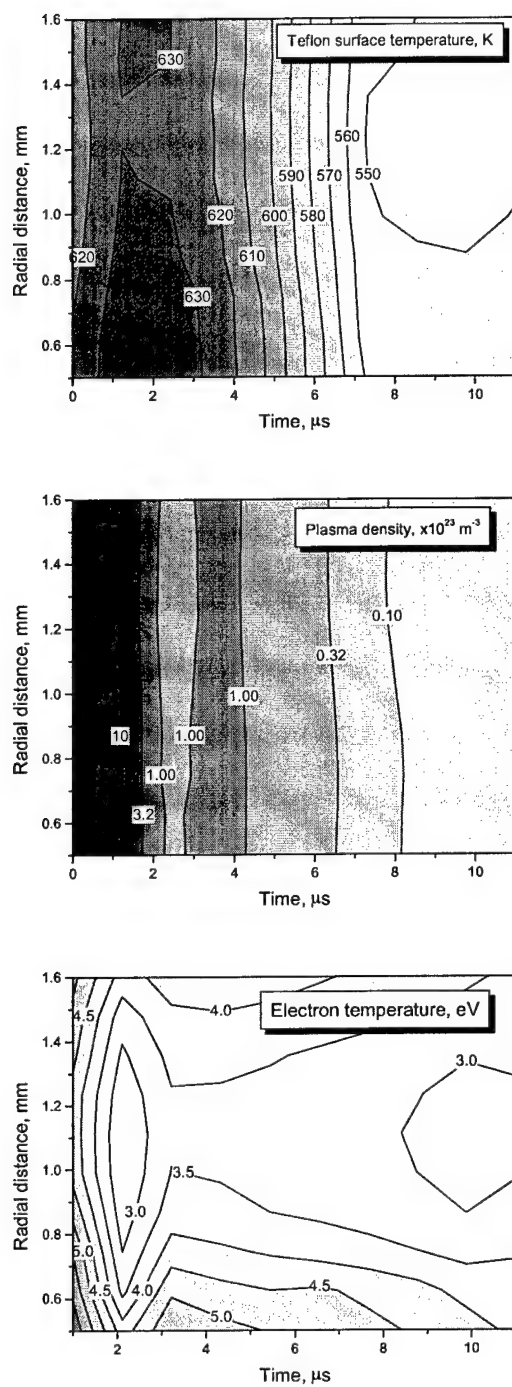**Figure 2**. Schematic of the near Teflon plasma layer

Figure 3. Teflon surface temperature, plasma density and elecrtron temperature distribution in the layer near the Teflon surface
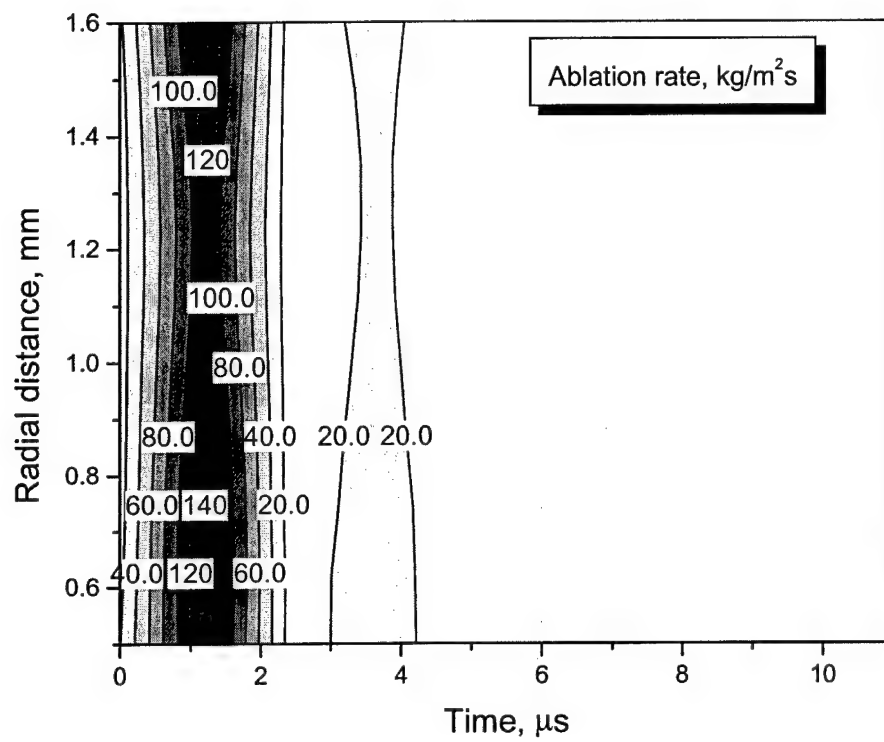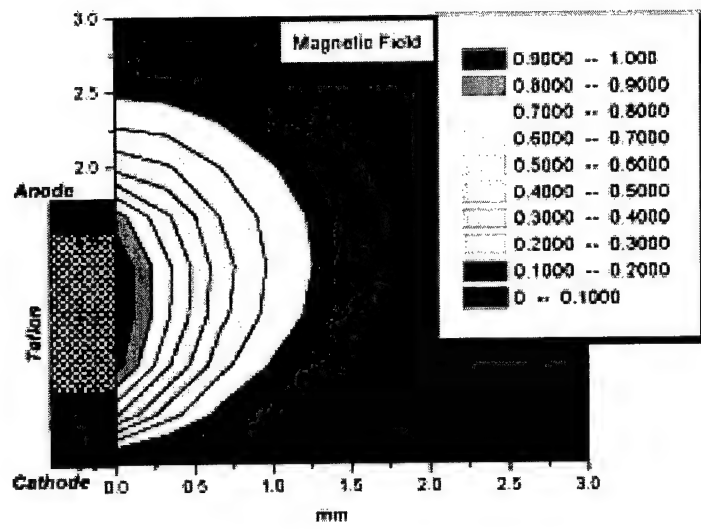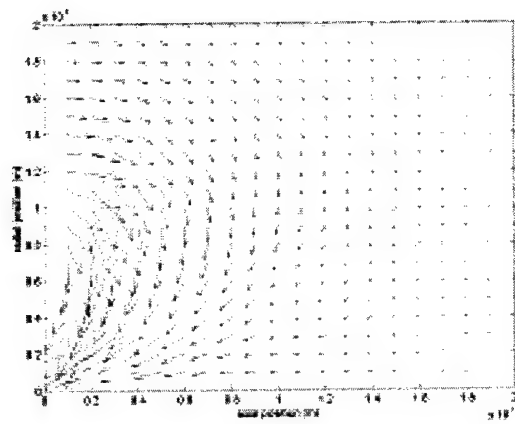
Figure 4. Ablation rate spatial and temporal distribution.

(a)

(b)

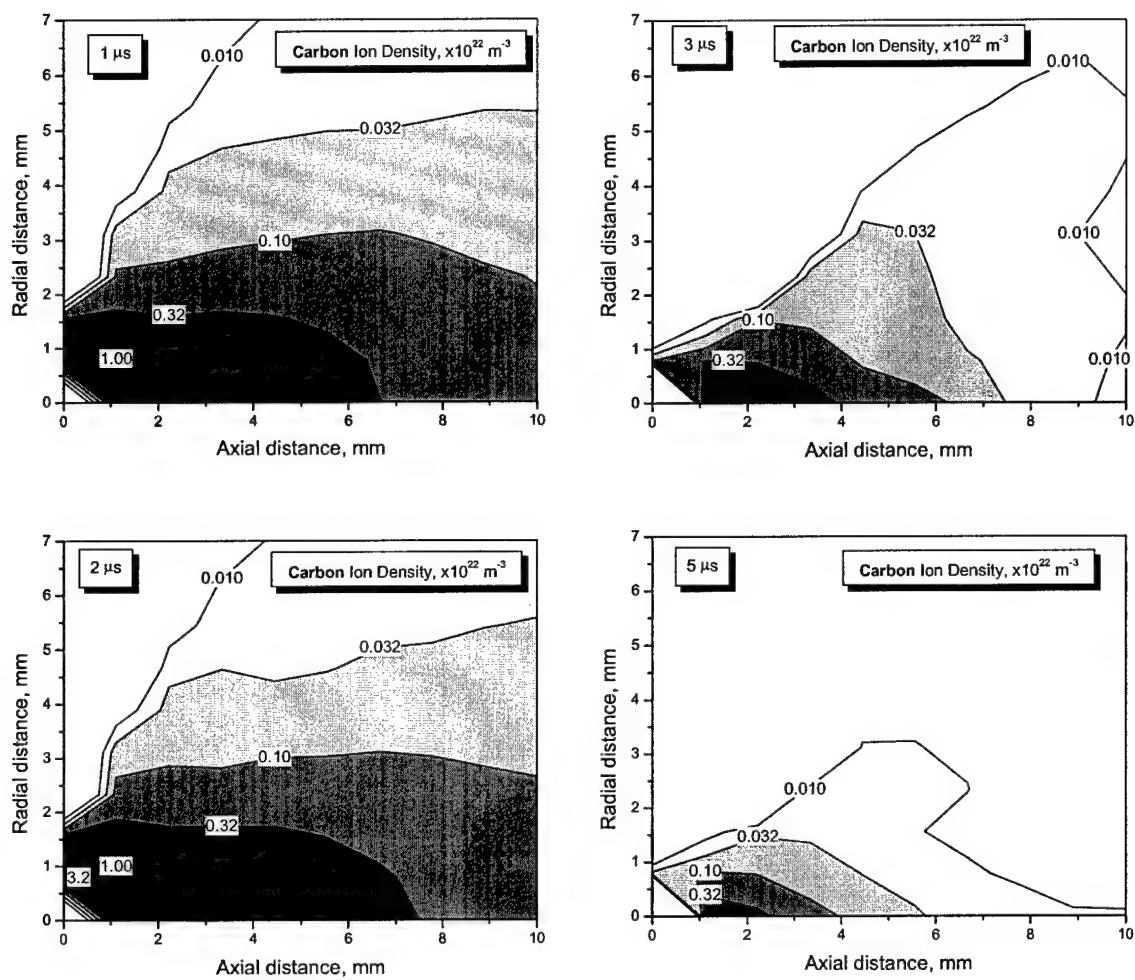**Figure 5.** (a) Magnetic field distribution and (b) current lines vectors in the near field of the micro-PPT.

17

Figure 6. Evolution of the Carbon ion density during the pulse
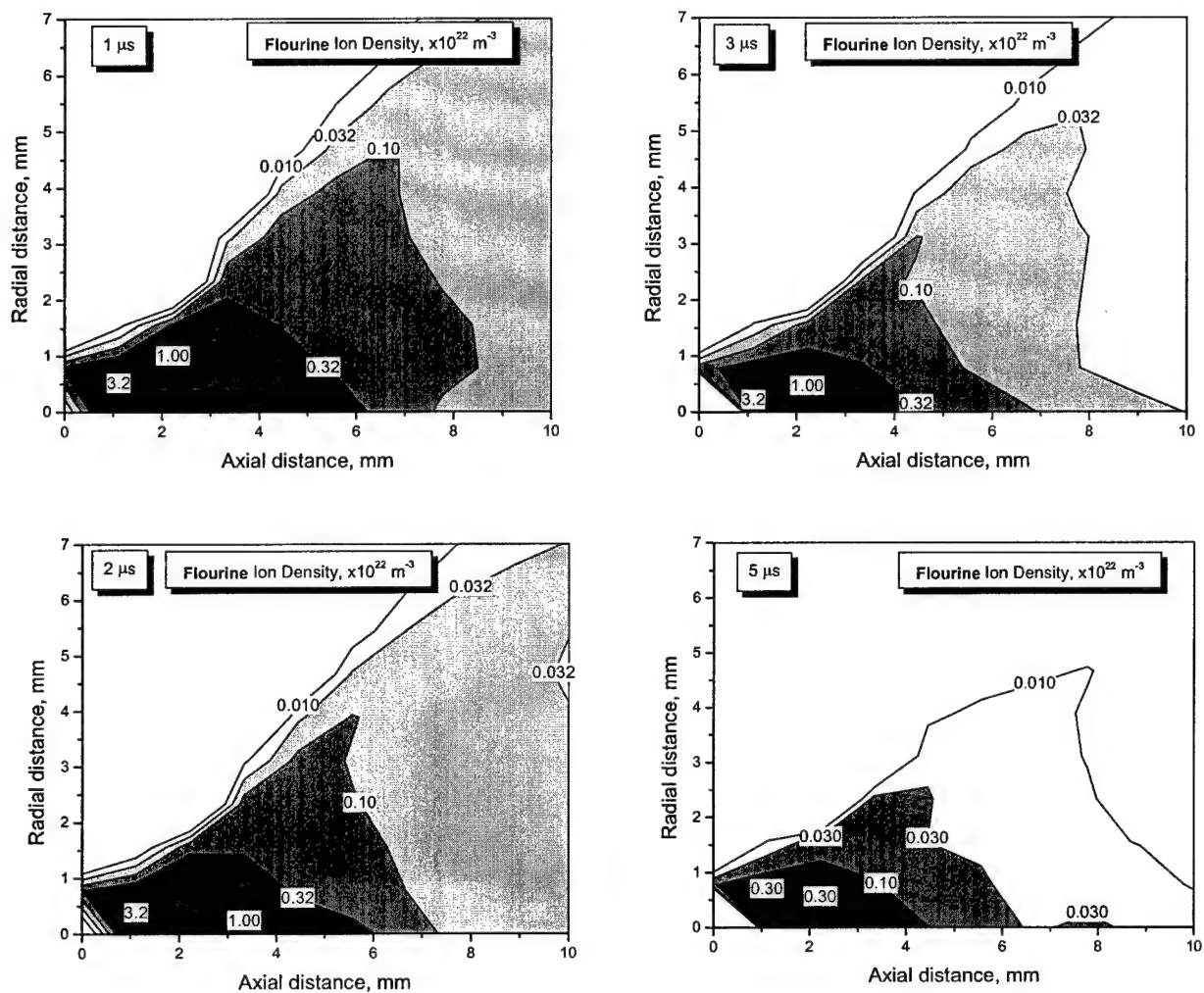
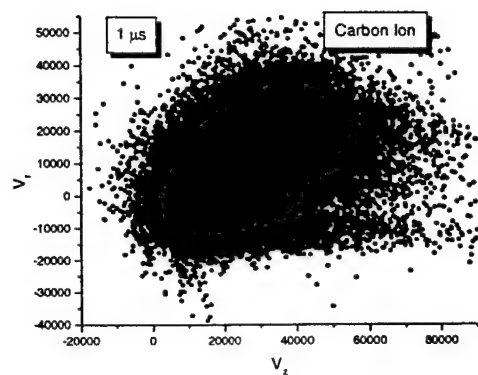**Figure 7**. Evolution of the Flourine ion density during the pulse

19
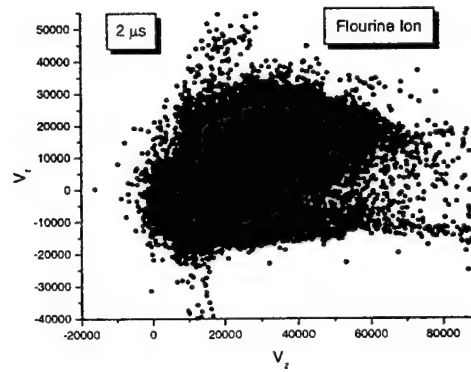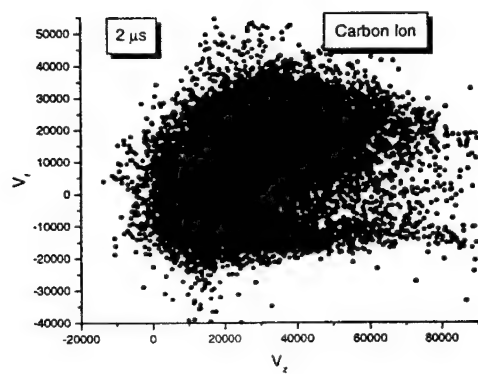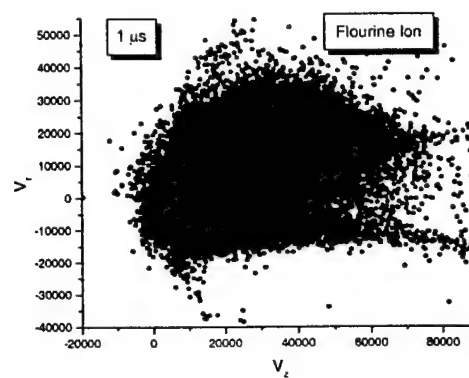
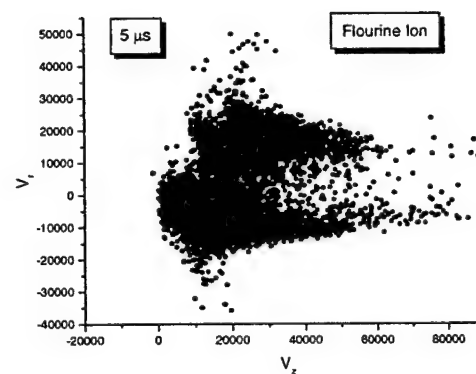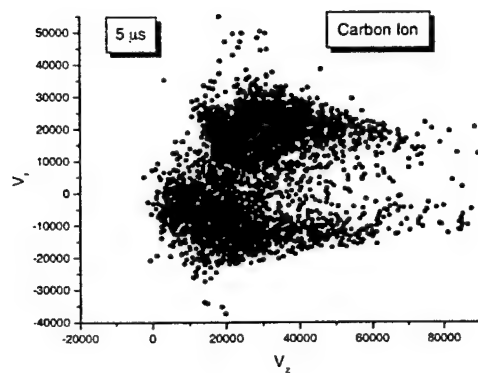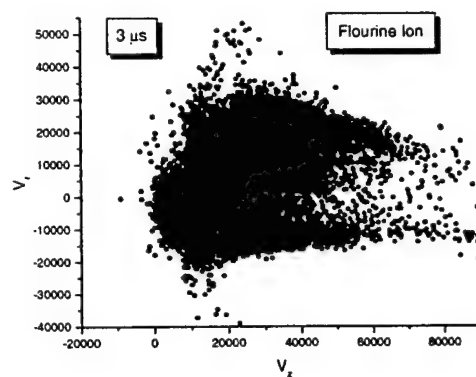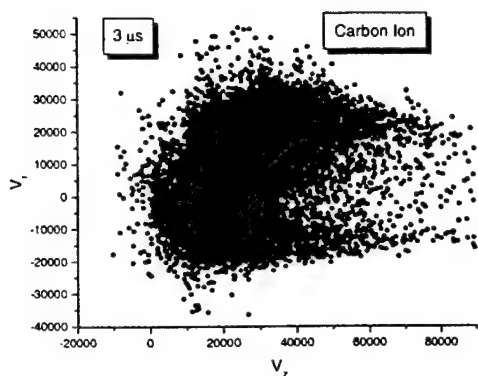**Figure 8**. Ion velocity phase. Early stage of the pulse

Figure 9. Ion velocity phase. Late stage of the pulse

23

AIAA-2001-3898

Performance Study of the Ablative Z-pinch Pulsed Plasma Thruster

Michael Keidar, Iain D. Boyd and Neal Lepsetz

University of Michigan, Ann Arbor MI 48109

Thomas E. Markusic, Kurt A. Polzin and Edgar. Y. Choueiri

Princeton University, Princeton NJ 08544

37th AIAA/ASME/SAE/ASEE Joint Propulsion Conference and Exhibit

8-11 July 2001
Salt Lake City, Utah

Performance Study of the Ablative Z-pinch Pulsed Plasma Thruster

Michael Keidar[♦], Iain D. Boyd* and Neal Lepsetz[♣]

Department of Aerospace Engineering, University of Michigan, Ann Arbor, MI 48109

Thomas E. Markusic[♥], Kurt A. Polzin[♥], and Edgar Y. Choueiri[♠]

Electric Propulsion and Plasma Dynamic Laboratory (EPPDyL), Princeton University,

Princeton, NJ 08544

Abstract

The ablative Z-pinch PPT utilizes the Z-pinch effect to produce an axially streaming plasma. When the current is fully pinched in this device, a large axial pressure gradient exists and thus plasma accelerates in the axial direction due to the gasdynamic force. In the present paper, a model of the electrical discharge in the Ablative Z-pinch Pulsed Plasma Thruster is developed. The model includes Joule heating of the plasma, heat transfer to the Teflon, and Teflon ablation. Mechanisms of energy transfer from the plasma column to the propellant include heat transfer by particle convection and by radiation. The computation of Teflon ablation is based on a recently developed kinetic ablation model. The average current density in the pinched region is used as a parameter of the model. The model predicts that the electron temperature peaks at about 4 eV and the plasma density peaks at about $8 \cdot 10^{23}$ m^{-3}. Thruster performance characteristics such as impulse bit, specific impulse and the mass bit are calculated. In the case of low pulse energy, all measured thruster performance characteristics agree with our model predictions when the average current density to the anode current density ratio α is about 0.55. In the case of high pulse energy, such an agreement with the experiment occurs when $\alpha \approx 0.7$-0.8, that suggests that in the case of higher pulse energy the current is more constricted near the anode tip. The model also predicts that the impulse bit decreases with increasing propellant inner diameter in agreement with experiment. The comparison of the model prediction with experimental data suggests that the pinch effect and the thrust-to-power ratio increase with the pulse energy.

[♦] *Research Scientist, Department of Aerospace Engineering, Member of AIAA*

[*] *Associate Professor, Department of Aerospace Engineering, Senior Member of AIAA*

[♣] *Undergraduate student, Department of Aerospace Engineering*

[♥] *Graduate student*

[♠] *Chief Scientist at EPPDyL. Assistant Professor, Applied Physics Group, Senior Member AIAA*

1. Introduction

Due to the combined advantages of system simplicity, high reliability, low average electric power requirement and high specific impulse, currently there is a renewed interest in pulsed plasma thrusters (PPT's) for a number of missions[1]. The PPT is considered as an attractive propulsion option for orbit insertion, constellation maintenance, drag makeup and attitude control of small satellites. Existing PPT's, however, have very poor performance characteristics with an efficiency[2] at the level of about 10% that leaves an opportunity for substantial improvement.

To improve the PPT performance, several directions are being considered, such as elimination of late-time ablation, choice of the proper current waveform etc[3]. Currently, new PPT devices using both an electromagnetic acceleration mechanism[4,5] or an electrothermal mechanism are under development[6,7]. One of the motivations for development of new PPT configurations is to achieve higher thrust-to-power ratio. Electrothermal PPTs that were developed by Burton at. al.[6,7] have thrust-to-power ratio >35 μN/W. Another approach for producing a high thrust-to-power PPT involves using the inverse Z-pinch effect, as demonstrated by Mikellides and Turchi et. al.[8].

Z-pinch plasmas produced by the magnetic compression of a cylindrical plasma column are used widely to produce hot and dense plasmas for many applications that include focusing of energetic particles, guiding intense optical laser pulses, and producing ultrahigh magnetic fields. While the macroscopic dynamics of the Z-pinch plasma can be described in terms of snowplow model the details of the current structure and other plasma properties are not completely understood[9]. The idea to use the Z-pinch geometry for a plasma thruster was first proposed by Jahn et. al[10]. Recently some interesting results on the application of the Z-pinch configuration for an ablative Pulsed Plasma Thruster were presented[11]. The Ablative Z-pinch PPT utilizes the pinch

effect to produce axially streaming plasma. It was found that a specific impulse of about 809 s, a thrust-to-power ratio of about 27.8 μN/W and a thrust efficiency of 8.95% were the highest performance values obtained for the best current AZ-PPT designs. When the current is fully pinched in this device, a large axial pressure gradient exists and thus the plasma accelerates in the axial direction. Therefore, the main mechanism of plasma acceleration is electrothermal due to the gasdynamic force. This motivates us to use a previously developed model for electrothermal PPT's to describe the Z-pinch PPT.

Another interesting effect that may enhance the AZ-PPT performances is the plasma macroparticle interactions. Macroparticles are large chunks (1-100 μm diameter) of the Teflon that are emitted during the pulse. Estimates have shown that the particulate emission consumes about 40% of the total propellant mass, while contributing only 1% to the total thrust[12]. Specific design of the AZ PPT allows the discharge chamber to act as a macroparticle trap as was mentioned in Ref. 11. Previously we showed that the macroparticle interaction with a discharge plasma may lead to complete decomposition of some macroparticles[13]. For instance, it was found[13] that a 5 μm diameter macroparticle would completely decompose during the 10 μs of the interaction with a plasma under typical conditions of an electrothermal PPT. Therefore macroparticle trapping can increase the time spent by the macroparticle in the discharge that will lead to increased macroparticle ablation and thus better propellant utilization.

In this paper, we describe the model of the electrical discharge in the AZ-PPT. Knowing the plasma parameter evolution during the pulse allows us to calculate the performance characteristics of the thruster such as specific impulse, impulse bit and mass bit. The present work is based on a previously developed model of the ablation controlled discharge[14,15]. This model was successfully used to model elecrtrothermal PPT's developed at the University of Illinois[6,7]

(PPT-4, PPT-7). The model includes Joule heating of the plasma, heat transfer to the Teflon, and Teflon ablation. Mechanisms of energy transfer from the plasma column to the propellant bar include heat transfer by particle convection and by radiation. The computation of Teflon ablation is based on a recently developed kinetic ablation model[16].

In the following section we will describe the model in brief that includes both sheath and quasi-neutral plasma as well as plasma-dielectric interaction.

2. The discharge model

The model considers the plasma generation processes (ablation, heating, radiation, ionization etc.) and plasma acceleration along a Teflon chamber. Some characteristic regions such as the Teflon surface, electrical sheath near the dielectric and quasi-neutral plasma are shown in Fig. 1. Different kinetic and hydrodynamic phenomena determine the main features of the plasma flow including plasma Joule heating, heat transfer to the dielectric and electrothermal acceleration of the plasma up to the sound speed at the cavity exit. Below, we will discuss the model in the different regions and the full system of equations including the final expressions obtained previously [15]. In addition, we will estimate the current distribution in the pinched area in order to obtain the current density that will be used in the energy balance.

Firstly, let us estimate the characteristic time for the pinch effect. In the frame of the simple snowplow model when the current rise is linear, it was shown that the time constant for pinch[17]:

$$\tau = (\mu\rho)^{1/4}L/(dI/dt)^2$$

where μ is the permittivity, ρ is the initial plasma density, dI/dt is the current rise, and L is the characteristic initial size. For the range of parameters typical for an AZ-PPT, an estimation shows that the current pinch time is $<10^{-7}$ s. This means that after that time, the current is strongly pinched. This statement is certainly supported by the experimental observations presented earlier [11]. Therefore, in our model, we have assumed that during the discharge (~10 μs) the current is fully pinched.

2.1. Electrostatic Sheath

According to our previous estimations[15] during the discharge pulse, a quasi-steady sheath structure is formed and that under typical PPT conditions, this sheath is unmagnetized (the self-magnetic field generated during the pulse is considered). In this case, the potential drop of the electrostatic sheath near the Teflon wall, is negative in order to repel the excess of the thermal electrons, so that the random electron current density j_{eth} is equal to the Bohm ion current density j_i. Under these conditions the potential drop in the sheath can be calculated as:

$$U_d = -T_e \ln (j_{eth}/j_i) \dots\dots\dots(1)$$

2.2. Teflon ablation

In the present work the Teflon ablation is modeled in the framework of the approximation[18] based on a previously developed kinetic model of metal evaporation in a surrounding plasma[19]. The mathematical description includes the model for two different layers between the surface and the plasma bulk: (1) a kinetic non-equilibrium layer adjusted to the surface with a thickness of about one mean free path; and (2) a collision-dominated layer with thermal and ionization non-

equilibrium. The plasma-wall transition layer also includes an electrical sheath described in the previous section. This model makes it possible to calculate the plasma parameters (density and temperature) at the interface between the kinetic and hydrodynamic layers. For known velocity and density at this interface, it is possible to calculate the ablation rate. The ablation rate is formulated according to Ref. 16 as follows:

$$\Gamma = mV_1 n_1 = n_1[(2kT_1/m)\cdot(T_2 n_2/2T_1 - n_1/2)/(n_1 - n_1^2/n_2)]^{0.5} \quad \text{...} \quad (2)$$

where n_1 and T_1 are the density and temperature at the kinetic layer edge, and n_2, T_2 are the density and temperature at the hydrodynamic layer-plasma bulk interface. Density n_2 and temperature T_2 are determined by the plasma bulk flow and energy balance (see next section). The density n_1 and temperature T_1 are determined by solution of the problem for the kinetic layer[18]. The system of equations is closed if the equilibrium vapor pressure can be specified that determines the parameters at the Teflon surface. In the case of Teflon, the equilibrium pressure formula is used [1]:

$$P = P_c \exp(-T_c/T_s) = n_s k T_s \quad \text{...} \quad (3)$$

where P is the equilibrium pressure, $P_c = 1.84 \times 10^{20}$ N/m^2 and $T_c = 20815$ K are the characteristic pressure and temperature, respectively.

2.3. Quasi-neutral plasma bulk

The schematic geometry of the thruster is shown in Fig. 1. Several simplifications are made in order to make it possible to develop a simple model. For instance, the anode spike is assumed to a cylinder as shown in Fig. 1. In the present model we assume that all parameters vary in the axial

direction, x (see Fig. 1), but are uniform in the radial direction. The axial component of the mass and momentum conservation equations reads:

$$A(\partial\rho/\partial t + \partial(\rho V)/\partial x) = 2\pi R_2 \Gamma(t,x) \quad \dots\dots\dots (4)$$

$$\rho(\partial V/\partial t + V\partial V/\partial x) = -\partial P/\partial x \quad \dots\dots\dots (5)$$

where A is the cross section of the Teflon chamber ($A=\pi(R_2^2-R_1^2)$), ρ is the plasma density, P is the pressure, V is the plasma velocity, $\Gamma(t,x)$ is the local instantaneous ablation rate, R_2 is the Teflon chamber radius and R_1 is the radius of the spike (see Fig. 1).

The energy transfer from the plasma column to the wall of the Teflon cavity consists of the heat transfer by particle fluxes and radiation heat transfer. In this case, the energy balance equation can be written in the form[15]:

$$\frac{3}{2}n_e (\partial T_e/\partial t + V\partial T_p/\partial x) = Q_J - Q_r - Q_F \quad \dots\dots\dots (6)$$

where T_e is the electron temperature, Q_J is the Joule heat, Q_r is the radiation heat and Q_F is the particle flux. The radiation energy flux Q_r includes the radiation in a continuum spectrum based on a theoretical model[20]. The Joule heat source is assumed to be concentrated in the pinch region by the abode tip (see Fig.1). The average current density in this region is used as a parameter of the model. The particle convection flux Q_F includes energy associated with electron and ion fluxes to the dielectric wall that leads to plasma cooling. Our estimations and previous calculation show[21] that the electron temperature varies only slightly with axial position and therefore we performed the calculation assuming $\partial T_e/\partial x=0$.

The temperature inside the Teflon wall can be calculated from the heat transfer equation:

$$\partial T/\partial t = a\partial^2 T/\partial r^2 \dotfill (7)$$

where a is the thermal diffusivity. This is the one-dimensional equation in the radial direction. This assumption can be made since the heat layer thickness near the surface is smaller than the Teflon cylinder curvature R_2 and also less than the characteristic length of plasma parameter changes in the axial direction. In order to solve this equation, we use the following boundary and initial conditions[15]:

$$- \lambda \partial T/\partial x (x=0) = q(t) - \Delta H \cdot \Gamma - C_p(T_s - T_o) \Gamma$$

$$\lambda \partial T/\partial x (x=\infty) = 0 \dotfill (8)$$

$$T(t=0) = T_o$$

where x=0 corresponds to the inner dielectric surface, ΔH is the ablation heat, Γ is the rate of Teflon ablation per unit area, T_o is the initial room temperature and q(t) is the density of the heat flux, consisting of the radiative and particle convection fluxes, and T_s is the Teflon surface temperature. The solution of this equation is considered for two limiting cases of substantial and small ablation rate very similar to that described in Ref. 15.

Having calculated the plasma density and electron temperature, we calculate the chemical plasma composition considering Local Thermodynamic Equilibrium (LTE) in the way described previously[15,22,23]. In the considered range of electron temperature (1-4 eV) and plasma density (10^{22}-10^{24} m^{-3}) we will assume that polyatomic Teflon molecules C_2F_4 fully dissociate and we will start our consideration from the point when we have gas containing C and F. The Saha

equations for each species (C and F) are supplemented by the conservation of nuclei and quasi-neutrality.

In the present model we use the experimental current waveform as an input condition. We assume that the pulse energy is supplied by a simple LRC circuit with fixed elements. In this case, the current produced by an underdamped LRC circuit can be approximated as:

$$I(t) = I_p \cdot \sin(\alpha t) \exp(-\beta t) \dotfill (9)$$

where $I_p = \sqrt{\dfrac{2E}{L}}$; $\alpha = \sqrt{\dfrac{1}{LC}}$; $\beta = \dfrac{R}{2L}$; L is the effective inductance in the circuit, C is the capacitance, R is the total circuit resistance, and E is the pulse energy. The best fit with the experimental waveform (frequency) corresponds to $\alpha = 0.9 \cdot 10^6$ s^{-1}. For C=33. 6 μF we can estimate that L in the circuit is about $3.7 \cdot 10^{-8}$ H. For an energy of 67 J, the amplitude of the current waveform I_p equals $6 \cdot 10^4$ A.

The current waveform was measured for AZ PPT-3 using an integrated Rogowski coil. The data that were taken for AZ-PPT3 fired at 25, 50 and 67J with the 33.6 microF capacitor are shown in Fig. 2. It can be seen that the thruster exhibits damped sinusoidal behavior typical of ablative pulsed plasma thruster. The measurement technique was the same as described in Ref. 11. The current waveform is used as an input parameter in our model.

It was estimated above that under the conditions considered, the current is fully pinched during the main part of the discharge. The current is concentrated between the anode tip end and the cathode as schematically shown in Fig. 1. In general, the current density distribution in that pinched area is two-dimensional and can be calculated using the magnetic transport equation.

9

However, in the framework of the present 1D model of the plasma flow, only the average current density is considered. The current density peaks at the anode spike tip, $j_a = I/\pi R_1^2$ and then decreases toward the cathode. In the present work we use the current density as a parameter in the range $(0.2 - 1) j_a$.

3. Results

In this section we present results of calculation of the plasma parameters during the discharge pulse for the AZ-PPT. As a working example, we consider AZ-PPT-3 as it shows the best device performance. This thruster has a Teflon chamber length of 57 mm, the radius of the Teflon $R_2 = 12.5$ or 19 mm, and the radius of the anode spike $R_1 \sim 6$ mm. The simulations are performed assuming a free stream condition at the thruster exit, e.g. the plasma velocity equals the local sound speed at $x = L$. Based on the calculated plasma parameter distribution, we calculate the thruster performance characteristics, such as mass ablated during the pulse, average specific impulse, and gasdynamic impulse bit.

The plasma density spatial and temporal distribution is shown in Fig. 3. The plasma density peaks at about $8 \cdot 10^{23}$ m^{-3} at 3 μs that corresponds to the first current peak. One can see also that the plasma density decreases towards the cathode (along x) as a result of the plasma acceleration. At the exit plane, the plasma density is about 60% of the plasma density near the anode base (x=0).

The electron temperature temporal variation is shown in Fig. 4 with discharge energy as a parameter. The electron temperature peaks at 3.7 eV in the case of 50 J and at 4.3 eV in the case of 75 J at about 1.5 μs. The electron temperature oscillations correspond to the discharge current oscillation shown above.

As a result of the oscillations in electron temperature and plasma density, the ionization degree calculated assuming LTE also oscillates as shown in Fig. 5. Initially, during the first current peak, the plasma is strongly ionized and the thruster produces a plume containing mainly C and F ions and electrons. At late time, the ionization degree at the peaks is about 0.5. This means that toward the pulse end the thruster produces a large amount of neutrals.

The calculated thruster performance characteristics integrated over the 15 μs pulse are shown in Fig. 6. Here we show an example of performance calculation for AZ-PPT 3 firing at 25 J. For comparison a parameter range measured experimentally is also shown. The impulse bit and mass bit strongly increase with parameter α, which is a measure of the current density in the pinched region. One can see that all measured parameters agree with our model predictions when the parameter $\alpha \approx 0.55$. This result suggests that even though the current is focused at the anode tip, the average current density in the pinched area is smaller than that at the anode. The effect of varying the Teflon chamber inner diameter ($2R_2$, see Fig. 1) is shown in Fig. 7. One can see that the model predicts a decrease of impulse bit with the increasing propellant inner diameter (ID) in agreement with experiment.

The calculation of the AZ-PPT-3 performance for the case of high pulse energy is shown in Fig.8. One can see that in this case, agreement with the experiment occurs when $\alpha \approx 0.7$-0.8. This means that in the case of the high pulse energy, the average current density is higher and closer to the anode current density. This is an expected result that means that in the case of higher pulse energy (higher current) the current is more constricted near the anode tip. The effect of the pulse energy on the thrust-to–power ratio is shown in Fig. 9 where pulse energy is used as a parameter. It can be seen that the thrust-to–power ratio decreases with the energy for the constant parameter α.

However, since in the experiment (Ref. 11) it was obtained that the thrust-to–power ratio actually increases with energy one can conclude that the parameter α must be higher in the case of high energy. Thus the comparison of the model prediction with experimental data suggests that the pinch effect increase with the pulse energy.

The simulated results are summarized in Fig. 10 where the dependence of the parameter α (average current density to the current density at the anode tip ratio) for which the agreement with the measured impulse bit was obtained is shown as a function of the pulse energy. Here also the Teflon chamber inner diameter (ID) is used as a parameter. Generally it can be seen that the average current density increases with the pulse energy as was mentioned above. An interesting result is the dependence of the average current density on the Teflon chamber ID. One can see that the average current density more significantly increases in the case of the large propellant ID. This observation can be explained as follows. When the propellant ID is larger, the model predicts that the plasma density in the channel is smaller. Therefore one can expect higher current density in the case of larger propellant ID since, in the pinched area, the current constriction is limited by the plasma pressure.

Taking into account that the average current density varies with the pulse energy, the dependence of the thrust-to-power ratio (T/P) on the Teflon chamber length L was calculated. These results are shown in Fig. 11. One can see that T/P much higher in the case of the smaller propellant ID. Also, in this case the T/P variation with the energy pulse is relatively moderate. In the case of the large propellant ID, T/P significantly increases with the pulse energy. In all cases there is an optimal length corresponded to the maximal T/P. In the case of 1" ID propellant the maximal T/P is predicted to be at L~40 mm, while in the 1.5" ID propellant case it corresponds to L~50 mm. After the maximum the T/P significantly decreases with L, especially in the case of smaller ID. In

this study we fix the length of the pinched area meaning that when the Teflon chamber length L increases the anode spike length also increases (see Fig. 1). As result the length of the pinched area normalized by the total length of the propellant decreases and therefore the plasma in the channel is less heated. This is the main reason why T/P decreases when L is high.

4. Summary

In this paper a model of the discharge in the recently developed Ablative Z-pinch Pulsed Plasma Thruster is presented. This device utilizes the pinch effect to produce an axially streaming plasma. The model includes Joule heating of the plasma, heat transfer to the Teflon, and Teflon ablation kinetics. Mechanisms of energy transfer from the plasma column to the propellant bar include heat transfer by particle convection and by radiation. In addition it was assumed that the current is fully pinched near the anode tip during the main part of the discharge. The average current density in the pinched area is used as a parameter of the problem. The model predicts that the electron temperature peaks at about 4 eV and the plasma density peaks at about $8 \cdot 10^{23}$ m^{-3}. During the initial stage of the discharge, plasma is predicted to be strongly ionized, while at the late time the ionization degree peaks at about 0.5. Thruster performance characteristics such as impulse bit, specific impulse, and the mass bit were calculated. In the case of low pulse energy, all measured thruster performance characteristics agree with our model predictions when the average current density to anode current density ratio α is about 0.55. In the case of high pulse energy, similar agreement with experiment occurs when $\alpha \approx 0.7$-0.8. This means that in the case of higher pulse energy (higher current) the current is more constricted near the anode tip. The model also predicts that the impulse bit decreases with increasing propellant inner diameter (ID) in agreement with experiment. The comparison of the model prediction with experimental data suggests that the pinch effect and the thrust-to-power ratio increase with pulse energy. It was

13

predicted that the thrust-to-power ratio dependence on the Teflon chamber length has a maximum. The non-monotonic behavior of the T/L with Teflon chamber length is more pronounced in the case of the smaller propellant inner diameter.

Acknowledgements

REFERENCES

[1] R. L. Burton and P. J. Turchi, "Pulsed plasma thruster", Journal of Propulsion and Power, vol.14, 5, 1998, pp. 716-735

[2] R. J. Vondra, "The MIT Lincoln laboratory pulsed plasma thruster", AIAA Paper 76-998, 1976.

[3] P. J. Turchi, Directions for improving PPT performance, *Proceeding of the 25th International Electric Propulsion Conference*, vol. 1, Worthington, OH, 1998, pp. 251-258.

[4] E. Antonsen, R.L. Burton and F. Rysanek, "Energy measurements in a co-axial electromagnetic pulsed plasma thruster", Paper AIAA-1999-2292.

[5] F. Gulczinski III, M. Dulligan, J. Lakes and G. Spanjers, "Micropropulsion research at AFRL", Paper AIAA-2000-3255

[6] R.L. Burton and S.S. Bushman, "Probe measurements in a Co-axial gasdynamic PPT", *35th Joint Propulsion Conference, Los Angeles, CA, June 1999*, AIAA Paper 99-2288.

[7] F. Rysanek and R.L. Burton, "Effects of geometry and energy on a coaxial Teflon pulsed plasma thruster", *36th Joint Propulsion Conference, Huntsville AL, July 2000*, AIAA Paper 2000-3429.

[8] I.G. Mikellides and P.J. Turchi, "Optimization of pulsed plasma thrusters in rectangular and coaxial geometries", IEPC Paper – 99-211.

[9] K.T. Lee, D.E. Kim and S.H. Kim, "Reversed current structures in a Z-pinch plasma", Phys. Rev. Lett., 85, 2000, 3834.

[10] R.G. Jahn, W. Jaskowsky, and R.L. Burton, "Ejection of a pinched plasma from an axial orifice", AIAA Journal, 3(10), 1965, pp. 1862-1866.

[11] T.E. Markusic, K.A. Polzin, J.Z. Levine, C.A. McLeavey and E.Y. Choueiri, "Ablative Z-Pinch Pulsed Plasma Thruster, AIAA Paper 2000-3257.

[12] G. G. Spanjers, J. S. Lotspeich, K.A. McFall, and R. A. Spores, Propellant losses because of particulate emission in a pulsed plasma thruster, *Journal of Propulsion and Power*, Vol. 14, 4, 1998, pp. 554-559.

[13] M. Keidar, I. D. Boyd and I.I. Beilis, "Model of particulate interaction with plasma in a Teflon Pulsed Plasma Thruster", J. Prop. Power, 17, No. 1, 2001, pp. 125-131.

[14] M. Keidar and I.D. Boyd, "Device and plume model of an electrothermal pulsed plasma thruster", Paper AIAA-2000-3430.

[15] M. Keidar, I.D. Boyd and I.I. Beilis, "Electrical discharge in the Teflon cavity of a coaxial pulsed plasma thruster', IEEE Trans. Plasma Sci., 28, 2000, p. 376-385.

[16] M. Keidar, I.D. Boyd and I.I. Beilis, "On the model of Teflon ablation in an ablation-controlled discharge", J. Phys. D: Appl. Phys., 34, June, 2001, pp. 1675-1677.

[17] N. A. Krall and A.W. Trivelpiece, Principles of Plasma Physics, McGraw-Hill, New York, 1973.

[18] M. Keidar, J. Fan, I.D. Boyd and I.I. Beilis, "Vaporization of heated materials into discharge plasmas", J. Appl. Phys., 89, 2001, pp. 3095-3099.

[19] I.I. Beilis, "Parameters of the kinetic layer of arc discharge cathode region", IEEE Trans. Plasma Sci.,1985, PS-13, p. 288-290.

[20] G. I. Kozlov, V. A. Kuznetsov, and V. A. Masyukov, "Radiative losses by argon plasma and the emissive model of a continuos optical discharge", Sov. Phys. JETP, 39, 1974, pp.463-468.

[21] P. Kovatya and J. J. Lowke, "Theoretical prediction of ablation stabilised arcs confined in cylindrical tubes", J. Phys. D: Appl. Phys., 17, 1984, pp. 1197-1212.

[22] P. Kovatya, "Thermodynamic and transport properties of ablated vapors of PTFE, alumina, perspex and PVC in the temperature range 5000-30000 K", IEEE Trans. Plasma Sci., 12, 1984 pp. 38-42.

[23] C.S. Schmahl and P.J. Turchi, , "Development of equation-of-state and transport properties for molecular plasmas in pulsed plasma thrusters. Part I: A two-temperature equation of state for Teflon", Proc. Inter. Electr. Propul. Conf. Pp. 781-788, 1997.
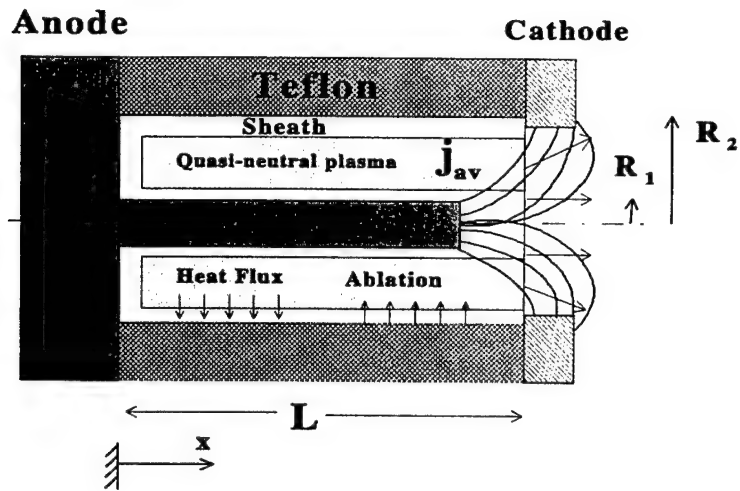
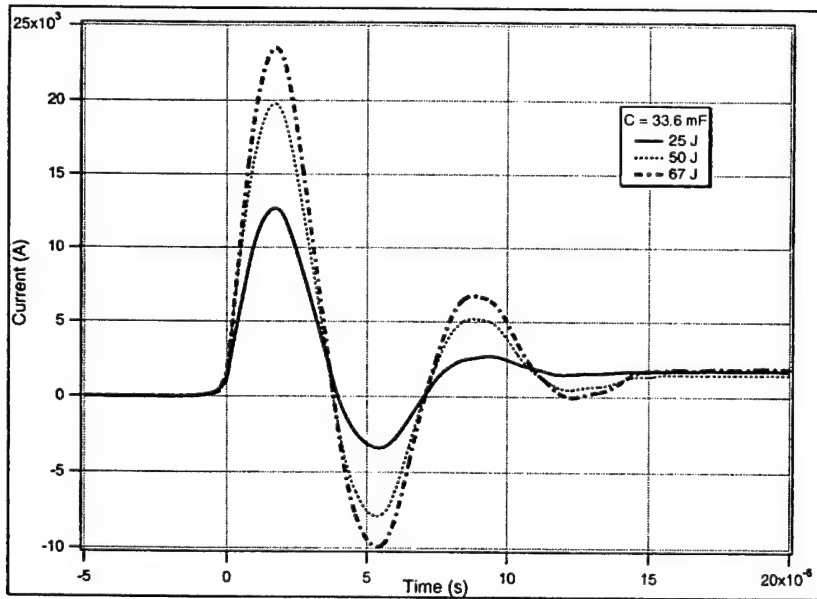*Figure 1. Schematic of the simplified AZPPT geometry adopted in the model*

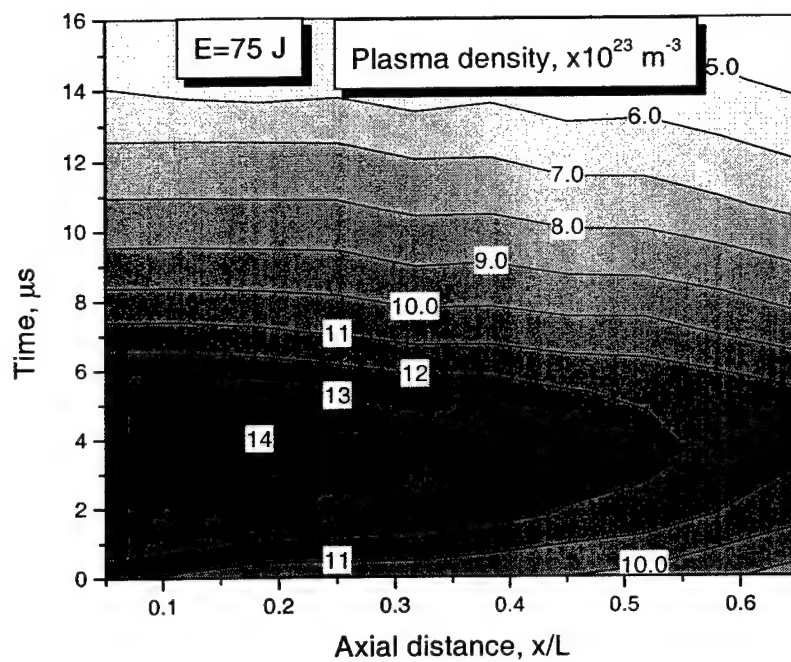

Figure 2. AZ-PPT-3 current waveform

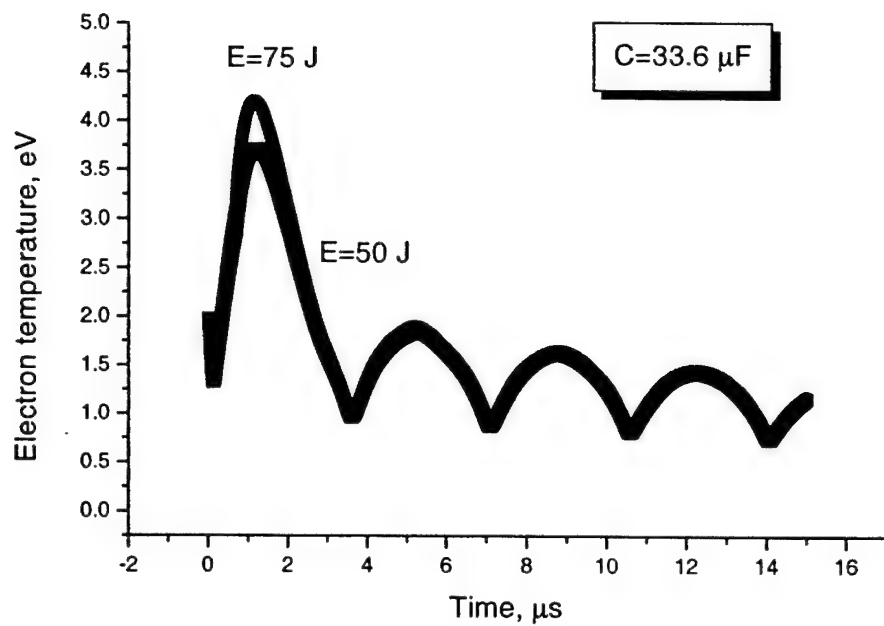**Figure 3.** *Plasma density temporal and axial (along channel centerline) variation during the pulse.*

Figure 4. *Electron temperature temporal variation during the pulse with the pulse energy as a parameter*
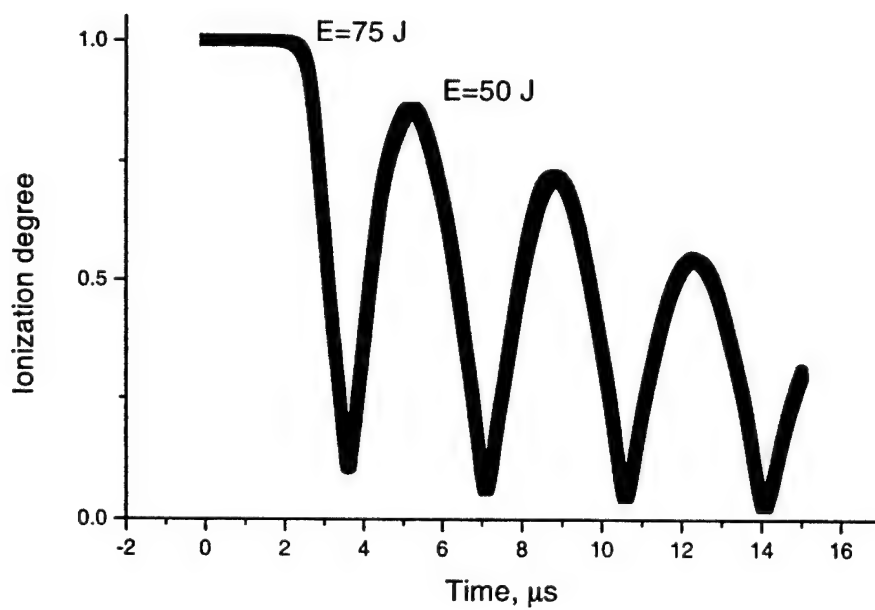

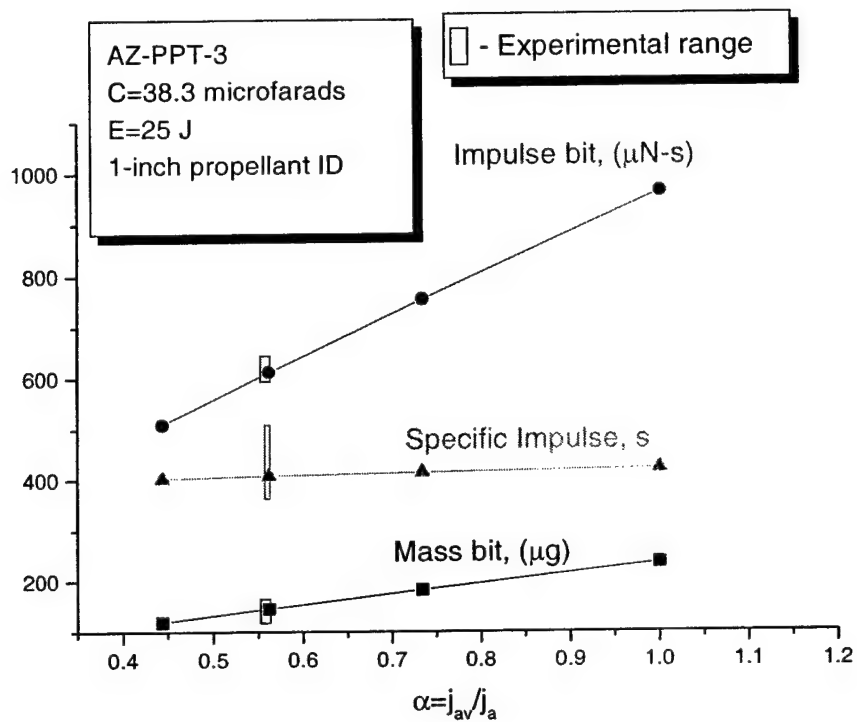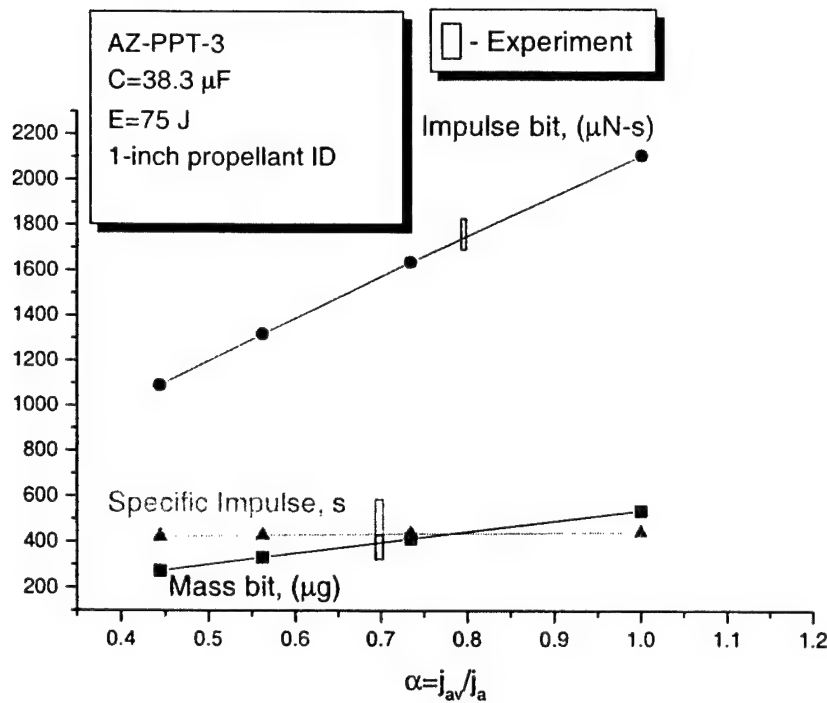**Figure 5.** *Ionization degree temporal variation during the pulse*

18

Figure 6. *AZ-PPT-3 performances as a function of average current density to the anode current density ratio and comparison with experiment*
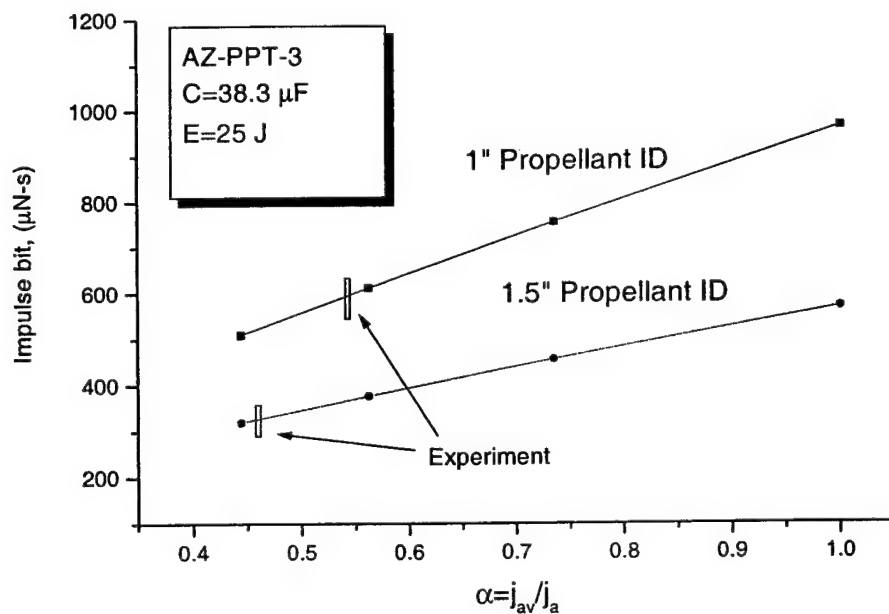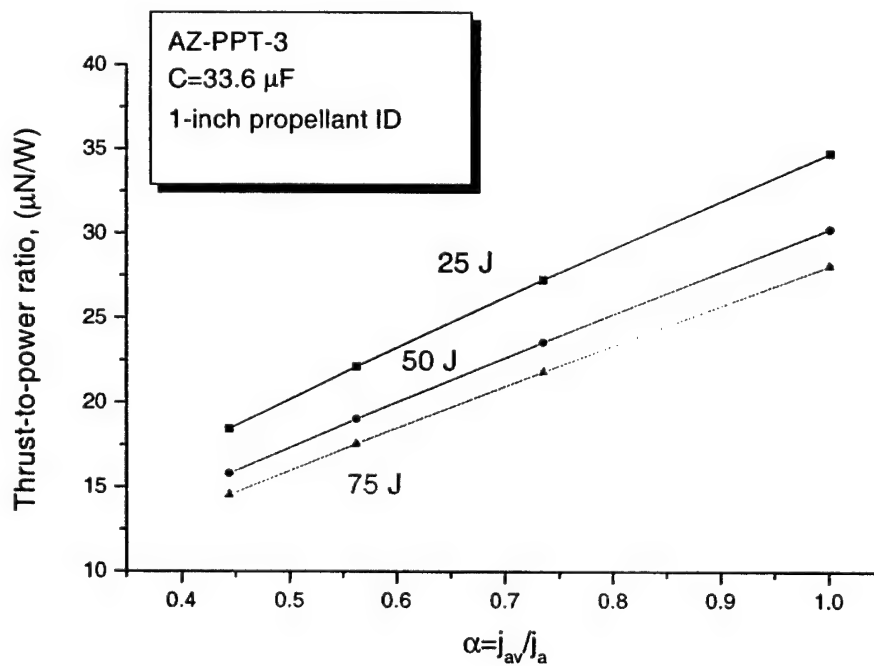

Figure 7. *AZ-PPT-3 impulse bit as a function of average current density to the anode current density ratio with propellant ID (2R₂) as a parameter*

Figure 8. *AZ-PPT-3 performances as a function of average current density to the anode current density ratio and comparison with experiment*

Figure 9. *Thrust-to-power ratio as a function of average current density to the anode current density ratio with pulse energy as a parameter*
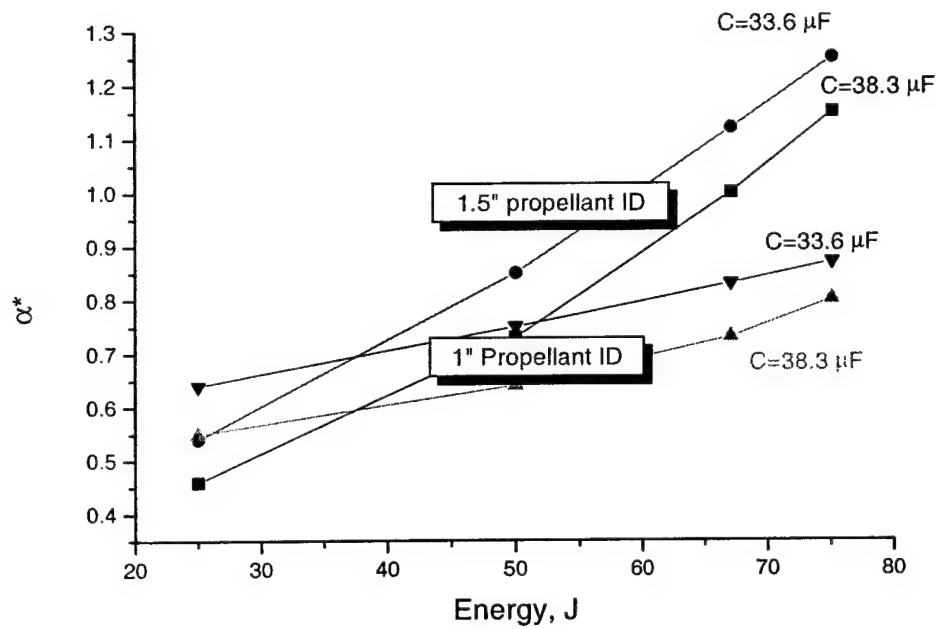
Figure 10. *Average current density to the anode current density ratio α* for which the model agree with experiment as a function of the pulse energy with capacitance and propellant ID as parameters*
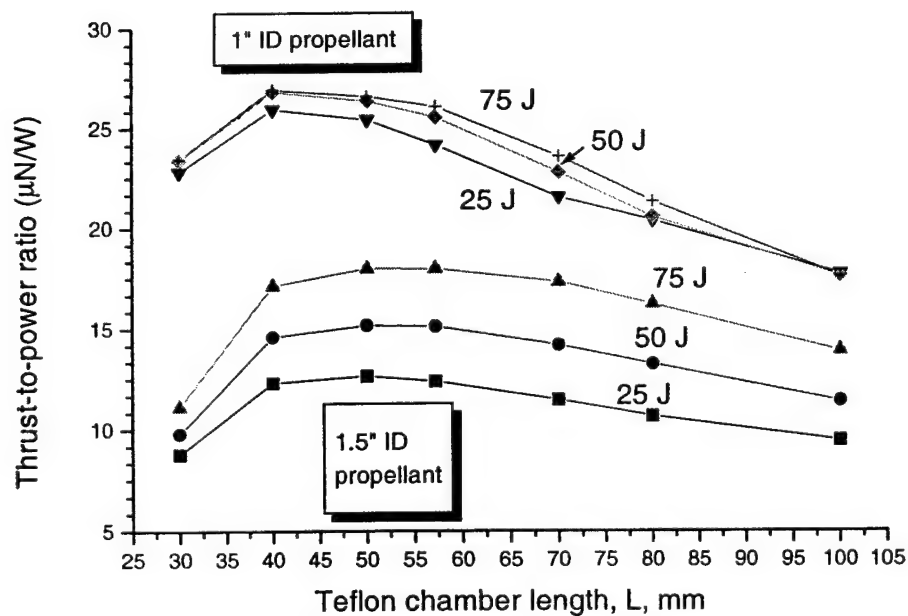

Figure 11. *Thrust-to-power ratio as a function of the Teflon chamber length with pulse energy and the propellant ID as parameters. C=38.3 μF.*

Analyses of Teflon surface charring and near field plume of a Micro-Pulsed Plasma Thruster

Michael Keidar and Iain D. Boyd

Department of Aerospace Engineering, University of Michigan, Ann Arbor MI 48109
734-764-7479, **keidar@engin.umich.edu**

Frank S. Gulczinski III, Erik L. Antonsen and Gregory G. Spanjers

Air Force Research Laboratory, Propulsion Directorate, Electric Propulsion Laboratory
Edwards AFB CA 93524

The Teflon ablation in a micro-Pulsed Plasma Thruster is studied with an aim to understand the charring phenomena. Microscopic analysis of the charred areas shows that it contains mainly carbon. It is concluded that the carbon char is formed as result of carbon flux returned from the plasma. A simplified model of the current layer near the Teflon surface is developed. The current density and the Teflon surface temperature have peaks near the electrodes that explain preferential ablation of these areas as was observed experimentally. The comparison of the temperature field and the ablation rate distribution with photographs of the Teflon surface shows that the area with minimum surface temperature and ablation rate corresponds to the charring area. This suggests that the charring may be related to a temperature effect. Electron densities predicted by the plume model are compared with near field measurements.

Introduction

Pulsed plasma thrusters (PPT's) have been investigated since the early 1960's and were among the first of various electrical propulsion concepts accepted for space flight mainly due to their simplicity and hence high reliability[1]. However, the PPT has an efficiency at the low level of 10% (Ref. 2) and therefore several ways for improvement have been suggested[3]. Currently, PPT's are considered as an attractive propulsion option for stationkeeping and drag makeup purposes of mass and power limited satellites[4,5]. Recently, a micro-PPT has being designed at the Air Force Research Laboratory for delivery of very small impulse bit[6]. This is a simplified miniaturized version of a conventional PPT with a thrust in the 10 µN range designed to provide attitude control and stationkeeping for microsatellites.

Complete assessment of the spacecraft integration effects requires characterization of the plasma plume exhaust of a PPT. Previously we have developed an end-to-end model of the PPT and its plume with application to electrothermal[7,8] and electromagnetic PPT's[9]. It became clear that the plasma distribution in the plume field heavily depends upon upstream boundary conditions. Therefore the model of the plasma generation in these devices becomes a very important aspect of accurate plasma plume simulation.

In the present paper we will focus on the MicroPPT. Inspection of the micro-PPT propellant surface after firing indicated signs of charring and preferential ablation near the electrodes[6,10]. We present also results of the microscopic analyses of the charring areas that is the useful tool for understanding of the charring mechanism. In order to understand this phenomenon a model of the plasma layer near the Teflon surface is developed. In addition, the solution of the model will provide boundary conditions for the plasma plume.

Microscopic analyses of the Teflon surface

The AFRL MicroPPT in development for TechSat21 uses a 3 electrode configuration[6]. A small diameter rod (center electrode) is encased in a small-diameter annulus of Teflon, which is then encased in a relatively small diameter tube, which acts as the intermediate electrode. This construction is then encased in a second larger diameter annulus of Teflon, which is then encased in a large diameter outer electrode. The MicroPPT is fired by a low-energy breakdown between the intermediate and central electrode. This discharge provides enough seed ionization to enable the higher energy conduction breakdown between the intermediate and out electrodes. The discharge between the intermediate and central electrode is referred to as the trigger discharge. The discharge between the intermediate and outer electrode is referred to as the "main discharge". Although a wide range of parameters are tested in various MicroPPT configurations, typically the trigger discharge will consume about 1/50 the energy of main discharge. In this fashion, the MicroPPT has demonstrated the ability to passively initiated a surface breakdown discharge across outer propellant diameters as high as ¼" using a relatively low voltage below 3000V. Without the 3-electrode configuration, up to 40 kV would be required to initiate the discharge across a ¼" diameter. Requiring a 40 kV charge would place excessive design requirements on the power-processing unit and on the spacecraft EMI shielding.

In this work, research is performed on 2-electrode MicroPPT configurations. The discharge occurs between an inner cathode rod and an outer anode tube, across a Teflon annulus. Understanding the physical processes in this simplified geometry has proven beneficial in advancing the optimization of the MicroPPT by separating the requirements for the

trigger and main discharges. Research[6,10] on small diameter 2-electrode designs, generally between 1-3 mm, is applicable to the trigger discharge. Research [6,11] on larger diameter 2-electrode designs, typically between 3 and 7 mm, are more applicable to the main discharge.

Micro-PPT propellant samples with 2 electrodes and different anode diameters were analyzed. These samples represent a fully charred, a partially charred and an uncharred Teflon surface. Microscopic analyses were performed on the Environmental Scanning Electron Microscope available at the EMAL Center at the University of Michigan. The sample chamber is held at a pressure of typically between 1-20 torr. The accelerating voltage is about 15-20 kV. X-ray Energy Dispersive Spectroscopy (XEDS) makes it possible to identify the chemical elements. Below we present some characteristic images taken from the fully charred sample.
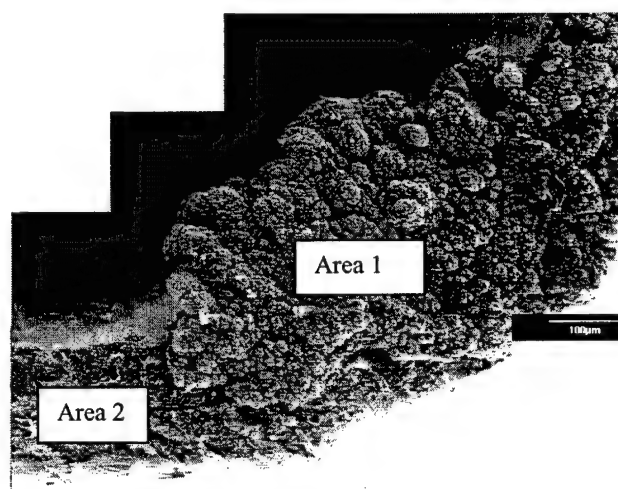

Figure 1. Charring area on the propellant surface of 3.6 mm micro-PPT

Generally two different structures are identified in the charred area (shown as Area 1 and Area 2 in Fig. 1) as can be concluded also from the high magnification images. One can conclude that Area 1 mainly contains Carbon and other small fractions of Fluorine, Copper (Cu), Silver (Ag) and Silicon (Si) as shown in Fig. 2. The images from Area 2 look very different as shown in Figure. 3. One can see that the main component here is Silicon. Small fractions of Cu and Ag are also found.

An analysis of the interface between Areas 1 and 2 as shown in Figure 1 suggests that the same structure (as in the image, Fig. 3) may lie under the Carbon charring. In order to verify this we removed the Carbon layer and analyzed the scratched area. We conclude from the element mapping that the scratched area contains Silicon as well as Fluorine.
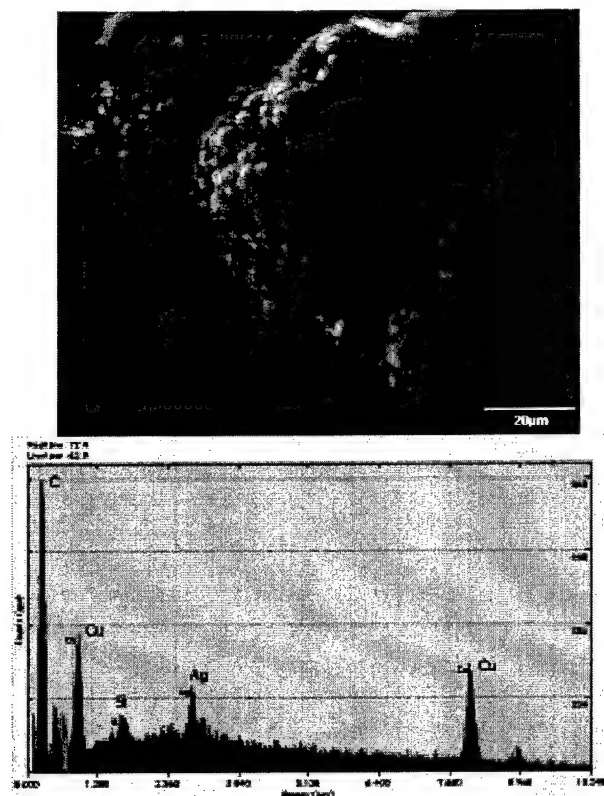

Figure 2. Image and XEDS results for the Area 1. The main peak corresponds to Carbon

Microscopic analyses of different fully and partially charred samples show that under the Carbon layer there is a layer of Silicon with some small amount of Copper. The origin of Copper is probably the outer electrode while Silicon may come from the diffusion pump or the vacuum facility.

In order to eliminate this possible source of Silicon the MicroPPT was fired in a chamber with a turbopump (glass bell jar). The image of this sample is shown in Fig. 4 and the typical image of the charred area is shown in Fig. 5.

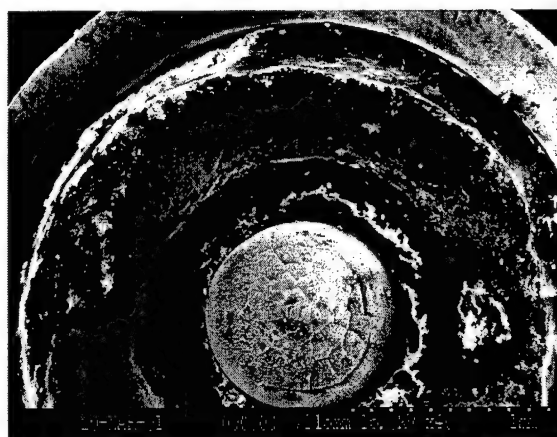*Figure 3. Image and XEDS results for the Area 2. The main peak corresponds to Silicon*

Figure 4. Propellant surface of 3.6 mm diameter micro-PPT

It is interesting to note that in the micro-PPT sample fired in the turbopumped chamber, there is no evidence of Silicon.

An important observation from the microscopic analyses is the presence in most samples of a layer of metal under the char. In those cases where no metal layer is found under the char, the charred area has the same appearance. It is concluded that the char formation therefore may be the same in both cases. This fact may suggest that the Carbon char is formed as result of the Carbon flux returned from the plasma rather than non-complete Teflon decomposition.

Figure 5. Charred area image and XEDS results. The main peaks corresponds to Carbon and Copper

Model

In this part we describe a model of the plasma layer near the evaporating surface with application to a micro-PPT that is shown schematically in Fig. 6.

The model includes the following features: Teflon ablation, plasma energy balance, heat transfer from the plasma to the Teflon, current spreading in the near field, and an equivalent RLC electrical circuit model. The Teflon ablation model is based on a recently developed kinetic ablation model.[12,13]
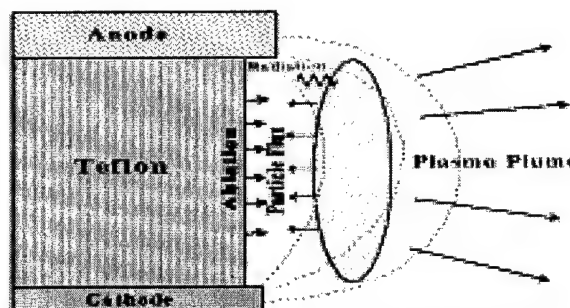

Figure 6. Schematic of the problem geometry and energy balance

The plasma energy balance and the heat transfer to the Teflon are based on a previously developed model of the ablation controlled discharge.[8,14] The energy balance in the layer has the following form:

$$3/2 \, ndT/dt = Q_J - Q_r - Q_F \dotfill (1)$$

where n is the plasma density, T is the plasma temperature, Q_J is the Joule heat, Q_r is the radiation heat and Q_F is the energy flux due to particle convection. Mechanisms of energy transfer from the plasma column to the propellant bar include heat transfer by particle convection and by radiation. The inputs for the model are thruster geometry, Teflon material properties, and Teflon equilibrium pressure dependence on the surface temperature.

In the transition region between the plasma and the ablated surface, two different layers are distinguished: a kinetic non-equilibrium layer adjusted to the surface with a thickness of about one mean free path; and (2) a collision-dominated layer with thermal and ionization non-equilibrium. The solution for these two layers is coupled with the quasi-neutral plasma that allows the calculation of the ablation rate. The energy input in Eq. 1 depends upon the current density distribution near the ablated surface. In order to calculate the current density, the problem of the current distribution in the thruster near field is solved.

Current distribution in the plasma plume near field

Assuming that the magnetic field has only an azimuthal component and after neglecting the

4

displacement current, the magnetic field in the near field plasma plume is calculated from the magnetic transport equation in the following form:

$$\partial\mathbf{B}/\partial t = 1/(\sigma\mu)\nabla^2\mathbf{B} - \nabla\times(\mathbf{j}\times\mathbf{B}/en) + \nabla\times(\mathbf{V}\times\mathbf{B}) \qquad (2)$$

where σ is the plasma conductivity, μ is the permittivity, $\mathbf{j}$ is the current density and $\mathbf{V}$ is the plasma velocity.

A scaling analysis shows that the various terms on the right hand side of Eq. 2 may have importance in different regions of the plasma plume and therefore a general end-to-end plasma plume analysis requires keeping all terms in the equation. In the case of the near plume of the MicroPPT with a characteristic scale length of about 1 cm, the magnetic Reynolds number $Re_m \ll 1$ and therefore the last term can be neglected. Taking this into account in the dimensionless form, Eq. 2 can be written as:

$$Re_m \partial\mathbf{B}/\partial t = \nabla^2\mathbf{B} - (\omega\tau)\cdot\{\nabla\times(\nabla\times\mathbf{B}\times\mathbf{B})\} \qquad (3)$$

here $(\omega\tau)$ is the Hall parameter that measures the Hall effect. Therefore, depending on the plasma density, the Hall effect may be important for the magnetic field evolution.

Our estimations show that the Hall parameter $\omega\tau \ll 1$ if the plasma density near the Teflon surface $N > 10^{23}$ m^{-3}. However, in general, the Hall parameter may vary for different devices and therefore in the future we will investigate the effect of the Hall parameter on the magnetic field distribution in the near field. From the magnetic field distribution the current density components can be calculated as follows:

$$J_r = - 1/\mu \; \partial B/\partial z$$
$$J_z = 1/\mu \; \partial B/\partial r$$

An example of the magnetic field distribution is shown in Fig. 7 for a 3.6 mm diameter propellant micro-PPT. The current density distribution is shown in Fig. 8. One can see that the thickness of the layer where the main part of the current is concentrated is about 1 mm from the Teflon surface. More details about the current and magnetic field distributions in the near field are presented in a recent paper[9].
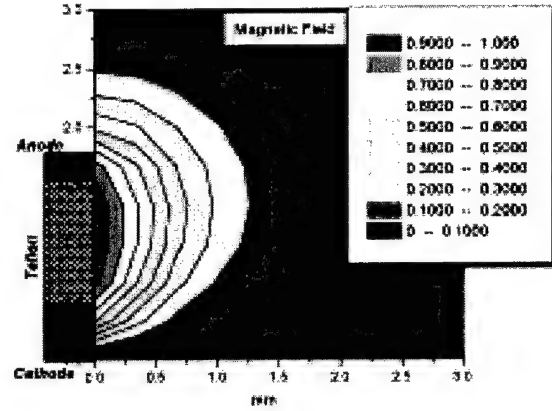

Figure 7. Magnetic field distribution in the near field of a 3.6 mm diameter micro-PPT
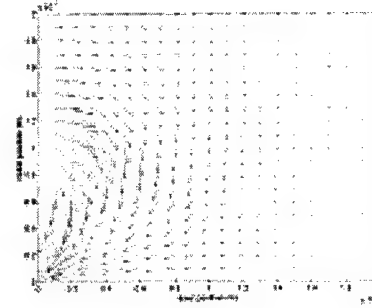

Figure 8. Current distribution in the near field of a 3.6 mm diameter micro-PPT

The current density radial distribution (according to Eqs. 2-4) near the Teflon surface is shown in Fig. 9.
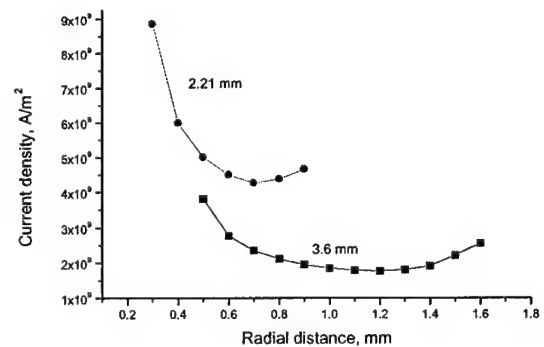

Figure 9. Current density near the Teflon surface

One can see that in the case of the smaller thruster (2.21 mm diameter) the current density is higher by a

factor of about 2 for the same total discharge current. The current density near the Teflon surface has a minimum due to the current spreading in r-z plane as shown in Fig. 8.

The dependence of the calculated ablated mass during the pulse is shown in Fig. 10 for two micro-PPT's with diameters of 3.6 mm and 2.21 mm.
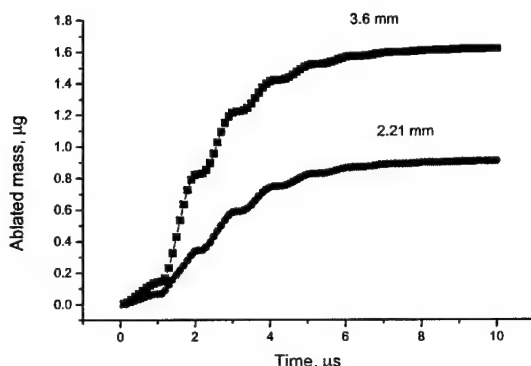

Figure 10. Ablated mass as a function of time with propellant diameter as a parameter

It should be noted that in the experiments, the average ablation mass was measured to be about 1.3 μg/shot in the case of the 2.21 mm diameter thruster. Our model predicts without any fitting parameter that the mass ablated per pulse is about 0.9 μg in this case. Taking into account that the late ablation in the form of macroparticles (that is not considered here but was observed in the micro-PPT[10]) may consume up to 40% of the mass[15], one can conclude that the model predicts the ablation rate reasonably well.

According to the energy balance (Eq. 1) and the heat transfer equation at the Teflon surface, the surface temperature should depend on the current density. The spatial and temporal variation of the Teflon surface temperature for the two thrusters is shown in Fig. 11. In these calculations, the experimental current waveform is used. In the case of the thruster with smaller diameter (2.21 mm), the Teflon surface temperature is higher by about 20 K and can be considered more uniform radially than that of the thruster with larger diameter during the whole pulse.
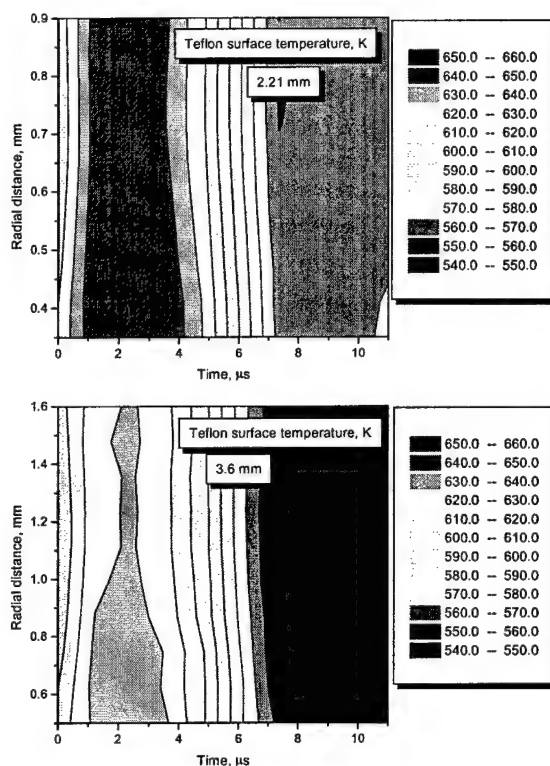

Figure 11. Teflon surface temperature (K) temporal and radial variation for two MicroPPT designs with diameter 2.21 mm and 3.6 mm

In the larger thruster (3.6 mm), the temperature has a minimum at radial distances of 1.1-1.3 mm. Since the Teflon ablation is approximately exponentially proportional to the surface temperature, the model predicts a lower rate of ablation in the areas where the surface temperature has a minimum. Taking this into account, the effect of the temperature distribution may be related to the preferential charring of the Teflon surface observed experimentally as shown in Fig. 12. It is interesting to note that comparison of the calculated temperature field and ablation rate with the photograph of the Teflon surface (see Fig. 12) shows that the area with surface temperature and ablation rate minimum corresponds to the charring area in the case of the 3.6 mm diameter thruster.

6

Figure 12. Teflon surface photo (Ref. 6) and the Teflon surface temperature field and the ablation rate in the case of 3.6 mm diameter micro-PPT

Effect of discharge energy

The current produced by an underdamped RLC circuit has the following form:

$$I(t) = I_p \sin(\alpha t) \cdot \exp(-\beta t)$$

where $\alpha = (1/LC - \beta^2)$, $\beta = R/2L$ and I_p is the current peak, $Ip = U_o/(L\alpha)$, where U_o is the initial voltage on the capacitor of capacitance C, R is the equivalent circuit resistance, L is the circuit inductance. From the comparison of I(t) with the experimental current waveform in the case of $C=0.3$ μF it is estimated that $R=0.3$ Ω and $L=3.6 \cdot 10^{-7}$ H.

We studied the effect of the discharge energy (CU_o^2) on the Teflon surface temperature and the Teflon ablation rate. These results are shown in Fig. 13. One can see that with the energy increase, the Teflon surface temperature and the ablation rate increase. These results suggest that increase of the discharge energy for constant capacitance leads to enhanced Teflon ablation.
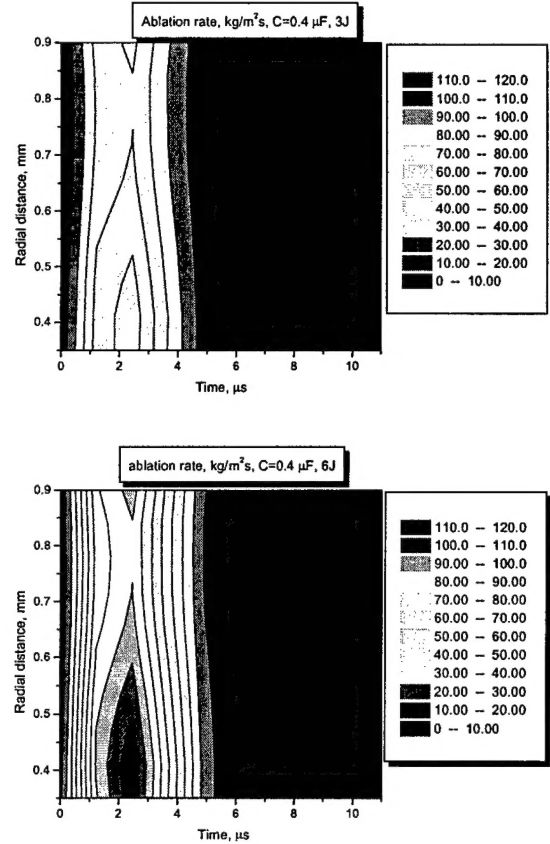
Figure 13. Ablation rate temporal and radial variation for discharge energies of 3J and 6J.

It was shown in experiment that the energy level affects the Teflon ablation. These experiments were conducted in the glass bell jar under a pressure of 10^{-6} torr. The char patterns for three different energies are shown in Fig. 14 after continuous firing for at least 8 hours and at 1 Hz. The cases with higher discharge energy were fired for longer duration to see if char would appear. There have been no experimental observations of cases where char appeared, only to be cleaned up by subsequent discharges at the same energy. (Cleaning of the char formation by firing at higher discharge energies has been observed experimentally, but is not considered within the context of this effort). For these tests a ¼" diameter 2-electrode MicroPPT was energized using a 0.417 uF capacitor. The charge voltage ranged from 2448V for the 1.25 J case, to 5364V for the 6 J case. Clearly

7

these voltages are insufficient to cause the surface breakdown needed for MicroPPT discharge initiation across a ¼" diameter. Rather than complicate the test setup by using the 3-electrode MicroPPT configuration[6], an auxiliary sparkplug, fired at 0.5 J, was used to initiate the discharge on command.

One can see that in the case of small energy, the charring in the area between the electrodes is observed while in the case of large energy, there is no charring. The middle energy case shows a level of char between the 2 extrema. This effect can be partially explained in terms of our model that shows that higher discharge energy leads to higher Teflon surface temperature
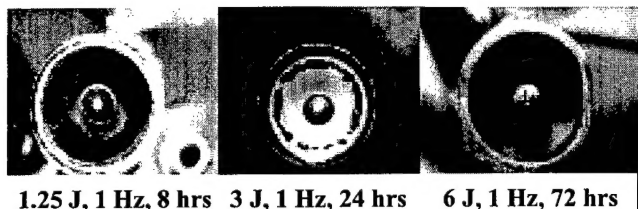

1.25 J, 1 Hz, 8 hrs   3 J, 1 Hz, 24 hrs   6 J, 1 Hz, 72 hrs

Figure 14. Photo of the micro-PPT propellant surface for discharge energies of 1.25 J, 3J and 6J.

Near field plume

In this section we will present measured and predicted electron density distributions in the near filed plume for one micro-PPT design. These data will be compared in order to verify our plume and device model.

Herriot Cell electron density measurement

An experimental basis for comparison is provided using a Herriott Cell interferometer. Electron density measurements are taken on a 6.35 mm (1/4") diameter MicroPPT at AFRL. The interferometer uses a single laser wavelength and quadrature heterodyne technique described by Spanjers *et al.*[16]

Addition of a Herriott Cell acts to confine a large number of laser passes into an area suitable for maximum exposure to the MicroPPT plume. This is achieved by focusing the laser between the two concave mirrors of the cell. The technique is used to

increase signal-to-noise ratio for diffuse plasmas by increasing laser exposure to the plasma over a characteristic path length.[17] Thirteen laser reflections in the Herriott Cell were focused to two points, separated by 3 mm. For data shown here, these points formed a plane parallel to the fuel face and 5 mm distant. A schematic of the beam geometry is shown in Fig. 15.
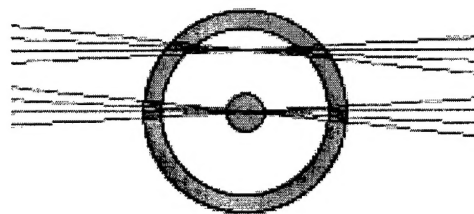

Figure 15. Schematic showing interferometer coverage of the Micro-PPT fuel face using the Herriott Cell. The beams are situated 5mm from the propellant face.

Figure 16 shows the experimental data from this geometry co-plotted with model predictions. The experimental data was taken at a discharge energy of 6.6 J from a 0.417 µF capacitor. Experimental waveforms of the current were obtained using a a self-integrating Rogowski coil. Peak density reaches $23\pm6\times10^{15}$ cm^{-3} with uncertainty due to shot-to-shot variations in thruster firing.

Near field plume simulations

Using the plasma layer model predictions as boundary conditions, we calculated the near field plume of the MicroPPT. This allows us to make direct comparison of our model predictions with measured data.

The general approach for the plume model is based on a hybrid fluid-particle approach that was used previously (Refs. 7). In this model, the neutrals and ions are modeled as particles while electrons are treated as a fluid. Elastic (momentum transfer) and non-elastic (charge exchange) collisions are included in the model. The particle collisions are calculated using the direct simulation Monte Carlo (DSMC) method[16]. Acceleration of the charged particles is computed using the Particle-In-Cell method (PIC)[17]. The ion dynamics is calculated by taking into account electromagnetic acceleration.

8

The electron dynamics is very important in the plasma plume of an electromagnetic PPT. Previously, our model was based on the assumption that electrons rapidly reach the equilibrium distribution and in the absence of a magnetic field can be described according to the Boltzmann distribution. While this was a satisfactory assumption in the case of an electrothermal thruster plume,[7] this is not suitable for the near field of an electromagnetic thruster. In the case of a magnetic field, the electron momentum equation reads (neglecting electron inertia):

$$0 = -e^2 n_e (\mathbf{E} + \mathbf{V_e} \times \mathbf{B}) - e \nabla P_e - \nu_{ei} m_e \mathbf{j}$$

The electric and magnetic field distributions in the plume are calculated from the set of Maxwell equations. More detailed study of the near field plume of the electromagnetic PPT was presented recently[9].
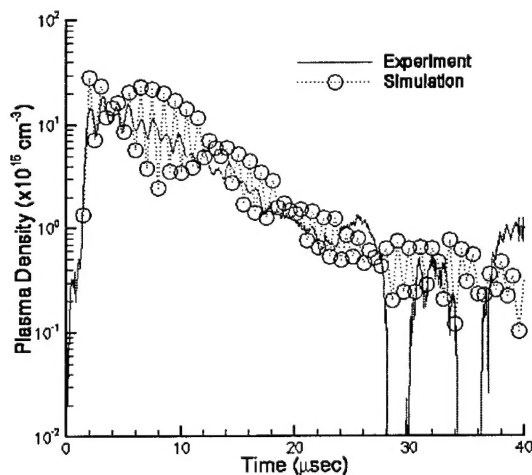

Figure 16. Comparison of predicted and measured electron density time variation at 5 mm from the propellant face at the axis in the case of 6.35 mm diameter micro-PPT firing at 6.6 J.

The calculated plasma density time variation at 5 mm from the propellant face at the axis is shown in Fig. 16. Plasma density peaks at about 3×10^{16} m^{-3} and decreases by few order of magnitude towards the pulse end. For comparison we show also measured plasma density (using Herriott Cell technique, see above section). One can see that our model correctly predicts both the plasma density level and temporal behavior during the entire pulse.

Summary

A model of the plasma layer near the Teflon surface of a PPT was developed that allows the calculation of the Teflon surface temperature and ablation rate self-consistently. It was found that the propellant size has an important effect on the Teflon surface temperature distribution and the ablation rate. For instance, in the case of the thruster with smaller diameter (2.21 mm) the Teflon surface temperature is higher by about 20 K and can be considered more uniform radially than that of the thruster with larger diameter during the whole pulse. In the larger thruster (3.6 mm), the temperature has a minimum at radial distances of 1.1-1.3 mm. The comparison of the temperature field and the ablation rate distribution with a photograph of the Teflon surface shows that the area with surface temperature and ablation rate minimum corresponds to the charring area in the case of the 3.6 mm thruster. This suggests that the charring may be related to the temperature effect. An analysis of the effect of the discharge energy E on the temperature distribution shows that the Teflon surface temperature and the ablation rate can be increased by increasing E. At the same time, the increase of capacitance leads generally to a smaller ablation rate, though this effect can be considered to be marginal.

A microscopic analysis of the charred areas showed that the charred area contained mainly Carbon. In some cases a metal layer was found under the Carbon char. The metal deposition is related to the electrode erosion while the Silicon is assumed to come from the diffusion pump. In fact, when a cryogen pumping system was used, no Silicon was obtained on the Teflon surface. In those cases where no metal layer was found under the char, the charred area has the same appearance. It is concluded that the char formation therefore may be the same in both cases. This fact may suggest that the Carbon char is formed as result of the Carbon flux returned from the plasma rather than non-complete decomposition of the Teflon.

Predicted electron density was directly compared with experimental data and very good agreement was obtained.

9

Acknowledgements

REFERENCES

[1] R. L. Burton and P. J. Turchi, "Pulsed plasma thruster", Journal of Propulsion and Power, Vol.14, No. 5, 1998, pp. 716-735.

[2] R.J. Vondra and K.I. Thomassen, "Flight qualified pulsed plasma thruster for satellite control", *Journal of Spacecraft and Rockets*, Vol. 11, No. 9, 1974, pp. 613-617.

[3] P. J. Turchi, Directions for improving PPT performance, *Proceeding of the 25th International Electric Propulsion Conference*, vol. 1, Worthington, OH, 1998, pp. 251-258.

[4] E. Y. Choueiri, "System optimization of ablative pulsed plasma thruster for stationkeeping", *Journal of Spacecraft and Rockets*, Vol. 33, No. 1, 1996, pp. 96-100.

[5] R. A. Spores, R. B. Cohen and M. Birkan, "The USAF Electric propulsion program", *Proceeding of the 25th International Electric Propulsion Conference*, vol. 1, Worthington, OH, 1998, 1997, p.1.

[6] Spanjers, G.G., White, D., Schilling, J., Bushman, S., Lake, J., Dulligan, M., "AFRL MicroPPT Development for the TechSat21 Flight," 27th Intl Electric Propulsion Conference, IEPC paper 2001-166, Pasadena, CA 2001.

[7] I. D. Boyd, M. Keidar, and W. McKeon, Modeling of a pulsed plasma thruster from plasma generation to plume far field, *Journal of Spacecraft and Rockets, Vol. 37, No. 3, 2000.*

[8] M. Keidar and I.D. Boyd, "Device and plume model of an electrothermal pulsed plasma thruster", Paper AIAA-2000-3430.

[9] M. Keidar and I.D. Boyd, "Electromagnetic effects in the near field plume exhaust of a pulsed plasma thruster", AIAA Paper 2001-3638

[10] Gulczinski, F., Dulligan, M., Lake, J., and Spanjers, G.G., :Micropropulsion Research at AFRL," Paper AIAA-2000-3255.

[11] Antonsen, E., Burton, R., Spanjers, G.G., "*High Resolution Laser Diagnostics in Millimeter-Scale Micro Pulsed Plasma Thrusters*", 27th Intl Electric Propulsion Conference, IEPC paper 2001-157, Pasadena, CA 2001.

[12] M. Keidar, J. Fan, I.D. Boyd and I.I. Beilis, "*Vaporization of heated materials into discharge plasmas*", J. Appl. Phys., 89, 2001, pp. 3095-3098.

[13] M. Keidar, I.D. Boyd and I.I. Beilis, "*On the model of Teflon ablation in an ablation-controlled discharge*", J. Phys. D: Appl. Phys., 34, 2001, pp. 1675-1677.

[14] M. Keidar, I.D. Boyd and I.I. Beilis, "*Electrical discharge in the Teflon cavity of a coaxial pulsed plasma thruster*", IEEE Trans. Plasma Sci., 28, 2000, p. 376-385.

[15] G.G. Spanjers, J.S. Lotspeich, K.A. McFall and R.A. Spores, "*Propellant losses because of particulate emission in a pulsed plasma thruster*", J. Prop. Power, 14, 1998, p. 554

[16] G.A. Bird, "*Molecular gas dynamics and the direct simulation of gas flows*" (Clarendon Press, Oxford, 1994).

[17] C.K. Birdsall and A.B. Langdon, Plasma Physics via Computer Simulation, Adam Hilger Press, 1991.

[16] G.G. Spanjers, K.A. McFall, F. Gulczinski III, R.A. Spores, "Investigation of Propellant Inefficiencies in a Pulsed Plasma Thruster, AIAA Paper 96-2723

[17] E.L. Antonsen, Herriott Cell Interferometry for Pulsed Plasma Density Measurements, MS Thesis, University of Illinois at Urbana-Champaign, 2001.